UNIVERSITÀ DEGLI STUDI DI MILANO

Department of Food, Environmental and Nutritional Sciences

PhD School in Food Systems

Cycle XXXI

STRUCTURAL PROPERTIES AND FUNCTIONAL TAILORING OF REFINED OR UNREFINED PLANT-BASED MATERIALS OBTAINED BY EXTRACTION OR BIO-TRANSFORMATION OF AGRO-FOOD WASTES

Settore disciplinare: AGR 15

Tutor: ***Professor Laura PIAZZA***

PhD coordinator: ***Professor Francesco BONOMI***

PhD thesis of:

Elisa ROCCHI – R11634

Academic Year: 2017 – 2018

Man orders the universe with his language and, when the concepts at stake no longer create order, he changes his concepts for others that create a more universal order. This is the only but true scientific progress. And I know well that I will soon give up my set of conceptual notions, which will become all false, in the sense the profane means this word. But it does not matter to me that I aspire only to order more and more the world and find the best "current" language in this purpose.

ANTOINE DE SAINT-EXUPÉRY

Abstract

The efficient exploitation of resources is a topic of concern worldwide, from both an environmental and economic point of view. The production of large amounts of agro-food residues is one of the main causes for the inefficiency of industrial-scale food production. These are materials of high organic load, where valuable natural compounds and structures can be identified and extracted in order to valorize wastes via physical, chemical or biotechnological processing. For this reason, an intensive investigation for the recovery of materials with improved functional properties has been carried out in the last years.

In this framework, this PhD doctoral project aimed to explore the potentiality of residue-derived ingredients for the food formulation. Structural and functional characterization of the proposed matrices was performed with a material science point of view, based on the quantitative analysis through mathematical models to promote and control adequate changes which can improve some functional properties in the food.

In the present thesis, four different materials were considered. Cellulose nanocrystals were characterized with a rheo-optical approach in order to provide an insight into the relationship between nematic ordering and kinetic arrest. Cell wall materials were studied as carrier of bioactive compounds, with the purpose of tuning the wall matrix organization to obtain a sustained release. Hemp seed meal fractions were evaluated because of their texturing and structuring abilities. The use of bacterial cellulose as support for the retain of volatile molecules was also investigated, along with its thickening ability.

Riassunto

L'impiego delle risorse in maniera efficiente è una tematica di interesse globale, sia da un punto di vista ambientale che economico. La produzione di grandi quantità di residui agro-alimentari è una delle principali cause di inefficienza a livello di produzione industriale. Questi materiali hanno ancora un elevato contenuto di materiale organico, ricco in composti naturali preziosi e peculiari strutture che, una volta identificati, possono essere estratti e valorizzati per via fisica, chimica o biotecnologica. Per queste ragioni, negli ultimi anni si osserva un crescente interesse sia scientifico che industriale per il recupero e la valorizzazione di materiali di scarto.

In questo contesto, questo progetto di dottorato si propone di investigare le potenzialità di ingredienti derivati da residui agro-alimentari per la formulazione alimentare. La caratterizzazione strutturale e funzionale delle matrici considerate ha seguito un approccio tipico della scienza dei materiali, basato sull'analisi quantitativa mediante modelli matematici per promuovere e controllare specifici fenomeni e modificazioni in grado di migliorare le proprietà funzionali del sistema formulato.

Nella presente tesi di dottorato sono stati considerati quattro diversi materiali. La cellulosa nano cristallina è stata caratterizzata da un punto di vista reo-ottico per meglio comprendere quale sia relazione esistente tra l'organizzazione nematica e lo stato cineticamente arrestato. Gli estratti di parete vegetale (CWM) sono stati studiati nell'ottica di un loro impiego come sistemi per il trasporto di composti bioattivi, agendo soprattutto sull'organizzazione della matrice polimerica di parete con lo scopo di poter meglio controllare il rilascio dei composti di interesse. Le frazioni di farina di semi di canapa sono state valutate in termini di capacità texturizzante e strutturante. La cellulosa batterica si è dimostrata invece un eccellente supporto per la ritenzione di molecole volatili.

Index

General Introduction:

FROM RESIDUES TO RE-USE

The current paradigm for industrial-scale food production is recognized as inefficient. Processes have been designed traditionally assuming abundant and cheap availability of resources, and require energy-intensive operations (i.e. thermal treatments, drying, freezing, cooled chain, purification steps) to enhance shelf-life, and obtain highly refined ingredients for food products manufacturing (van der Goot *et al.*, 2016). One of the main causes for the inefficiency relates to the production of large waste or by-product streams (Raak *et al.*, 2017). FAO (2011) estimated that 45% of fruit and vegetable biomass is wasted during all food supply chain, including agriculture post-harvest, processing, distribution and consumption (**figure I.1**).

Pre-consumer	**FOOD PRODUCTION** → agricultural waste	*e.g. wheat straw*
	FOOD PROCESSING → food processing	*e.g. tomato pomace*
	FOOD DISTRIBUTION → transport and retailer	*e.g. damaged food products*
Post-consumer	**FOOD DISTRIBUTION** → mixed domestic food waste production & waste packaging	*e.g. meal preparation waste*

Figure I.1 Simplified food waste chain modified from Pfaltzgraff *et al.* (2013)

Within parts of plants or animals that cannot be consumed (e.g. seeds, stems, peels, bones), many functional components and nutrients are loss during industrial transformation. Moreover, traditional manufacturing is focused on the use of purified and refined materials for the production of food products or ingredients that consist of a single compound or a defined mixture of components. The aim of this strategy is reducing the complexity and variability in favor of standardization, which allows global sourcing, an easier control of the performance, and simpler handling (Ibarz and Barbosa-Canovas, 2002).

On the other hand, the unprecedented scale of food waste in global food supply chains is attracting increasing concern due to its environmental, social and economic impacts (EPA, 2013; Government of South Australia, 2010; Defra, 2011). The management and disposal of side stream products represent an onerous task, thus the current approach for resource management is grounded on the notion that 'waste' can be a 'resource' (Bringezu and Bleischwitz, 2009). In this context, the concept of 3R's (*Reduce, Re-Use, Recycle*) was recently introduced as a hierarchy of strategies (**figure I.2**) with the aim of minimizing waste (Kroyer, 1995). In the first instance, the hierarchy places priority on preventing waste arising, and relegates disposal, a term that encompasses landfilling, to the least favored waste management option (Papargyropoulou *et al.*, 2014). Improved management structures and quality monitoring in food chains can help to reduce waste production, but it cannot be completely avoided. Historically, the exploitation of agro-food wastes for animal feeding represented the first strategy for their re-use. More recently, global attention addressed toward the usage of residues as raw materials for the production of bioenergy, through direct incineration or a fermentation process (biofuels) (Kelzer *et al.*, 2010, Liguori *et al.*,

2013). Pushed by international policy (FAO, EU, national governments), an intensive investigation for the recovery of valuable components and the exploiting the potentiality of recycling has been carried out (Galanakis, 2012). The aim is obtaining materials whose economic value and functional advantages are more than the cost of collection and processing for recycling. Among the intermediate waste management options, reuse and recycling is preferred to energy recovery since it is more environmentally sound (Lin *et al.*, 2013).

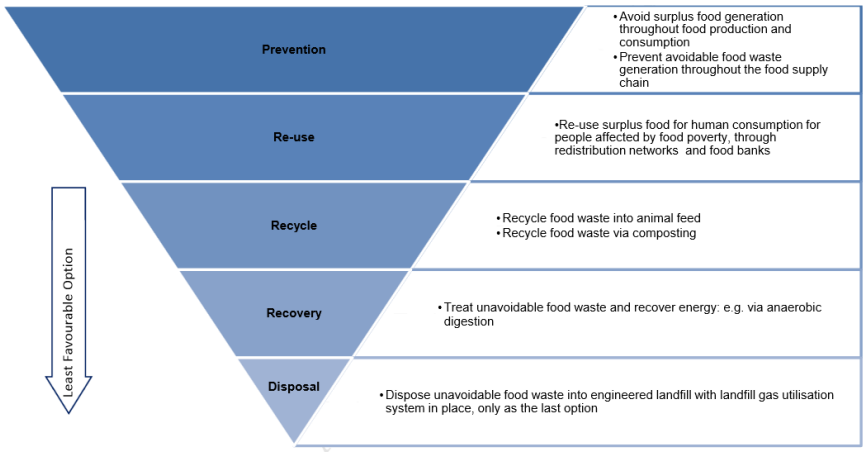

Figure I.2 The waste hierarchy, adapted from Directive 2008/98/EC (European Parliament and Council, 2008).

Agro-food residues are materials of high organic load, composed of a complex and variable mixture of molecules interacting each other and arranged in a supramolecular organization. In this complex framework, valuable natural compounds and structures can be identified and extracted in order to valorize wastes via physical, chemical or biotechnological processing. According to the degree of intervention on the waste matrix, we can distinguish three different approaches: i) the recovery of target compounds, ii) the mild-fractionation to obtain unrefined materials, and iii) the utilization as substrate for bio-transformation.

i) By-products are an abundant source of biopolymers, such as proteins and carbohydrates (e.g. dietary fibers, starch) (Bonarius *et al.*, 2014; Ramachandran *et al.*, 2007), and bioactive components, such as carotenoids and phenolic compounds (Moure *et al*., 2001, Wijngaard *et al.*, 2012). Also components not suitable for foods or feed, such as aliphatic compounds derived from lignin, could be an attractive starting material in the fine chemical and pharmaceutical industry (van der Goot et al., 2016, Zakzeski, Bruijnincx, Jongerius & Weckhuysen, 2010). Thus, the economic potential of by-products is wide and diverse, stimulating an intense investigation about extraction technologies to obtain purified compounds. The main challenges of extraction process are the efficient purification from impurities and toxic compounds, avoidance of deterioration and functionality loss during processing and guarantee of the food grade nature of the final product, besides economic feasibility (Galanakis, 2012). The selectivity of the extraction steps represents a critical factor which requires an intensive treatment of the material. In these terms, conventional extraction processes showed some limitation related to energy-efficiency and environmental sustainability. For this reason, new methods based on emerging technologies are rising interest (Alexandre *et al*, 2017) for the extraction of high value molecules. However, it should also be considered that the recovery of target compounds is generally an individual process integrated into a multi-product system (i.e. biorefinery).

ii) Mild-fractionation enables to produce multicomposite ingredients in which part of the natural structure and interactions are still present. They represent materials enriched in specific components, with a reduced purity compared to conventional ingredients. Despite limited standardization, the production of unrefined materials is more advantageous in terms of resources exploitation. In addition, impurities removal may reduce part of the system functionality, which is enhanced by interaction and cooperation of microcomponents with the main components (Wu *et al.*, 2007; Wang *et al.*, 2002). Also from a nutritional point of view, recent studies indicate that the use of pure ingredients leads to disadvantages inducing micronutrient deficiency (Bhutta, 2008, Black *et al.*, 2008) and over-nutrition of energy-dense components (Ng *et al.*, 2014).
At the present, most of the investigation is focused on polysaccharide-rich fractions, more sustainable alternative source of proteins (Day, 2013; Van der Spiegel, Noordam & Van der Fels-Klerx, 2013) and fibers (de Almeida Costa, da Silva Queiroz-Monici, Reis & de Oliveira, 2006) providing technological and nutritional properties. More recently, a new interest in fractions enriched in bioactive compounds with biological properties (i.e. antioxidant) is rising for nutraceutical and technological applications (Batista-Gonzalez et al., 2012).

iii) The bio-transformation of agri-food residues into high added-value materials involves the action of living organisms (i.e. bacteria, fungi, yeast and actinomycetes) or bio-catalytic polymers (i.e. enzymes) that feed on organic matter to reduce and convert organic waste into high quality products (Grumezescu & Holban, 2017). Firstly, anaerobic digestion and composting were the exploited to convert organic wastes in an energetic source with the release of biogases and heat (Dietrich *et al.*, 2016). Over the years, the use of food wastes as substrate for industrial fermentation aimed at producing specific compounds has gained importance due to their economic and environmental advantages. The development of second-generation bioethanol by bioconversion of lignocellulosic biomass is a representative example, especially in solving the problem of land and crops competition with food and feedstock applications (Menon, & Rao, 2012). More recently, the same family of materials was investigated as substrate for the bio-synthesis of valuable ingredients dedicated to food manufacturing: i.e. cellulose, vanillin (Castro *et al.*, 2011; Zamzuri & Abd-Aziz, 2013).

Despite the striking advantages in terms of renewability and sustainable production, the path to the effective industrial exploitation of organic residues is still studded with challenges to be faced. The standardization of the composition is a critical factor, since agro-food residues can be really heterogeneous as effect of the different geographical origin, weather conditions, post-harvesting processing and botanical variety (Pfaltzgraff *et al.*, 2013). It should also be considered that the diversity in the chemical composition and in structural organization at macro-, meso-, and microscopic levels is responsible for defining functionality. Thus, a comprehensive understanding of the technological performance requires a multiscale approach, able to capture how material composition and architecture decline into functional properties. The mathematical tolls allow to describe the technological performance of the food matrix from a quantitative point of view, using models able to explain or predict their behavior, according to food engineering (Capuano *et al.*, 2017). This approach is typical of empirical models, obtained from mathematical analysis of process data, with the final target of promoting and controlling adequate changes which can improve some sensorial and/or functional properties in the food. On the other hand, theoretical models developed on the basis of chemical and physical principles can be applied to calculate specific parameters and obtain structural information to describe the matrix (Mikleš & Fikar, 2000). Quantitative description is a crucial point for the optimization of ingredients functionality,

also through the rational set up of the processing parameters (Breannan, 2016). In this sense, the optimization of operative conditions requires effective models for process simulation and the development of reliable design procedures.

For this reason, the present project was addressed to the mathematical description of functional behaviour and processes, exploring a variety of different materials classified as follows: refined and multicomposite self-assembled materials, functional fractions, and bio-transformation products.

References

Alexandre, E. M., Moreira, S. A., Castro, L. M., Pintado, M., & Saraiva, J. A. (2017). Emerging technologies to extract high added value compounds from fruit residues: sub/supercritical, ultrasound-, and enzyme-assisted extractions. *Food Reviews International*, 1-32.

Batista-Gonzalez, A.E., Silva, A., Vidal-Novoa, A., Pinto, J.R., Mancini, D.A.P., & Mancini-Filho, J.(2012). Analysis of in vitro and in vivo antioxidant properties of hydrophilic fractions from the seaweed *Halimeda monile* L.. *Journal of Food Biochemistry*, 36 (2), 189-197.

Bhutta, Z. A. (2008). Micronutrient needs of malnourished children. *Current Opinion in Clinical Nutrition & Metabolic Care*, 11(3), 309-314.

Black, M. M. (2008). Effects of vitamin B12 and folate deficiency on brain development in children. *Food and nutrition bulletin*, 29(2), S126-S131.

Bonarius, G. A., Vieira, J. B., van der Goot, A. J., & Bodnár, I. (2014). Rheological behaviour of fibre-rich plant materials in fat-based food systems. *Food Hydrocolloids*, 40, 254-261.

Brennan, C. S. (2016). Food ingredients, processing, structure and functionality: the success for the global food industry. *International Journal of Food Science & Technology*, 51(1), 1-2.

Bringezu, S., & Bleischwitz, R. (2009). Sustainable resource management. Trends, visions and policies for Europe and the World. *Greenleaf*, Sheffield.

Capuano, E., Oliviero, T., & van Boekel, M. A. (2017). Modeling food matrix effects on chemical reactivity: Challenges and perspectives. *Critical reviews in food science and nutrition*, 1-15.

Castro, C., Zuluaga, R., Putaux, J. L., Caro, G., Mondragon, I., & Gañán, P. (2011). Structural characterization of bacterial cellulose produced by Gluconacetobacter swingsii sp. from Colombian agroindustrial wastes. *Carbohydrate Polymers*, 84(1), 96-102.

Day, L. (2013). Proteins from land plants–potential resources for human nutrition and food security. *Trends in Food Science & Technology*, 32(1), 25-42.

de Almeida Costa, G. E., da Silva Queiroz-Monici, K., Reis, S. M. P. M., & de Oliveira, A. C. (2006). Chemical composition, dietary fibre and resistant starch contents of raw and cooked pea, common bean, chickpea and lentil legumes. *Food chemistry*, 94(3), 327-330.

Defra. (2011). Government review of waste policy in England 2011.

Dietrich, T., Villaran Velasco, M. C., Echeverrià, P.J., Pop, B., & Rusu A. (2016). Crop and plant biomass as valuable material for BBB. Alternatives for valorization of green wastes. In: Poltronieri, P., & D'Urso, O.F. (Eds.), *Biotransformation of Agricultural Waste and By-Products* (pp. 1-19)

EPA (2013) Putting Surplus Food To Good Use. Washington DC

European Parliament and Council (2008). Directive 2008/98/EC on Waste.

FAO (2011) Global food losses and food waste: Extent, Causes and Prevention. Food and Agriculture Organization of the United Nations, Rome.

Galanakis, C. M. (2012). Recovery of high added-value components from food wastes: conventional, emerging technologies and commercialized applications. *Trends in Food Science & Technology*, 26(2), 68-87.

Government of South Australia. (2010). Valuing Our Food Waste. *South Australia's Household Food Waste Recycling Pilot*. Adelaide.

Grumezescu, A. M., & Holban, A. M. (2017). Preface for Volume 2: Food Bioconversion. In Food Bioconversion (pp. xxi-xxiv).

Kelzer, J. M., Kononoff, P. J., Tedeschi, L. O., Jenkins, T. C., Karges, K., & Gibson, M. L. (2010). Evaluation of protein fractionation and ruminal and intestinal digestibility of corn milling co-products. *Journal of dairy science*, 93(6), 2803-2815.

Kroyer, G. T. (1995). Impact of food processing on the environment—an overview. *LWT-Food Science and Technology*, 28(6), 547-552.

Ibarz, A., & Barbosa-Canovas, G.V. (2002). Introduction to unit operations: fundamental concepts. In: *Unit operations in food engineering*. CRC Press

Liguori, R., Amore, A., & Faraco, V. (2013). Waste valorization by biotechnological conversion into added value products. *Applied Microbiology and Biotechnology*, 97(14), 6129-6147.

Mancini-Filho, J., Vidal-Novoa, A., & Silva, A.M.O. (2013). Antioxidant properties of algal components and fractions. In. Dominguez, E. (Ed.), *Functional Ingredients from Algae for Foods and Nutraceuticals* (pp. 255-286). Elsevier

Menon, V., & Rao, M. (2012). Trends in bioconversion of lignocellulose: biofuels, platform chemicals & biorefinery concept. *Progress in Energy and Combustion Science*, 38(4), 522-550.

Fikar Mikleš, J., & Fikar, M. (2000). Mathematical modelling of processes. In: *Process Modelling, Identification, and Control* (p. 14) Slovak Technical University Press.

Fito, P., & Chiralt, A. (2003). Food matrix engineering: the use of the water-structure-functionality ensemble in dried food product development. *Food Science and Technology International*, 9(3), 151-156.

Moure, A., Cruz, J. M., Franco, D., Domínguez, J. M., Sineiro, J., Domínguez, H., ... & Parajó, J. C. (2001). Natural antioxidants from residual sources. *Food chemistry*, 72(2), 145-171.

Ng, M., Fleming, T., Robinson, M., Thomson, B., Graetz, N., Margono, C., ... & Abraham, J. P. (2014). Global, regional, and national prevalence of overweight and obesity in children and adults during 1980–2013: a systematic analysis for the Global Burden of Disease Study 2013. *The lancet*, 384(9945), 766-781.

Papargyropoulou, E., Lozano, R., Steinberger, J. K., Wright, N., & bin Ujang, Z. (2014). The food waste hierarchy as a framework for the management of food surplus and food waste. *Journal of Cleaner Production*, 76, 106-115.

Pfaltzgraff, L. A., Cooper, E. C., Budarin, V., & Clark, J. H. (2013). Food waste biomass: a resource for high-value chemicals. *Green Chemistry*, 15(2), 307-314.

Raak, N., Symmank, C., Zahn, S., Aschemann-Witzel, J., & Rohm, H. (2017). Processing-and product-related causes for food waste and implications for the food supply chain. Waste management, 61, 461-472.

Ramachandran, S., Singh, S. K., Larroche, C., Soccol, C. R., & Pandey, A. (2007). Oil cakes and their biotechnological applications–A review. *Bioresource technology*, 98(10), 2000-2009.

van der Goot, A. J., Pelgrom, P. J., Berghout, J. A., Geerts, M. E., Jankowiak, L., Hardt, N. A., ... & Boom, R. M. (2016). Concepts for further sustainable production of foods. *Journal of Food Engineering*, 168, 42-51.

Van der Spiegel, M., Noordam, M. Y., & Van der Fels-Klerx, H. J. (2013). Safety of novel protein sources (insects, microalgae, seaweed, duckweed, and rapeseed) and legislative aspects for their application in food and feed production. *Comprehensive Reviews in Food Science and Food Safety*, 12(6), 662-678.

Wang, M., Hamer, R. J., van Vliet, T., & Oudgenoeg, G. (2002). Interaction of water extractable pentosans with gluten protein: effect on dough properties and gluten quality. Journal of Cereal Science, 36(1), 25-37.

Wijngaard, H., Hossain, M. B., Rai, D. K., & Brunton, N. (2012). Techniques to extract bioactive compounds from food by-products of plant origin. *Food Research International*, 46(2), 505-513.

Wu, W., Clifford, M., & Howell, N. K. (2007). The effect of instant green tea on the foaming and rheological properties of egg albumen proteins. *Journal of the Science of Food and Agriculture*, 87(10), 1810-1819.

Zakzeski, J., Bruijnincx, P. C., Jongerius, A. L., & Weckhuysen, B. M. (2010). The catalytic valorization of lignin for the production of renewable chemicals. *Chemical reviews*, 110(6), 3552-3599.

Zamzuri, N. A., & Abd-Aziz, S. (2013). Biovanillin from agro wastes as an alternative food flavour. *Journal of the Science of Food and Agriculture*, 93(3), 429-438.

Aim of the Work

The aim of this PhD doctoral thesis is to present the information collected from the structural and functional characterization of different novel food ingredients, to demonstrate the potentiality of residue-derived ingredients for the food formulation. Biological systems are approached from a material science point of view, to obtain relationships that described their multi-scale structure and behaviour.

The instigated systems were really heterogeneous, from both a structural and processing point of view. For this reason, the results are presented in four subheadings, one for each material.

In particular, the first subheading (**topic 1**) investigates the different transitions which take place in nanocrystalline cellulose. The coexistence of sol-gel and iso-anisotropic transitions requires the coupling of rheological and rheo-optical techniques to characterize the behaviour, and the consequent technological performance, of this nanoranged structures.

The work reported in the second subheading (**topic 2**) is aimed to the setup of a release system for bioactive compound by using cell wall materials (CWM) as carrier. The application of mathematical modelling to the release profiles allowed to identify the mechanisms involved in the migration of entrapped molecules through the CWM matrix. In the first paragraph (**experiment 3**), anionic dyes were used as models to investigate the behaviour of CWM in different release media. Subsequently, ascorbate was selected as delivered molecule with technological purposes; data about the release kinetic and protective effect of encapsulation against thermal degradation are discussed in the second paragraph (**experiment 4**). In order to improve the sustainability of the extraction process, it was proposed a new procedure to obtain plant-based unrefined ingredients. In the third paragraph (**experiment 5**) the release behaviour of the model dye from the two delivery systems (obtained with traditional and novel extraction) were compared. Moreover, the applicability of folic acid as release bioactive was assessed, also by tuning the CWM structure with calcium ions addition.

The aim of the work reported in the third subheading (**topic 3**) is to evaluate the possibility of obtaining protein-enriched products by simple fractionation of hemp seed meal (HSM) that residues from hemp seed oil cold pressing extraction. Firstly (**experiment 6**), the attention was focussed on the effect of different factors (*i.e.* cultivar, defatting pre-treatment, granulometry and pH) on the technological performance of HSM. In the following paragraph (**experiment 7**), the thermal stability of HSM protein fraction after a pasteurization treatment was investigated, in view of the application of this material in a real food system.

The last subheading (**topic 4**) relates the potentiality of bacterial cellulose in retaining volatile compounds, compared to a cellulosic commercial support for flavour molecules.

Topic 1

SELF-ASSEMBLED MATERIALS: BOTTOM-UP APPROACH

The development of nanomaterials involves the understanding of the precise assembly and ordering of structures on a molecular scale that subsequently controls the organization and integration of structures over several length scales. Thus, an extensive comprehension and control of the interactions and assembly behavior of nanoranged components is on the basis of tuning food structure, rheology and functional properties at the macroscopic scale (Sanguansri & Augustin, 2006). For instance, the interaction of water with amorphous carbohydrates is associated with length scales of a few Ångströms and the diffusion of both water and flavor compounds involves mechanisms at the molecular level (Ubbinik *et al.*, 2008).

At the moment, the commercial scale production of nanomaterials is dominated by a "*top-down*" approach, based on removing building block from the substrate to form the nanostructure. By constrast, nanoscience is now advancing toward a "*bottom-down*" approach that relies on the self-assembling properties of molecules under thermodynamic control to build supramolecular structures, microstructures and higher hierarchical structures to produce functional materials (Förster & Konrad, 2003). Self-assembly and self-organization are concepts derived from biology that involve creating conditions such that individual atoms and molecules arrange themselves in a specific way to create a material, through integration into larger functional units and structural hierarchies (Seeman, N.C. & Belcher, A.M. (2002). In nature self-assembly is often used to make complex structures. At present, the mastery of self-assembly is limited to relatively simple systems.

Molecular self-organization can be achieved by setting a balance between different non-covalent forces (i.e. van der Waals, electrostatic, and hydrophobic interactions, hydrogen and coordination bonds) (Dickinson, 2003; Whitesides & Grzybowski, 2002). There must be the co-existence of both long-range repulsion (e.g. thermodynamic incompatibility, phase separation, excluded volume, and columbic repulsion) and short-range attraction (e.g. covalent bonds and electric dipole interaction). This can occur in macromolecules of defined shape that self-assemble due to the effects of excluded volume interactions and in block co-polymers consisting of binary polymer structures that self-assemble via phase separation effects (Förster & Konrad, 2003). The nature of the self-assembled structures formed is dependent on the size of the polymer, its shape, composition of the solution and its bulk phase, and environmental stresses (Sanguansri & Augustin, 2006).

Examples of self-assembled nanostructures in food include the organization of the casein micelle, the structures formed in protein–polysaccharide coacervates and liposomes. Also, nanoemulsions and nanoparticles have been recently developed using a range of edible materials (McClemens & Rao, 2011; Tiede *etal.*, 2008), but food application is still at its infancy. At the moment most of the research interest is focused on vesicular organization, while less attention is still paid to anisotropic structures (Teo & Sun, 2008). Among them, liquid crystals (LCs) are self-assembled dynamic functional soft materials which possess both order and mobility at molecular, supramolecular and macroscopic levels (Bisoyi & Kumar, 2011).

Nanocrystalline cellulose

The material is isolated from cellulosic fibers through acid treatment. The hydrolysis with sulfuric acid entails the removal of amorphous and paracrystalline regions, along with the introduction of semi-esters negatively charged. The result is a colloidal suspension of highly crystalline nano-ranged rodlike particles, able to spatially self-assemble in different orientations and self-order into liquid crystalline chiral nematic structures under specific conditions (Revol *et al.*,1994). For optimization purposes it is possible to control the morphology and the periodic length via block lengths and polymer concentration.

These nanoranged structures have found application primarily as reinforcing additive for biocompossites, with interesting applications in the food packaging (Mariano *et al*., 2014;) and in drug delivery systems (Honorato Rios *et al*., 2016). But more recently rheological behavior, water absorption and absence of cytotoxic and genotoxic properties of nanocellulose have facilitated its use as food ingredient, with the role of stabilizer and functional ingredient (e.g. dietary fiber) (Koh *et al*., 2016).

In the past, nanocrystals of cellulose were extensively isolated from different vegetal and animal source (Beck-Candanedo *et al.*, 2005; Teixeira *et al.*, 2010; van den Berg *et al.*, 2007). During the recent years, agro-food residues have attracted the attention as source of cellulosic materials and several studies were reported describing the extraction of cellulose fibers and nanofibers from waste products (Teixeira *et al.*, 2011; Rosa *et al.*, 2012; Purkait *et al.*, 2010). Currently, new processes for the production of cellulose nanocrystals are object of investigation (dos Santos *et al.*, 2013; Henrique *et al.*, 2013), even though their application is limited to the manufacture of high-performance materials able to generate important added value.

Beck-Candanedo, S., Roman, M., & Gray, D. G. (2005). Effect of reaction conditions on the properties and behavior of wood cellulose nanocrystal suspensions. *Biomacromolecules*, 6(2), 1048-1054.

Bisoyi, H. K., & Kumar, S. (2011). Liquid-crystal nanoscience: an emerging avenue of soft self-assembly. *Chemical Society Reviews*, 40(1), 306-319.

Dickinson, E. (Ed.). (2003). Food Colloids, Biopolymers and Materials (Vol. 284). *Royal Society of Chemistry*.

dos Santos, R. M., Neto, W. P. F., Silvério, H. A., Martins, D. F., Dantas, N. O., & Pasquini, D. (2013). Cellulose nanocrystals from pineapple leaf, a new approach for the reuse of this agro-waste. *Industrial Crops and Products*, 50, 707-714.

Förster, S., & Konrad, M. (2003). From self-organizing polymers to nano-and biomaterials. *Journal of Materials Chemistry*, 13(11), 2671-2688.

Henrique, M. A., Silvério, H. A., Neto, W. P. F., & Pasquini, D. (2013). Valorization of an agro-industrial waste, mango seed, by the extraction and characterization of its cellulose nanocrystals. *Journal of environmental management*, 121, 202-209.

Honorato-Rios, C., Kuhnhold, A., Bruckner, J. R., Dannert, R., Schilling, T., & Lagerwall, J. P. (2016). Equilibrium liquid crystal phase diagrams and detection of kinetic arrest in cellulose nanocrystal suspensions. *Frontiers in Materials*, 3, 21.

Koh, A., Spinella, S., Maiorana, A., & Gross, R. (2015, August). Characterizing the effect of modification on cellulose nanocrystal pickering emulsions. In: *Abstracts of papers of the american chemical society* (vol. 250). 1155 Washington, DC.

Mariano, M., El Kissi, N., & Dufresne, A. (2014). Cellulose nanocrystals and related nanocomposites: review of some properties and challenges. Journal of Polymer Science Part B: Polymer Physics, 52(12), 791-806.

McClements, D. J., & Rao, J. (2011). Food-grade nanoemulsions: formulation, fabrication, properties, performance, biological fate, and potential toxicity. *Critical reviews in food science and nutrition*, 51(4), 285-330.

Purkait, B. S., Ray, D., Sengupta, S., Kar, T., Mohanty, A., & Misra, M. (2010). Isolation of cellulose nanoparticles from sesame husk. *Industrial & Engineering Chemistry Research*, 50(2), 871-876.

Revol, J. F., Godbout, L., Dong, X. M., Gray, D. G., Chanzy, H., & Maret, G. (1994). Chiral nematic suspensions of cellulose crystallites; phase separation and magnetic field orientation. Liquid Crystals, 16(1), 127-134.

Rosa, S. M., Rehman, N., de Miranda, M. I. G., Nachtigall, S. M., & Bica, C. I. (2012). Chlorine-free extraction of cellulose from rice husk and whisker isolation. *Carbohydrate Polymers*, 87(2), 1131-1138.

Sanguansri, P., & Augustin, M. A. (2006). Nanoscale materials development–a food industry perspective. *Trends in Food Science & Technology*, 17(10), 547-556.

Seeman, N.C. & Belcher, A.M. (2002) Emulating biology: building nanostructures from the bottom up. Proc. Natl. Acad. Sci. USA 99 (Suppl. 2), 6451–6455

Teo, B. K., & Sun, X. H. (2006). From top-down to bottom-up to hybrid nanotechnologies: road to nanodevices. *Journal of cluster science*, 17(4), 529-540.

Teixeira, E., Corrêa, A. C., Manzoli, A., de Lima Leite, F., de Oliveira, C. R., & Mattoso, L. H. C. (2010). Cellulose nanofibers from white and naturally colored cotton fibers. *Cellulose*, 17(3), 595-606.

Teixeira, E., Bondancia, T. J., Teodoro, K. B. R., Correa, A. C., Marconcini, J. M., & Mattoso, L. H. C. (2011). Sugarcane bagasse whiskers: extraction and characterizations. Industrial Crops and Products, 33(1), 63-66. Tiede, K., Boxall, A. B., Tear, S. P., Lewis, J., David, H., & Hassellöv, M. (2008). Detection and characterization of engineered nanoparticles in food and the environment. *Food Additives and Contaminants*, 25(7), 795-821.

Ubbink, J., Burbidge, A., & Mezzenga, R. (2008). Food structure and functionality: a soft matter perspective. *Soft matter*, 4(8), 1569-1581.

van den Berg, O., Capadona, J. R., & Weder, C. (2007). Preparation of homogeneous dispersions of tunicate cellulose whiskers in organic solvents. *Biomacromolecules*, 8(4), 1353-1357.

Whitesides, G. M., & Grzybowski, B. (2002). Self-assembly at all scales. *Science*, 295(5564), 2418-2421.

Experiment 1:

Rheo-optical characterization of cellulose nanocrystals suspensions

Despite wide interest in this new family of materials, a complete characterization of the behaviour and the consequent technological performances is still far to be achieved. The coexistence of different concentration-dependent phenomena (i.e orientation of the nanorods and sol-gel transition) requires a more complex and complete analytical approach to access the samples features from both mechanical and optical point of view. For this reason, rheological and rheo-optical analysis were coupled to investigate the influence of surface charge on the equilibrium between anisotropic transition and behavior at kinetic arrest state.

1.1 Experimentals

1.1.2 Cellulose nanocrystals (CNCs)

The table below summarizes the information about two cellulose suspensions obtained at different hydrolysis conditions (Melodea Ldt., Sweden). As it is evident, the two samples have a similar aspect ratio (that is *L/D*, equal to 17.8 and 18.4 for sample 61 and 64 respectively) but they differ in the sulfur content, and thus in the negative surface electrical state. The different composition along with comparable dimensions allowed us to study their (rheological) behavior only in light of the role of charge density.

Table 1.1 Physico-chemical characterization of CNCs samples (identified as 61 and 64): dimensional (length, *L*, and diameter, *D*), compositional (sulfur content, *S%*), and electrical (surface charge) parameters.

Sample name	**Size**		**% S**	**Surface charge [e/nm^2]**
	L [nm]	D[nm]		
61	101.3	5.7	0.27	0.116
64	101.1	5.5	0.574	0.237

1.1.3 Rheological characterization

The shear rheology was assessed using a CMT (combined motor and transducer) rheometer (DHR-2, TA instruments) equipped with 40 mm diameter cone-plate geometry. All the measurements were performed with a gap of 28 μm, at a temperature of 25 °C. The aqueous suspensions of CNC were analyzed at different concentration values included in the region of coexistence of isotropic and anisotropic phases.

Oscillatory measurements in frequency sweep were performed on each sample from 0.1 to 100 rad/s, with a 0.2% deformation. The strain is within the linear viscoelastic region (LVE) as determined by strain sweep experiments, performed from 0.1% to 100% of strain at a frequency of 1 rad/s.

The relaxation behavior was also evaluated in the transient regime, the stress response was measured after an initial step strain (varying from 10% to 300%) for 180 minutes.

1.1.4 Polarized microscopy

A microlitre drop of the solution was sandwiched between glass slides separated by Mylar film spacers (yielding a 10 μm gap). Images were acquired on a Nikon TE200 inverted microscope with a Nikon DS-5M camera. Liquid crystalline domains were characterized with polarized transmission microscopy.

1.1.5 Rheo-optical characterization

Rheo-optical characterization was performed on a RheOptiCAD cell (CAD Instruments), a linear, strain-controlled shearing device coupled to a Nikon Ti-S inverted microscope and a CCD camera (AVT Prosilica GX1050), which allows both transmission and reflection imaging. A low, 2x magnification was chosen to ensure a large field of view; two crossed polarizers were inserted along the optical path, before and after the sample, at 45 degrees relative to shearing direction to maximize sensitivity to optical anisotropy. Two glass slides confined the sample within a gap of 200 μm. Stacks of images were acquired at 20-50 fps via Labview custom software and processed via ImageJ or custom Matlab code.

1.2 Results

1.2.1 Macroscopic characterization of phase transition

Table 1.2 provides the critical concentrations, quantified by means of macroscopic observation of the bulk sample through cross polarized filters, and are defined as: *c**, that is the minimal concentration to get iso-anisotropic phase separation, and the concentration corresponding to the gelling point (c_g), identified by the presence of a fuzzy interface.

Table 1.2 Critical concentration values (liquid crystalline inset, *c**, and gelling point, c_g) obtained by macroscopical observation.

Sample name	**c***		**c_g**
	[wt%]	pH	[wt%]
61	0.5	3.3	1.75
64	2.49	2.71	4.75

1.2.2 Polarized microscopy

Polarized microscopy was an efficient tool to visualize the sol-gel and iso-anisotropic transitions through the analysis of microscopic textures, and the micrograph for CNC 64 and 61 are reported in **figure 1.1**.

Sample 64 at a concentration lower than 5 % (**figure 1.1a-b**) showed characteristic stripes of N* phase in coexistence with isotropic. This texture is the expression of the periodicity typical of the nematic conformation, as also described by Shafiei-Sabet and his group (2012). However, this characteristic texture is only barely recognizable at 3%, while it clearly evident at 4%. At 5%, the fraction of nematic phase is still lower than unity but in **figure 1.1c** we can recognize a diffused birefringence, enhanced at 5.9 % (**figure 1.1d**). Thus, microscopy textures get "frozen" and show increased birefringence, along with disappearance of detectable N* periodicity. Such observations mark the appearance of a kinetically arrested phase, in which N* regions are supposedly jammed.

If we consider sample 61, the micrographs display an evolution by increasing concentration. At 1.4% and 2.1% (**figure 1.1e-f**) we can recognize a weak birefringence while at 2.8% (**figure 1.1g**) some liquid crystal domains with fingerprint textures, characteristic of chiral nematic structure, are detectable. However, birefringent arrested structure was never reached despite the critical value (c_g = 1.75%) reported after macroscopic observation.

It could be deduced that the lower surface charge of CNC 61 determines a decrease of the effective diameter and apparent volume of the charged rods. It is reflected in stronger chiral interactions which produce birefringent structures at lower concentrations compared to CNC 64 (Hirai *et al.*, 2008).

1.2.3 Rheological Analysis

Gelation Criterion I: Yield strain

Strain sweep tests were performed in order to quantify the stress measured at *G'* and *G''* cross-over (σ_y), marking the transition from a solid-like to a liquid-like response (Derakhshandeh *et al.*, 2013), a possible estimate of yield stress.

The results shown in **figure 1.2a** confirmed the fluid-like behavior of the sample at 3%, since the loss modulus-maintained values higher than the storage modulus on the whole range of deformations investigated. The increment in yield stress between samples at 5% and 5.9% can be related to a glass transition (O'Hern *et al. 2011*). On the contrary, sample 61 (**figure 1.2b**) showed

a fluid-like behavior at all concentration values tested, since G'' maintained higher values than G' in the whole range of strain tested.

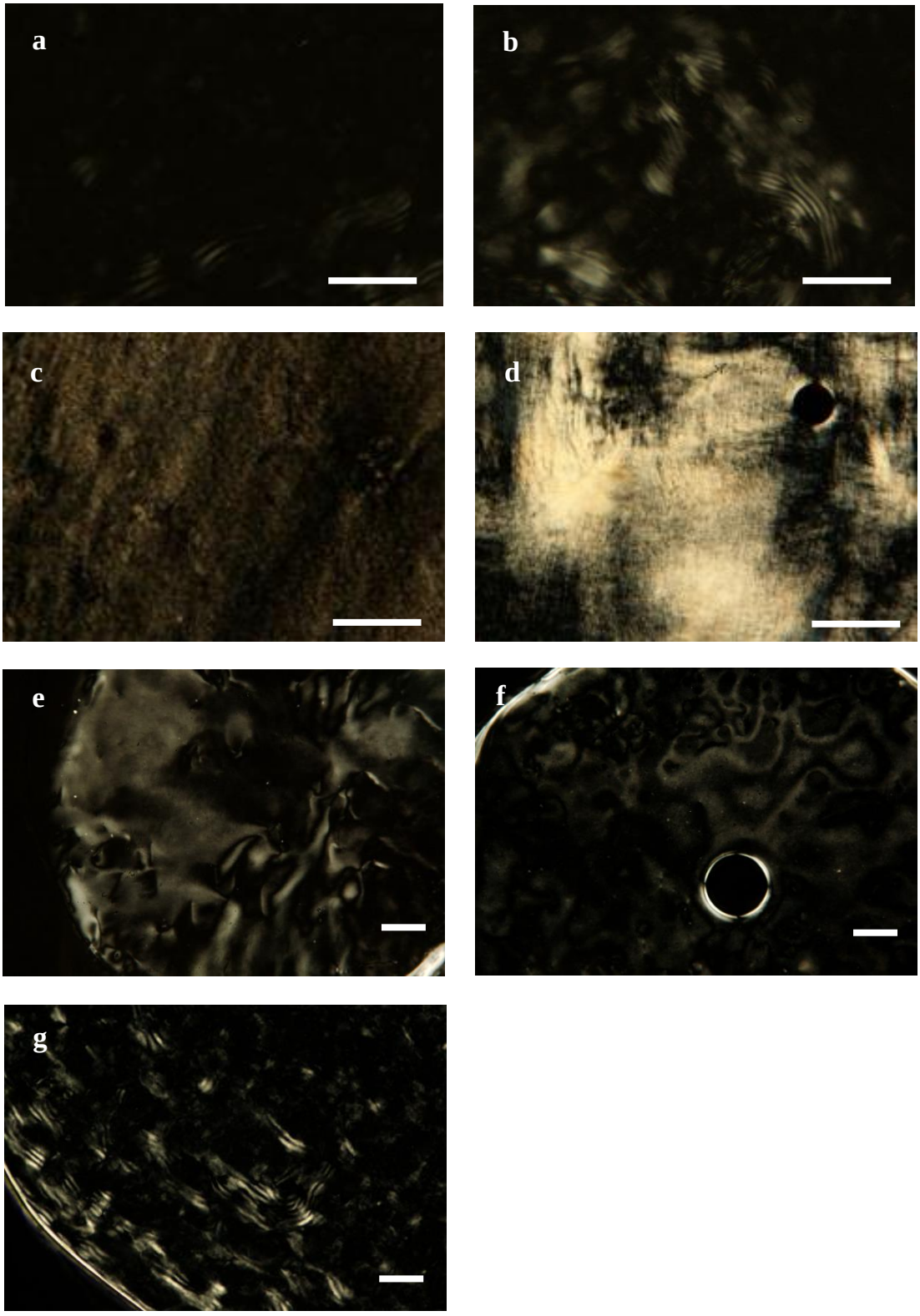

Figure 1.1 CNC-64: typical polarized textures for cellulose at 3% (a), 4% (b), 5% (c), 5.9% (d); size bar: 200 µm. CNC-61: typical polarized textures for cellulose at 1.4% (e), 2.1% (f), 2.8% (g); size bar: 200 µm.

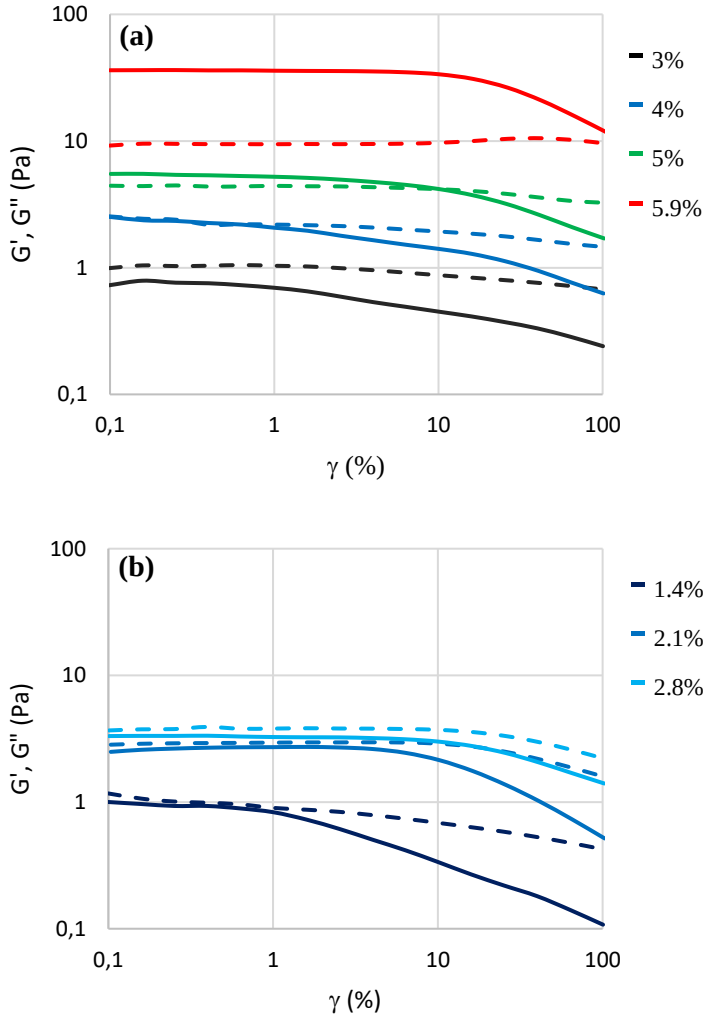

Figure 1.2 Non-linear rheology. Storage modulus *G'* (continuous lines) and loss modulus *G"* (dashed lines) as a function of oscillation amplitude (ω = 10 rad/s), for CNC 64 (a) and CNC 61 (b) at various concentrations.

Gelation Criterion II: Mechanical spectra

In order to determine the critical concentration where sol-gel transition occurs, oscillatory tests were performed in a range of frequencies spanning from 0.1 to 200 rad/s. As follows from graphs in **figures 1.3**, it is clear that the trend of the dynamic moduli shows a power law dependence on the frequency with a different scaling between storage and loss modulus.

$$G'(\omega) \propto \omega^n; G''(\omega) \propto \omega^m \qquad \text{(eq. 1.1)}$$

Observing the viscoelastic spectra presented for sample 64 in (**figure 1.3a**), we can recognize a power law trend for all the curves. Yet three different behaviors can be identified by increasing the concentration, as already observed for cellulose physical gels by Shafiei-Sabet and his group (2014).

The 3% CNC suspension showed a trend typical for fluid samples, as clear from the high dependence of the dynamic moduli on the frequency (highlighted by the exponents in **table 1.3**) and the predominance of *G"* on *G'* over the entire range of frequencies investigated. The 4% sample seemed to be quite close to the critical concentration for gelling. Indeed, according to the criterion of Winter-Chambon (1986), the loss and storage moduli were almost identical and proportional to $\omega^{1/2}$ over a wide range of frequencies at the gel point. In this case, the increase of

G' and *G''* as a function of the frequency shows the same log-log slope of 0.47. For the 5% suspension, the sample displayed a gel-like behavior, and indeed the storage modulus is dominant on the storage modulus over almost the entire range of frequencies investigated. In the end, the most concentrated sample (5.9%) shows a slight dependence on frequency ($n < 0.2$), suggesting that a transition from gel to glassy behavior occurs. In the end, the viscoelastic response of the same sample at 5.9% identified a typical solid-like behavior.

About CNC 61, all the three concentrations investigated show a dominant fluid behavior, since *G''* > *G'* over the most of the range of frequencies applied (**figure 1.3b**). In addition, the absence of a sol-gel transition is confirmed through the power law fitting (**eq. 1.1**) which did not show significant changes of exponent values (n) for different concentration, as reported in **table 4**. The liquid-like nature of the most concentrated samples is not in agreement with the value of gel transition (c_g = 1.75 %) obtained by macroscopic observation.

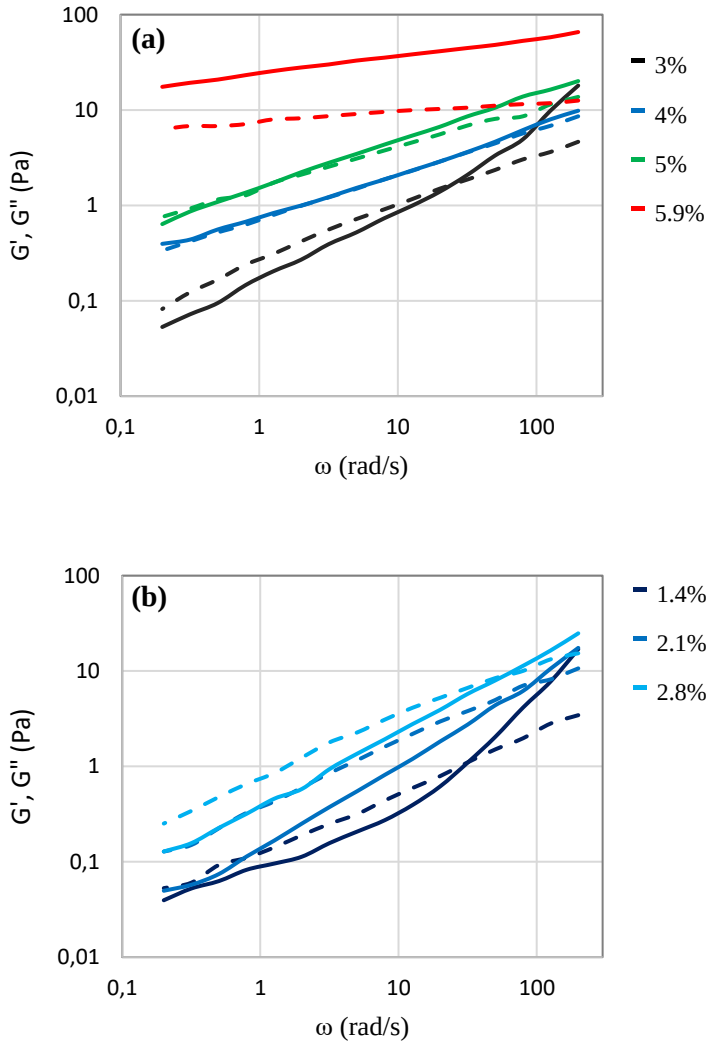

Figure 1.3 Linear rheology. Storage modulus *G'* (continuous lines) and loss modulus *G''* (dashed lines) as a function of angular frequency (γ = 0.5%), for CNC 64 (a) and CNC 61 (b) at various concentrations.

Table 1.3 Exponent of the power law fitting (**eqs. 1.1**) for the two dynamic moduli as from frequency sweep spectra for CNC samples at four concentrations.

	n	***m***
CNC 64		
3%	0.75	0.54
4%	0.47	0.47
5%	0.48	0.40
5.9%	0.18	0.10
CNC 61		
1.4%	-	0.63
2.1%	0.92	0.62
2.8%	0.78	0.57

We can also observe that the effect of stronger chiral interactions in CNC 61 was not reflected significantly in the rheological behavior, and in particular its gelling transition.

Stress relaxation

Nanocrystalline cellulose represent a complex matrix, where a multiplicity of different phenomena takes place. Increasing concentration is responsible for orientation of the nanorods (from iso- to anisotropic transition) and sol-gel transition. While the mechanisms leading to liquid crystalline organization are clear, the physical origin of the gelation process is not well understood even if the formation of a percolated network of liquid crystal domains is hypothesized (Tzoumaki *et al*., 2010; Dufresne, 2103).

In the present paragraph we describe the results obtained only for gel samples (namely CNC 64 at 4, 5 and 5.9%), while the behavior of other cannot be discussed because of the low stress values acquired are too close to the instrument sensitivity. **Figure 1.4** shows the stress relaxation curves with different initial strains (γ_i: 10, 40, 100 and 300%) for the three concentrations.

The less concentrated suspension (4%) relaxes completely before the end of the test, for initial deformation < 80%. While the same sample underwent a single power law relaxation for higher strains. This behavior was reported to be characteristic of critical gels (Winter, 2013) and relaxation curves were described according to the following model (Ng *et al*., 2008; Le Goff *et al*., 2015):

$$G(t) = S \cdot t^{-n} \qquad \text{(eq. 1.2)}$$

where $G(t)$ is the relaxation modulus which decays as a function of the stiffness (S) and of the time (t) with an exponent $-n$.

At 5% and 5.9% of concentration, two relaxation phenomena can be clearly identified. The faster process is characterized by power law decay with a quite constant slope (intended as *n* value, 0.50-0.55 at 5% and 0.30-0.35 at 5.9%). After 1 s, an additional relaxation event occurs.

Only for cellulose suspension at 5.9% (at γ = 100% and 300%) and 5% (at γ = 300%) it was possible to identify the mathematical model able to describe the relaxation at longer time. It can be hypothesized that also in other cases a similar mechanism occurred but the test duration was not long enough to monitor the completely the second stress decay.

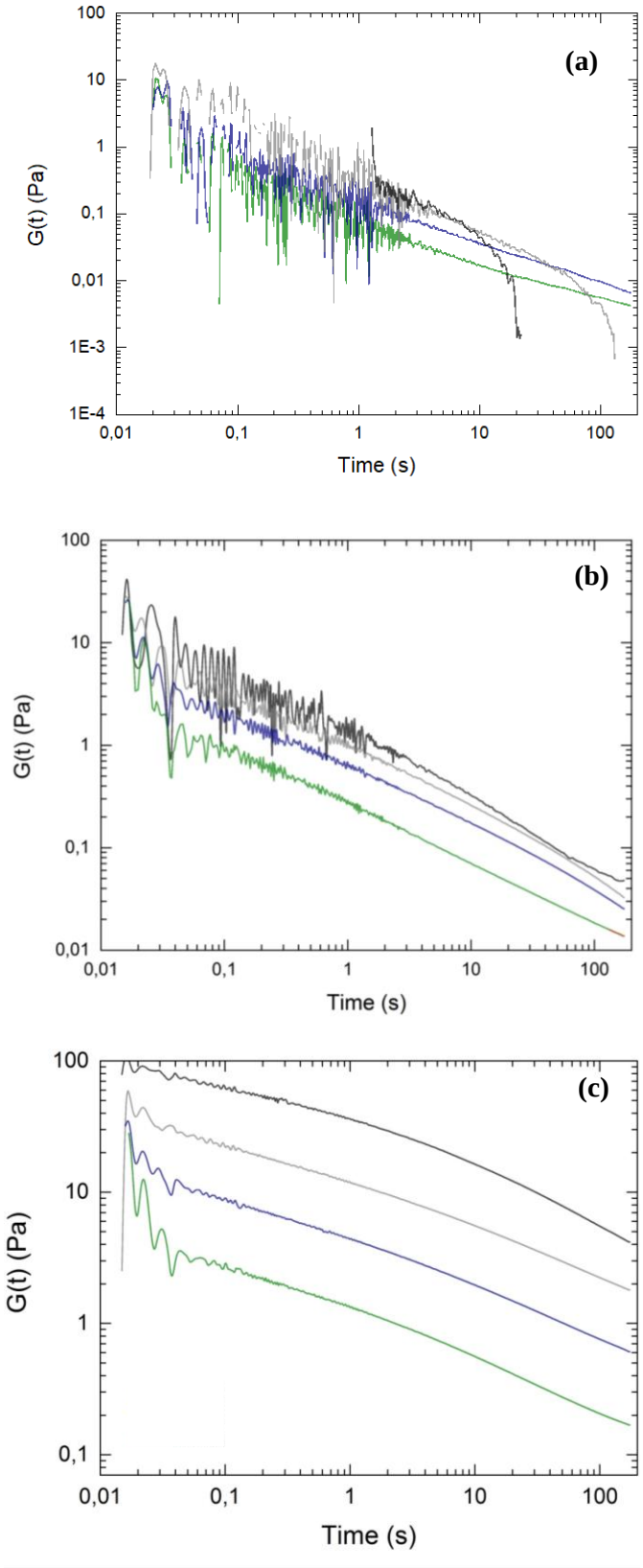

Figure 1.4 Stress relaxation curve of CNC-64 at different concentration (4%: a; 5%: b; 5.9%: c) after a step deformation of 10% (black line), 40% (grey line), 100% (blue line), 300% (green line).

Curves obtained with the most concentrated CNC suspension showed a final exponential decay, and thus were analyzed using the following model:

$G(t) = S \cdot t^{-n} + a * exp(-t/\tau)$ (eq. 1.3)

where a represents the amplitude of the curve and τ and is the relaxation time associated to the phenomenon. The values of τ calculated for the different γ_i are shown in **table 1.4**. As previously discussed in **section 1.2.1**, the sample at 5.9% can be considered a strong gel. The solid-like behavior is confirmed also in transient regime, indeed a residual stress is observed at long time for $\gamma_i > 100\%$.

A multistage character of the relaxation curves possibly reflects different processes. As already described for similar systems, two main relaxation mechanisms influence the overall behavior; the shortest time is generally associated with reorientational dynamic, while the longer one was ascribed to chain entanglement (Lerouge & Berret, 2009; Song *et al*, 2010).

As clear from the graphs, stress relaxation behavior is affected by two main factors, that are concentration (Ureña-Benavides *et al*., 2011) and initial strain (Gray & Mu, 2016).

Concerning the faster power law region of the curves, a decrease in slope value is observed for increasing concentrations (**table 1.4**). The slowdown of the relaxation phenomenon can be related to an increase of the anisotropic fraction. Indeed, anisotropic phase in the matrix seems to stabilize the system against shear induced reorganization (Makarova *et al*., 2013). On the other hand, the exponent *n* was maintained quite constant despite the different strain applied. It would be expected that the initial shear would have caused a modification in CNC rods alignment and loss of chirality (Gray & Mu, 2016) but such differences cannot be appreciated through rheological analysis.

The exponential relaxation seems to be sensitive both to cellulose concentration and the initial step strain. In the first case, a higher concentration of nanocrystals in reflected into an increased entanglement density (Song et al, 2010). This slows the chains relaxation of almost 1 order of magnitude, as evident by comparing relaxation times for samples at 5% and 5.9% (with an initial deformation of 300%).

Only for cellulose suspension at 5.9% it is possible to compare long relaxation time values at different strain. It can be hypothesized that for the other two samples the test duration was not long enough to monitor the completely the second stress decay. It is evident, from the different values shown in **table 1.4**, that a wider initial deformation determines a faster relaxation.

Table 1.4 Stress relaxation parameters (eq. 1.3) indicative of a fast (*n*) and slower decay (τ) for sample 64 at four different concentrations.

	n	**τ (s)**
c = 4%, γ = 40%	0.81	
c = 4%, γ = 100%	0.63	---
c = 4%, γ = 300%	0.46	---
c = 5%, γ = 40%	0.50	
c = 5%, γ = 100%	0.51	
c = 5%, γ = 300%	0.55	1.70
c = 5.9%, γ = 40%	0.30	
c = 5.9%, γ = 100%	0.34	12.07
c = 5.9%, γ = 300%	0.35	8.66

1.2.4 Rheo-optics

Since material microstructure controls rheology as well as optical properties (Wagner, 1998), rheological characterization gave only a partial probe of material microstructure and molecular or mesoscale dynamics. For this reason, optical methods were required to have a complete insight of CNC arrangement and response. The sample was observed by means of a polarized microscope during a step deformation and the consequent relaxation. The average intensity (*I*) of light transmitted through the crossed polarizers was quantified in order to estimate the effect of deformations on the overall degree of alignment. Indeed, for isotropic samples *I* is nearly zero while aligned regions are characterized by birefringence detected as an increase in *I* value.

In **figure 1.5**, we report the evolution in time of the average intensity (*I*) of light transmitted in a defined region of interest while applying the stress relaxation protocol for the CNC at 5.9%. The value reported in the ordinates are normalized to the value at maximum peak (I_{max}), corresponding to the *I* value when the complete deformation is applied. The transient optical alignment is quickly relaxed for small deformations. For large imposed shear some residual birefringence persists for much longer times. This behavior could be explained by an overall system rearrangement of the nanorods when the material is 'fluidized' due to the deformation applied (Echeverria et al., 2015).

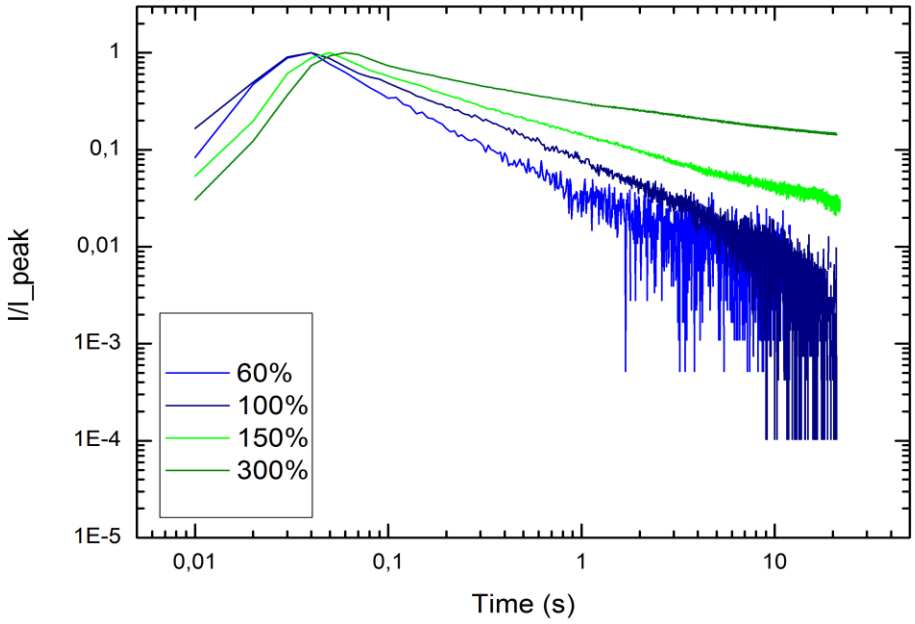

Figure 1.5 Transmitted intensity *I* through crossed polarizers normalized for the value at the maximum peak (I_{max}) for CNC at 5.9 %, during step deformations at different amplitudes and relaxation after deformation cessation.

Conclusions

In the effort of understanding the relationship between nematic structures assembling ang kinetic arrest, nanocrystalline cellulose aqueous dispersions were evaluated through macroscopic observation, rheological analysis and rheo-optics. The transition from an isotropic to an anisotropic system did not seem to affect the gelling behaviour, assessed in terms of viscoelastic properties. Some discrepancies were observed in the identification of the gelling concentration between rheological and macroscopic evaluations, likely due to the involvement of different mechanisms in defining the fuzzy interface. On the contrary, a permanent alignment of CNC was observed applying deformations able to induce a fluid state in the sample.

Acknoledgments

I acknowledge the kind gift of CNC samples from Doron Kam (Hebrew University of Jerusalem), and Giuliano Zanchetta (Dept. of Medical Biotechnology and Translational Medicine, UNIMI) for performing optical and rheo-optical analysis.

References

Derakhshandeh, B., Petekidis, G., Shafiei Sabet, S., Hamad, W. Y., & Hatzikiriakos, S. G. (2013). Ageing, yielding, and rheology of nanocrystalline cellulose suspensions. *Journal of Rheology*, 57(1), 131-148.

Dufresne, A. (2013). Nanocellulose: a new ageless bionanomaterial. *Materials Today*, 16(6), 220-227.

Echeverria, C., Almeida, P. L., Feio, G., Figueirinhas, J. L., Rey, A. D., & Godinho, M. H. (2015). Rheo-NMR study of water-based cellulose liquid crystal system at high shear rates. *Polymer*, 65, 18-25.

Gray, D. G., & Mu, X. (2016). Twist–bend stage in the relaxation of sheared chiral nematic suspensions of cellulose nanocrystals. *ACS Omega*, 1(2), 212-219.

Hirai, A., Inui, O., Horii, F., & Tsuji, M. (2008). Phase separation behavior in aqueous suspensions of bacterial cellulose nanocrystals prepared by sulfuric acid treatment. *Langmuir*, 25(1), 497-502.

Le Goff, K. J., Gaillard, C., Helbert, W., Garnier, C., & Aubry, T. (2015). Rheological study of reinforcement of agarose hydrogels by cellulose nanowhiskers. *Carbohydrate polymers*, 116, 117-123.

Lerouge, S., & Berret, J. F. (2009). Shear-induced transitions and instabilities in surfactant wormlike micelles. In *Polymer Characterization* (pp. 1-71). Springer, Berlin, Heidelberg.

Makarova, V. V., Tolstykh, M. Y., Picken, S. J., Mendes, E., & Kulichikhin, V. G. (2013). Rheology–Structure Interrelationships of Hydroxypropylcellulose Liquid Crystal Solutions and Their Nanocomposites under Flow. *Macromolecules*, 46(3), 1144-1157.

Ng, T. S., & McKinley, G. H. (2008). Power law gels at finite strains: the nonlinear rheology of gluten gels. *Journal of Rheology*, 52(2), 417-449.

O'Hern, C. S., Langer, S. A., Liu, A. J., & Nagel, S. R. (2001). Force distributions near jamming and glass transitions. *Physical review letters*, 86(1), 111.

Shafiei-Sabet, S., Hamad, W. Y., & Hatzikiriakos, S. G. (2012). Rheology of nanocrystalline cellulose aqueous suspensions. *Langmuir*, *28*(49), 17124-17133.

Shafiei-Sabet, S., Hamad, W. Y., & Hatzikiriakos, S. G. (2014). Ionic strength effects on the microstructure and shear rheology of cellulose nanocrystal suspensions. *Cellulose*, 21(5), 3347-3359.

Song, H., Zhang, J., Niu, Y., & Wang, Z. (2010). Phase transition and rheological behaviors of concentrated cellulose/ionic liquid solutions. *The Journal of Physical Chemistry B*, 114(18), 6006-6013.

Tzoumaki, M. V., Moschakis, T., & Biliaderis, C. G. (2009). Metastability of nematic gels made of aqueous chitin nanocrystal dispersions. *Biomacromolecules*, 11(1), 175-181.

Ureña-Benavides, E. E., Ao, G., Davis, V. A., & Kitchens, C. L. (2011). Rheology and phase behavior of lyotropic cellulose nanocrystal suspensions. *Macromolecules*, 44(22), 8990-8998.

Wagner, N. J. (1998). Rheo-optics. *Current Opinion in Colloid & Interface Science*, 3(4), 391-400.

Winter, H. H., & Chambon, F. (1986). Analysis of linear viscoelasticity of a crosslinking polymer at the gel point. Journal of rheology, 30(2), 367-382.

Winter, H. H. (2013). Glass transition as the rheological inverse of gelation. *Macromolecules*, 46(6), 2425-2432.

Experiment 2:

Seeing Is Believing: Coupling Between Liquid Crystalline Ordering and Rheological Behaviour in Cellulose Nanocrystals Suspensions

Within the liquid crystalline and gel phases of CNC, some of the pre-shear protocols typically used in rheological measurements - involving mechanical yielding imposed via large amplitude oscillations or continuous shear - are associated to perturbation and persistent alignment of CNC domains along the shear direction, which in turn weaken the linear mechanical CNC response. Complete relaxation of shear-induced ordering and full recovery of linear moduli only occur over hundreds of seconds. We thus show that the combination of optical and rheological characterization can provide a valuable tool for the assessment of non-linear behavior in complex fluids like CNC suspensions.

2.1 Materials and methods

2.1.1 Materials and sample preparation

CNCs samples, a kind gift of D. Kam (Hebrew University of Jerusalem), were obtained from waste cellulosic material (from paper industry), following an established protocol which involves sulfuric acid hydrolysis, washing and sonication steps (Bondeson *et al.*, 2006; Abraham *et al.*, 2016).

The CNC sample described here has been characterized via Dynamic Light Scattering, Atomic Force Microscopy and cryogenic Transmission Electron Microscopy to determine CNC size; relatively narrow distributions have been found, with average length L = 100 nm (90 % between 50 and 175 nm) and average diameter D = 5.5 nm (90 % between 3 and 8 nm). The presence of aggregates was detected, possibly due to low sonication time/power. Surface charge, as determined by Zeta Potential, is -0.237 e/nm^2. The stock solution, 5.9 % in weight, was diluted with milliQ water to obtain lower c_{CNC} samples.

2.1.2 Rheological and rheo-optical characterization

Rheological measurements, oscillatory and continuous shear, were performed with a DHR-2 rheometer (TA Instruments) equipped with 40 mm diameter cone-plate geometry, with a gap of 28 μm. Care was taken that samples were fully homogenous within the timescale of measurements.

Rheo-optical characterization was performed on a RheOptiCAD cell (CAD Instruments), a linear, strain-controlled shearing device coupled to a Nikon Ti-S inverted microscope and a CCD camera (AVT Prosilica GX1050), which allows both transmission and reflection imaging. A low, 2x magnification was chosen to ensure a large field of view; two crossed polarizers were inserted along the optical path, before and after the sample, at 45 degrees relative to shearing direction to maximize sensitivity to optical anisotropy. Two glass slides confined the sample within a gap of 200 μm. Stacks of images were acquired at 20-50 fps via Labview custom software and processed via ImageJ or custom Matlab code. Both types of measurements were performed at 25 °C.

2.2 Results and Discussion

2.2.1 Phase diagram

We evaluated the phase diagram via a combination of macroscopic and polarized optical microscopy observations, finding the expected transition from isotropic to coexisting isotropic and N* phases at c_{CNC} = 2.5 %. In **figure 2.1** we report the fraction of N* phase Φ_{N^*} as a function of c_{CNC}, together with microscope textures showing the characteristic stripes of N* phase in coexistence with isotropic. For c_{CNC} > 5 %, when Φ_{N^*} is still lower than unity, the macroscopic interface gets fuzzy and phase separation is completely suppressed at c_{CNC} = 5.9 %. Correspondingly, microscopy textures get "frozen" and show increased birefringence, along with disappearance of detectable nematic (N*) periodicity. Such observations mark the appearance of a kinetically arrested phase, in which N* regions are supposedly jammed.

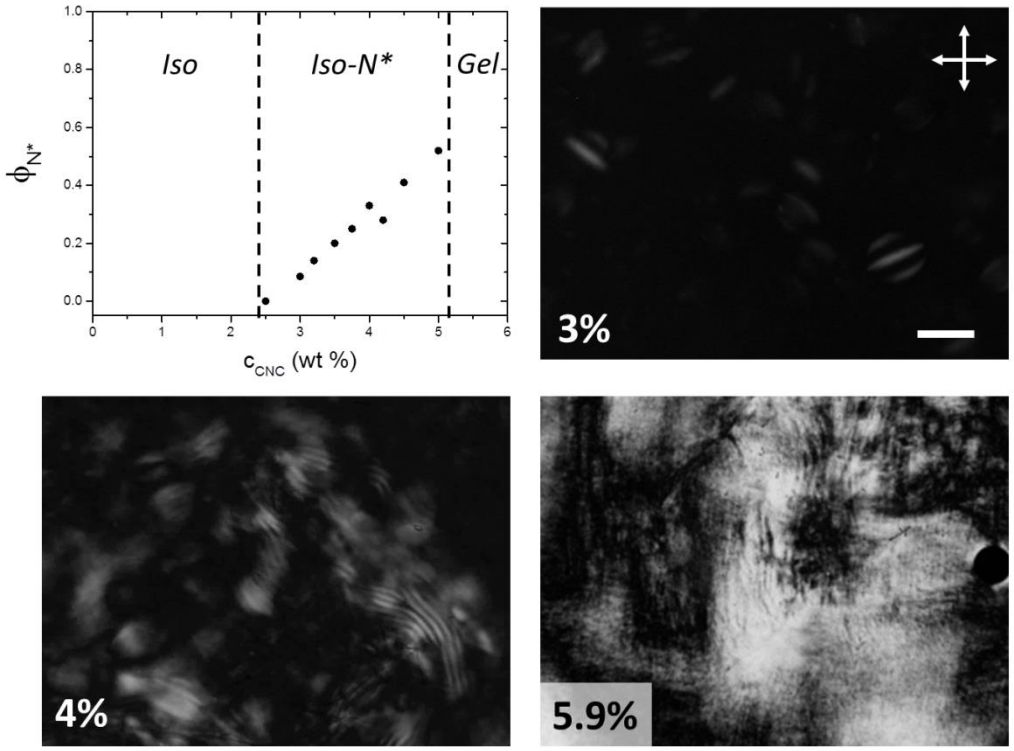

Figure 2.1 CNC phase diagram. Top left: volume fraction of N* phase as a function of CNC concentration. Other panels show typical polarized microscopy textures for the indicated concentrations.

2.2.2 Linear and non-linear rheological characterization

Materials that contain more than one phase can be considered structured fluids since their rheological behaviour is affected by the interactions of the constituents. We performed linear oscillatory rheology measurements in the same c_{CNC} range. In **figure 2.2**, we show the storage modulus G' and loss modulus G'' as a function of frequency. For samples up to 5 %, the mechanical response is mostly fluid-like, with a non-negligible elastic component, yet vanishing at low frequency. On the contrary, for c_{CNC} = 5.9 %, CNC behaviour shows a clear discontinuity, consistent with macroscopic and microscopic observations: G' prevails over G'' and becomes nearly frequency-independent. Some of these features are reminiscent of critical gels (characterized by similar power-law scaling of G' and G'' with frequency); however, at this stage it is not yet clear if aggregates play any role in such behaviour.

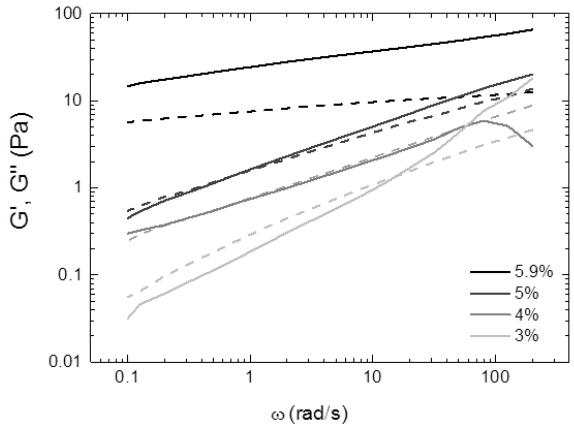

Figure 2.2 Linear rheology. Storage modulus G' (continuous lines) and loss modulus G'' (dashed lines) as a function of angular frequency (left, 0.5% amplitude), for various CNC concentrations.

2.2.3 Coupling between rheological response and degree of ordering

Within the Iso-N* region, different pre-shearing protocols yield similar and reproducible effects. On the contrary, at c_{CNC} = 5.9 %, i.e. within the kinetically arrested phase, we observed a marked dependence of the measured linear moduli on the type and extent of pre-shear. In **Figure 2.3a**, we show linear frequency sweep measurements for the same sample, either only allowed to relax for 15 minutes after loading, or subjected to different deformations and immediately tested after pre-treatment. While 100% oscillations produce only slight weakening of the elastic response, 300% oscillations and continuous shear at high shear rate dramatically impact sample properties, which only recover after several tens of minutes. Furthermore, **figure 2.3b** displays the measured G' during a non-linear, 300 % oscillation and its time evolution (as measured through a linear 0.5 % oscillation) during the subsequent 300 seconds interval, for several repeated cycles. An almost immediate G' recovery is observed after each cessation, followed by a slow relaxation to a plateau value. Overall, the effect of each cycle of large oscillations adds to the previous one with a progressive weakening effect.

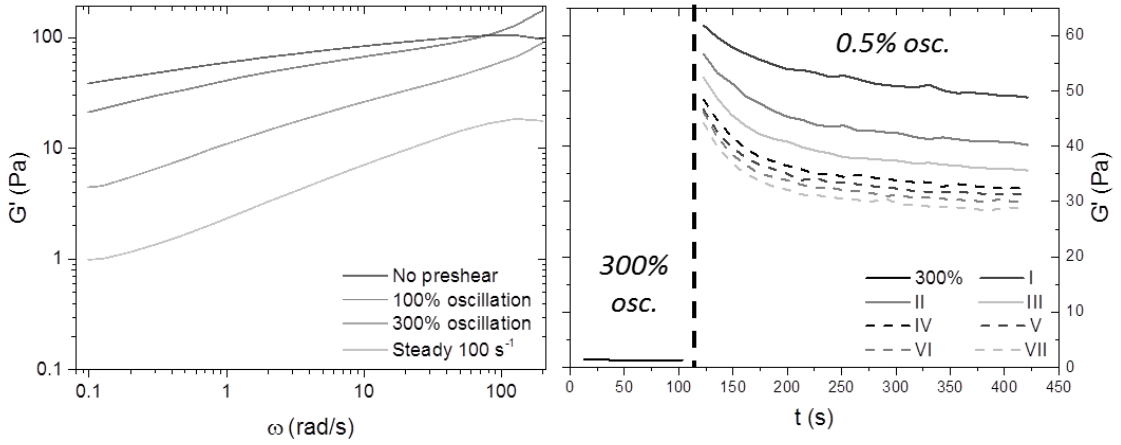

Figura 2.3 History dependence. Left: frequency dependence of G' for different pre-shearing protocols. Right: measured G' for a 300% oscillation and linear response during recovery time, for various consecutive cycles.

The arrested phase of CNC is made up by a large fraction of partially ordered, tightly packed N* domains (which however cannot be singularly resolved). Therefore, a possible contribution to the elasticity of the phase may come from networks of defects between neighbouring domains. Indeed, a significant interplay between defects and shear properties has been reported for LC polymers like PBLG and Hydroxypropyl Cellulose (Echeverria *et al.*, 2015) and in thermotropic LCs (Ramos *et al.*, 2002).

To get better insight into CNC arrangement and response, we placed the high c_{CNC} sample in a microscope shear cell and observed it during different applied deformations. Polarized microscopy allows to highlight the extent and spatial distribution of birefringent, i.e. aligned, regions. We chose a low magnification to access a large portion of the sample, at the expenses of spatial resolution. Furthermore, since the response of the sample is rather uniform across the field of view, to estimate the effect of deformations on the overall degree of alignment we extracted from each image the average intensity I_T of light transmitted through the crossed polarizers. I_T would be expected to be nearly zero for a quiescent isotropic sample (or for a set of perfectly disordered domains). This is clearly not the case for our sample, which shows a significant birefringence in the gel phase (see f**igure 2.1**), possibly resulting from domains sheared and aligned upon cell loading, and from structuring at substrates. In any case, the relative variation of I_T can provide a meaningful estimate of sample alignment evolution.

We subjected CNC to oscillatory deformations at various amplitudes, ranging from linear to strongly non-linear regimes. Because the system is not a simple dispersion of independent rods but rather it is composed by jammed N* domains, the optical response to deformation is a complex phenomenon, resulting from the combination of mechanical resistance and yielding, tendency to align along the shear direction, and ongoing relaxation phenomena. This non-trivial behaviour can be appreciated in the inset of **figure 2.4**, which shows the transmitted intensity at start-up for a 300% oscillation. However, we are here interested in the resulting effect of deformations on the time scale of seconds to minutes relevant for rheology experiments; therefore, we average I_T over the oscillation period.

In **figure 2.4**, we report the time evolution of the averaged I_T during and after the applied deformation for different amplitudes. Oscillations with amplitudes in the linear regime and amplitudes slightly below yield strain *reduce* the overall intensity, which we can attribute to partial relaxation of previous, "frozen" alignment. Instead, for amplitudes at yield strain and above, during the application of oscillations I_T grows and reaches a plateau within few seconds, corresponding to fluidization of the sample and further alignment of N* regions, which partially relaxes after stopping the oscillation. Small oscillations bring the sample to a lower degree of order and only slightly affect the defect network; large oscillations increase the overall alignment and push the sample towards a well-aligned, thermodynamically stable N* phase, which however has weaker elastic component.

When looking for an appropriate pre-shear protocol for complex anisotropic samples like CNC at high concentration, one should thus consider what kind of material and what kind of phase - stable or metastable, isotropic or anisotropic - has to be measured. Reproducibility of linear tests may not be enough to ensure that the system is not affected by the shear itself. For the gel phase of CNC, our measurements suggest that oscillations with amplitude around the yield strain may provide the best compromise between fluidization and imposed alignment.

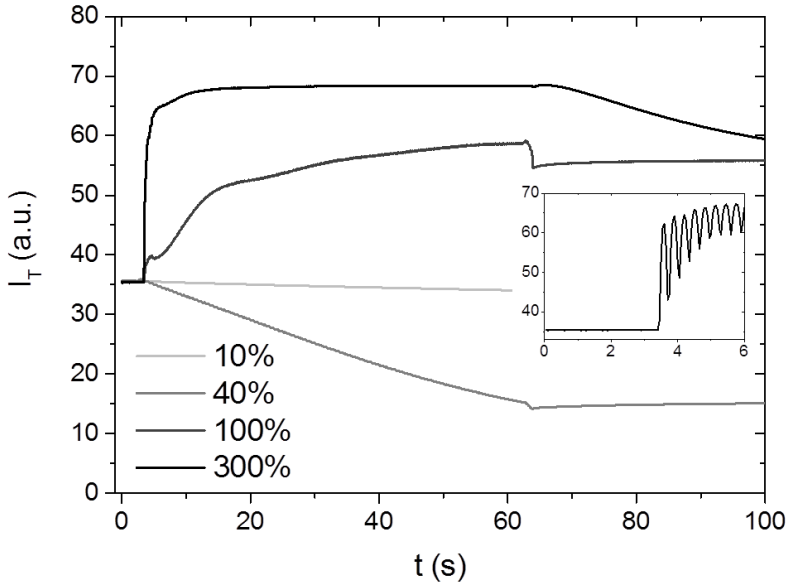

Figure 2.4 Transmitted intensity IT through crossed polarizers for CNC at 5.9 %, during oscillations at different amplitudes and after cessation. IT is averaged over each oscillation period. Inset: non-averaged IT for the start-up at 300 %.

Conclusions

We combined rheological measurements and microscopy observations under shear to characterize the N* and gel phases of CNC dispersion. In particular, we investigated the correlation between the degree of alignment and the elasticity of the phase. We found that large and fast deformations, typically applied in colloidal gels to rejuvenate the samples, in CNC anisotropic phases promote sample alignment which in turn lowers its mechanical properties. In such situations, optical access to the sheared textures can prove extremely beneficial to establish reliable protocols.

Acknoledgments

I acknowledge the kind gift of CNC samples from Doron Kam (Hebrew University of Jerusalem), and Giuliano Zanchetta (Dept. of Medical Biotechnology and Translational Medicine, UNIMI) for performing optical and rheo-optical analysis.

References

Abraham E., Kam D., Nevo Y., Slattegard R., Rivkin A., Lapidot S., Shoseyov O., 2016, Highly Modified Cellulose Nanocrystals and Formation of EpoxyNanocrystalline Cellulose (CNC) Nanocomposites, ACS Appl. Mater. Interfaces, 8, 28086-28095.

Bondeson D., Mathew A., Oksman K., 2006, Optimization of the Isolation of Nanocrystals from Microcrystalline Cellulose by Acid Hydrolysis, Cellulose, 13, 171-180.

Cunha A. G., Mougel J.-B., Cathala B., Berglund L., Capron I., 2014, Preparation of double Pickering emulsions stabilized by chemically tailored nanocelluloses, Langmuir, 30, 9327-9335.

Echeverria C., Almeida P. L., Feioa G., Figueirinhas J. L., Rey A. D., Godinho M. H., 2015, Rheo-NMR study of water-based cellulose liquid crystal system at high shear rates, Polymer, 65, 18-25.

Gómez C. H., Serpa A., Velásquez-Cock J., Gañán P., Castro C., Vélez L., Zuluaga R., 2016, Vegetable nanocellulose in food science: A review, Food Hydrocolloids, 57, 178-186.

Gonçalves A. P. B., Cruz A. M. F., de Sales J. C., Souza M. C., da Silva F. L. B. M, Guimarães F. L. B. M, Mattedia S., José N. M., 2016, Achievement and Characterization of Cellulose Nanowhiskers of Palm (Elaeis Guineensis) and Bromelia Fibers (Neoglaziovia Variegate), Chemical Engineering Transactions, 50, 403-408.

Klemm D., Kramer F., Moritz S., Lindström T., Ankerfors M., Gray D., Dorris A., 2011, Nanocelluloses: A New Family of Nature-Based Materials, Angew. Chem. Int. Ed., 50, 5438-5466.

Lagerwall J. P. F., Schütz C., Salajkova M., Noh J., Park J. H., Scalia G., Bergström L., 2014, Cellulose nanocrystal-based materials: from liquid crystal self-assembly and glass formation to multifunctional thin films, NPG Asia Materials, 6, e80.

Portela I., González Alriols M., Labidi J., Llano-Ponte R., 2015, Cellulose Nanofibers from Recycled Cellulose Pulp, Chemical Engineering Transactions, 45, 937-942.

Ramos L., Zapotocky M., Lubensky T. C., Weitz D. A., 2002, Rheology of defect networks in cholesteric liquid crystals, Phys. Rev. E, 66, 031711.

Topic 2

SELF-ASSEMBLED MATERIALS: BIOLOGICAL STRUCTURES

Biological materials have capabilities that are far beyond of those of man-made ones with similar phase composition (Carlson *et al.*, 2005; Srinivasan *et al.*, 1991). As proof of this, some of nature-made materials are still widely used for industrial manufacturing (i.e. natural fibers for textile fabrication) and biologically made structures inspire the synthesis of novel materials with advantages characteristic of biological systems (i.e. honeycomb, gecko adhesive system) (Aizenberg & Fratzl, 2009). Moreover, synthetic materials are generally processed in harsh conditions conversely to ambient conditions used by nature, and the fabrication of biologically derived materials produces lower amounts of waste and pollution, where the result is mostly biodegradable or recyclable (Meyers *et al*., 2008).

The capabilities performed by biological structures can be outstanding considering the weak constituents from which they are assembled. But it should be considered that evolution was the occasion for nature to 'experiment' with various solutions to its challenges and has improved the successful ones (Bar-Cohen, 2005). The main strategies exploited by natural materials include hierarchy, multifunctionality, self-organization, and self-healing capability (Meyers *et al*., 2008). Functionality is directly dependent on the material architecture at different multiscale levels. The majority of biological creatures are constituted by cell-based structure, which offers the ability to grow with fault-tolerance and self-repair, while performing all of the physiological functions. The use of materials that perform multiple tasks allows nature to use more effectively resources.
At a macromolecular level, composite materials that consist of fibers bonded by a matrix are widely diffused in animals and plants. The combination of fiber and matrix provides great stiffness, flexibility and low weight of the constructed structure. These properties of composite materials made them very attractive and they are now widely used in commercial parts and structures (Bar-Cohen, 2005).

One of the most important structural elements in vegetal materials is represented by the cell wall, which was many important functions in a cell including mechanical support and molecules transport government (Cosgrove, 2005). In this chapter, the behaviour of cell wall materials (CWM) extracted from vegetal products will be investigated in view of their utilization as multifunctional food ingredients.

CWM

The use in food formulations of single biopolymers extracted from plant cell walls is recognised since long: in particular several groups of these polymers are found to play a role as food thickeners, stabilizers, and emulsifiers.
In recent years a new approach based on solvent extraction from vegetal sources has allowed to obtain a new family of multicomposite ingredients, which maintain the intrinsic supramulecular organization. Cell wall materials can be described as a self-assembled network of cellulose microfibers embedded in a matrix of pectin and hemicellulose and this particular organization imparts them peculiar technological performances, other than a recognized nutritional role (Kunzek *et al*., 2002; Torres *et al.*, 2009).

The cell walls of higher plants are multicomposite materials consisting of cellulose macrofibrils, which provides the structural girders, imbibed in a hydrated matrix of non-cellulosic polysaccharides (i.e. pectins and hemicelluloses), polyphenols (i.e. lignin), and structural glycoproteins (i.e. extensin) (Hansen *et al*., 2011; Foster, 2011). Recently NMR techniques (Dick-Perez *et al*, 2011) permitted the study of these materials in native environments. This new

analytical approach highlighted the important role of proteins for the structural function, and determined the review of the two-network paradigm, highlighting how structural function of plant cell walls is accomplished by all three types of polysaccharides. The complexity of spatial organization of wall components is the results of years of evolution and optimization by nature in order to reply to specific necessities of living beings, and is credited to be at the root of the physiological multifunctionality of the cell wall. Indeed Cell wall is the structure designated to perform a multiplicity of physiological tasks contextually, from regulating shape, to contrasting cellular turgor and furnishing striking mechanical properties, beyond its fundamental role in cell growth and diversification (Cosgrove, 2005).

Until now, most of scientific knowledge concerns the rheological behaviour of plant cell wall water suspensions (Hansen *et al.*, 2011; Roversi *et al.*, 2016), intended for use as structuring materials in manufactured products. Concentrated dispersions of cell-wall materials were found to behave as colloidal dispersions of irregular deformable particles, and always showed dominant elastic properties (Day *et al.*, 2010) along with a complete reversible stress softening. Besides, plant cell walls are ideal candidates as swelling and thickening agents of many formulated foods due to their natural affinity to water (Harris & Smith, 2006; Roversi & Piazza, 2016). Recent studies have started to investigate the emulsifying properties of cell wall extracted from vegetal sources, but we are yet far from understand the mechanism underlying such functionality. There is still some debate about whether their ability to form stable emulsions is primarily due to their surface activity (Leroux *et al.*, 2003) or the ability to thicken the aqueous phase (Wellcan *et al.*, 2015; Dickson, 2003). On the contrary, little attention has been paid to the possibility to release small molecules from CWM. At the present, most of the research attention is focussed on the release of micronutrients naturally associated with fruit and vegetables, and how the presence of structured polysaccharides affects their bioaccessibilty (Bot *et al.*, 2018; Lemmens *et al*., 2014). But the potential exploitation of cell walls powders as delivery systems that carry, protect, and deliver encapsulated bioactive compounds to their specific site remains an unexplored field. Since stability and availability of sensitive nutrients are affected by the conditions encountered during the entire food production chain up to the moment of consumption and digestive conditions (Zandi, 2017), the hollow architecture of CWM might be an excellent alternative strategy to increase the stability and limit the degradation of such compounds acting as hydrogel-based delivery devices.

Aizenberg, J., & Fratzl, P. (2009). Biological and biomimetic materials. *Advanced Materials*, 21(4), 387-388.
Bar-Cohen, Y. (2005) Biomimetics: biologically inspired technologies. CRC Press.

Bot, F., Verkerk, R., Mastwijk, H., Anese, M., Fogliano, V., & Capuano, E. (2018). The effect of pulsed electric fields on carotenoids bioaccessibility: The role of tomato matrix. *Food Chemistry*, 240, 415-421.

Carlson, J., Ghaey, S., Moran, S., Tran, C. A., & Kaplan, D. L. (2005). Biological materials in engineering mechanisms. *Biomimetics: Biologically Inspired Technologies*, 365-380.

Cosgrove, D. J. (2005). Growth of the plant cell wall. *Nature reviews molecular cell biology*, 6(11), 850.

Day, L., Xu, M., Øiseth, S. K., Lundin, L., & Hemar, Y. (2010). Dynamic rheological properties of plant cell-wall particle dispersions. *Colloids and Surfaces B: Biointerfaces*, 81(2), 461-467.

Dickinson, E. (2003). Hydrocolloids at interfaces and the influence on the properties of dispersed systems. *Food hydrocolloids*, 17(1), 25-39.

Dick-Pérez, M., Zhang, Y., Hayes, J., Salazar, A., Zabotina, O. A., & Hong, M. (2011). Structure and interactions of plant cell-wall polysaccharides by two-and three-dimensional magic-angle-spinning solid-state NMR. *Biochemistry*, 50(6), 989-1000.

Foster, T. J. (2011). Natural structuring with cell wall materials. *Food hydrocolloids*, 25(8), 1828-1832.

Hansen, S. L., Ray, P. M., Karlsson, A. O., Jørgensen, B., Borkhardt, B., Petersen, B. L., & Ulvskov, P. (2010). Mechanical properties of plant cell walls probed by relaxation spectra. *Plant Physiology*, pp-110.

Harris, P. J., & Smith, B. G. (2006). Plant cell walls and cell-wall polysaccharides: structures, properties and uses in food products. *International journal of food science & technology*, 41, 129-143.

Kunzek, H., Müller, S., Vetter, S., & Godeck, R. (2002). The significance of physico chemical properties of plant cell wall materials for the development of innovative food products. *European Food Research and Technology*, 214(5), 361-376.

Lemmens, L., Colle, I., Van Buggenhout, S., Palmero, P., Van Loey, A., & Hendrickx, M. (2014). Carotenoid bioaccessibility in fruit-and vegetable-based food products as affected by product (micro) structural characteristics and the presence of lipids: A review. *Trends in Food Science & Technology*, 38(2), 125-135.

Leroux, J., Langendorff, V., Schick, G., Vaishnav, V., & Mazoyer, J. (2003). Emulsion stabilizing properties of pectin. *Food Hydrocolloids*, 17(4), 455-462.

Meyers, M. A., Chen, P. Y., Lin, A. Y. M., & Seki, Y. (2008). Biological materials: structure and mechanical properties. *Progress in Materials Science*, 53(1), 1-206.

Roversi, T., & Piazza, L. (2016). Supramolecular assemblies from plant cell polysaccharides: Self-healing and aging behavior. *Food Hydrocolloids*, 54, 189-195.

Srinivasan, A. V., Haritos, G. K., & Hedberg, F. L. (1991). Biomimetics: Advancing man-made materials through guidance from nature. *Applied Mechanics Reviews*, 44(11), 463-482.

Torres, F. G., Troncoso, O. P., Lopez, D., Grande, C., & Gomez, C. M. (2009). Reversible stress softening and stress recovery of cellulose networks. *Soft Matter*, 5(21), 4185-4190.

Wallecan, J., McCrae, C., Debon, S. J. J., Dong, J., & Mazoyer, J. (2015). Emulsifying and stabilizing properties of functionalized orange pulp fibers. *Food Hydrocolloids*, 47, 115-123.

Zandi, M. (2017). Evaluation of the Kinetics of Ascorbic Acid (AA) Release from Alginate-Whey Protein Concentrates (AL-WPC) Microspheres at the Simulated Gastro–Intestinal Condition. *Journal of Food Process Engineering*, 40(1), e12334.

Experiment 3:

Plant-derived supramolecular aggregates, intended as carrier of bioactive compounds: Kinetic study of release mechanisms

The past decade has seen the rapid development of functional foods through the addition of bioactive compounds, due to their potential health benefits to humans, but this approach still holds many technological challenges. The encapsulation of nutraceutical and functional food components in appropriate edible delivery systems was is an advantageous strategy to protect these molecules from food processing, adverse environmental conditions, and digestion (McClements *et al.*, 2009; Fang, & Bhandari, 2010). Furthermore, the presence of a physical barrier slowing down molecules migration allows to control the release kinetic, optimizing both the extent and the rate of absorption in the body (Faulks & Southon, 2008). Conventionally, encapsulation technology is focused on vesicular and particulate systems, which require specific technologies to produce the desired architectures able to effectively encapsulate and protect bioactive compounds.

The hollow shape of CWM represents a suitable location for the entrapment of bioactive molecules through precipitation reactions. In addition, CWM can be considered a hydrogel-based material with swelling properties (Roversi & Piazza, 2016), and understanding the mechanism driving the matrix behavior in aqueous media can be useful to control the migration of bioactives through the wall layer. This study aims at evaluating the ability of supramolecular plant-derived assembles (i.e. CWM) to retain a water-soluble model compound with low molecular weight (fluorescein) and to identify the release mechanisms through this matrix at different pH and ionic strength conditions, in an effort to reproduce the digestive environments. The mathematical modelling of experimental data provides a useful tool to gain insight into the transport mechanisms involved.

3.1 Materials and methods

Fresh-cut rocket salad, *Eruca sativa*, (Bonduelle, Italy) was purchased at a local market in Milano (Italy) and stored at 4 °C prior to processing. Tracing dyes, sodium fluorescein salt and methylene blue, and all chemicals were supplied by Sigma-Aldrich (Germany). Simulated fluids consisted of an aqueous solution of 0.125 M NaCl, 0.045 M $NaHCO_3$, 0.007 M KCl (Pizzolitto *et al.*, 2012) characterized by a different pH, corresponding to 2 and 7 for simulated gastric (SGF) and intestinal (SIF) fluids respectively.

3.1.1 CWM preparation

Cell wall material was obtained according to the procedure described by Roversi *et al*. (2016). Briefly, salad leaves were boiled in 95% (v/v) ethanol for 30 min to inactivate potential wall-modifying enzymes. After the homogenization at top speed in a Polytron (Brinkam Instruments) for 1 min, the dispersion was filtered under pressure with Glass Microfiber Filters (Whatman), pore size 125 μm. The resulting pellets were washed with a methanol-chloroform solution (1:1) until their complete discoloration. In the end, cell walls underwent acetone washing to remove loosely associated water. Final samples were dried at room temperature overnight, and particles with a diameter between 125 and 250 μm, corresponding to small clusters of cells (Day *et al.*, 2010), were selected by sieving.

Sodium fluorescein and methylene blue were selected as model molecules to easily trace the release behaviour during the kinetic study. According to the procedure proposed by Paunov and his group (2007), 0.5 g of CWM was poured into 60 ml of alcoholic solution of methylene blue (0.46 g/100 ml) for two hours. The imbibed material was filtered under pressure with Glass Microfiber Filters (Whatman) washing with water until removing the excess of dye. Subsequently, the CWM was deepened into 60 ml of aqueous solution of sodium fluorescein (0.46 g/100 ml), which interacts with the methylene blue leading to the formation of a less soluble complex. The reduced solubility of the product compound was exploited to load particles. CWM particles were filtered as previously described for methylene blue and washed exceeding water to remove every excess of free fluorescein. The amount of adsorbed fluorescein was quantified by subtracting the amount of fluorescein contained into the water used for the washing operations to the amount of fluorescein of the initial loading solution.

3.3.2 Release kinetic study

The release studies were conducted in sink conditions, dispersing 0.2 g of CWM, loaded with the ionic dye complex, in 50 ml of dissolution medium under stirring. Deionized water or simulated digestive fluids were used for the release experiments. Aliquots (0.2 ml) were periodically withdrawn from the dissolution medium and the concentration of fluorescein was quantified using a UV-VIS spectrophotometer (Jasco V-650, Japan). The wavelength of maximal absorbance considered varied as a function of pH and was equal to 491, 440, 495 nm in water, SGF and SIF respectively. The results are expressed as relative release (*RR%*) or fractional release (*f*):

$$RR\% = \frac{M_t}{M_{CWM}} \qquad \text{(eq. 3.1)}$$

$$f = \frac{M_t}{M_\infty} \qquad \text{(eq. 3.2)}$$

where M_t is the amount of fluorescein release at time *t*, M_{CWM} the amount of fluorescein loaded in CWM, and M_∞ is the amount of fluorescein released at the equilibrium (after 24 hours).

3.2.3 Mathematical analysis

In order to study the transport mechanisms of fluorescein from CWM, empirical and semi-empirical models were considered to fit the experimental data obtained from kinetic release studies.

The zero-order model describes a linear release profile, as clear from the following equation:

$$f = k_0 t \quad \text{(eq. 3.3)}$$

where k_0 is the kinetic dissolution constant. In this case the release rate is constant all over the investigated period of time. Thus, the amount of released agent is only function of time, and not of the solute concentration.

In typical first-order kinetics, the release is proportional to the amount of the bioactive remaining into the interior. The linearized equation is expressed as:

$$\log M_t = \log M_0 + \frac{k_1 t}{2.303} \quad \text{(eq. 3.4)}$$

where M_0 is the initial amount of bioactive in the solution and k_1 is the first-order constant.

Higuchi model is the most commonly used equation to describe solutes dissolution from solid matrix systems, driven by Fickian diffusion. Baker and Lonsdale (1974) adjusted Higuchi function with the aim of modelling release specifically from spherical matrices. The equation is linearized as follows:

$$\frac{3}{2}\left[1 - (1-f)^{2/3}\right] - f = kt \quad \text{(eq. 3.5)}$$

where k is the release constant.

Weibull equation is a distribution function, and represents another descriptive model. The equation is expressed in terms of bioactive fraction accumulated in the solution at time t:

$$f = 1 - \exp\left[\frac{(-kt)^b}{a}\right] \quad \text{(eq. 3.6)}$$

where the scale parameter a defines the time scale of the process, while the shape parameter b describes the different curve shapes (Costa & Sousa Lobo, 2001).

Korsmeyer and Peppas model is a semi-empirical power law equation, and it is a useful tool for the study of release kinetics from polymeric system when the release mechanism is not known or when more than one type of phenomenon is involved. The equation establishes an exponential relationship between the fractal release and the time:

$$f = kt^n \quad \text{(eq. 3.7)}$$

where k is the release velocity constant and n is the exponent related to the release mechanism (Korsmeyer & Peppas, 1981).

Since diffusion and relaxation of polymeric chains can be considered as additives mechanism (Alfrey *et al.*, 1966), Peppas and Sahlin (1989) developed a release kinetic model constituted by the sum of two power laws:

$$f = K_D t^m + K_R t^{2m} \quad \text{(eq. 3.8)}$$

In this equation, K_D is the release kinetic constant for diffusion, K_R is the release kinetic constant for polymers relaxation, and m is a constant coefficient.

The diffusion coefficients, D_E and D_L, were calculated using the early-time (**eq. 3.9**) and late-time (**eq. 3.10**) approximation equations, respectively, obtained when solving Fick's second law under initial and boundary conditions (Fu & Kao, 2010; Crank 1979). The early-time approximation is defined as follows:

$$\frac{M_t}{M_{CWM}} = 6\left(\frac{Dt}{\pi\delta^2}\right)^2 \quad \text{(eq. 3.9)}$$

where M_t is the amount of the bioactive released at time t, M_{CWM} is the total mass of bioactive loaded into the particle, D is the diffusion coefficient of the bioactive within the cell wall matrix, and δ is the diffusional distance. This approximation holds for the release of the first 60% of the

cumulative release. The late approximation, which holds for the final portion of the drug release (*i.e.* $0.4 \leq Mt/MCWM \leq 1$), is described by the following equation:

$$\frac{M_t}{M_{CWM}} = 1 - \left(\frac{6}{\pi^2}\right) exp[(-\pi^2 Dt)/\delta^2] \qquad \text{(eq. 3.10)}$$

3.2 Results and Discussion

3.2.1 Release of fluorescein from cellulose as model system

CWM was loaded with the product of the ionic reaction of two oppositely charged dyes (methylene blue and fluorescein sodium salt) in order to monitor the release process. The loading procedure, set up according to the indications of Paunov *et al*. (2007), determined a final amount of adsorbed fluorescein equal to 0.16 g for each gram of CWM. The effective incorporation of the two dyes was also confirmed by means of optical microscopy, as shown in **figure 3.1**.

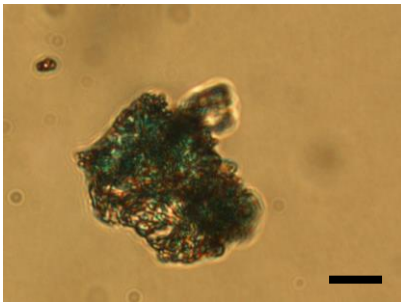

Figure 3.1 Image of CWM loaded with the ionic product of the reaction between methylene blue and fluorescein sodium salt, obtained by optical microscopy (40x). Size bar = 20 µm.

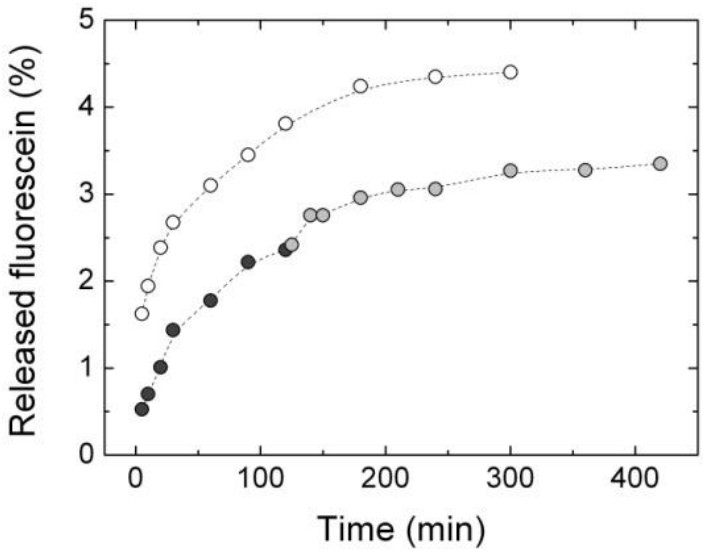

Figure 3.2 Release profile of fluorescein from CWM in water (hollow circle), and simulated digestive fluids (black and grey circles for SGF and SIF respectively).

The release behavior of the samples obtained was investigated at different *in vitro* conditions. At first the release kinetic was performed in deionized water for 5 hours to understand the behavior in pure solvent. Further, the release profile was carried out in simulated gastric and intestinal fluids (SGF and SIF respectively) to investigate the influence of pH and of the presence of the ionic force, simulating the digestive process conditions. The release profile of fluorescein from CWM in water and in simulated fluids, expressed as relative amount of released fluorescein

(*RR%*), as a function of time is showed in **figure 3.2**. From the graph it can be seen that the three curves reached an equilibrium value at a different time, reported in **table 3.1**. This parameter (t_∞), which represents the time required by the delivery system to reach the plateau value of released fluorescein (*RR%*), is useful to predict whether the release is sustained for a long time. In the case of water, the equilibrium is reached after about 120 min, while the curve obtained in SIF got a plateau value in about 90 min. On the contrary, a release equilibrium is never reached during the time of analysis, such behavior is confirmed also by the equilibrium value (after 24 hours). For this reason, the amount of released fluorescein at t = 24 hours, reported in **table 3.1**, was considered as the equilibrium value and used to compare the release processes in different conditions.

Table 3.1 Equilibrium parameter related to the release kinetic of fluorescein in different medium conditions.

	Water	**SGF**	**SIF**
t_{eq} *(min)*	120	-	90
RR_{eq} *(%)*	4.57	2.69	1.09

The material displayed a maximum release corresponding to the 4.37% of the entrapped fluorescein in water, and to 3.36% after the complete simulated digestion *in vitro*. The relative release at equilibrium was equal to 2.69% in SGF, and to 1.09% if we consider only the contribution of the release in SIF. The different portion of released fluorescein at the same time (24 hours) can partially be explained by a reduced solubility of fluorescein as a function of pH, which shows a minimum value between pH 3 and 4 (Diehl & Markuszewski, 1985). However, the solubility limitation is not sufficient to justify the different shape of the curve, as follows from **figure 3.3**.

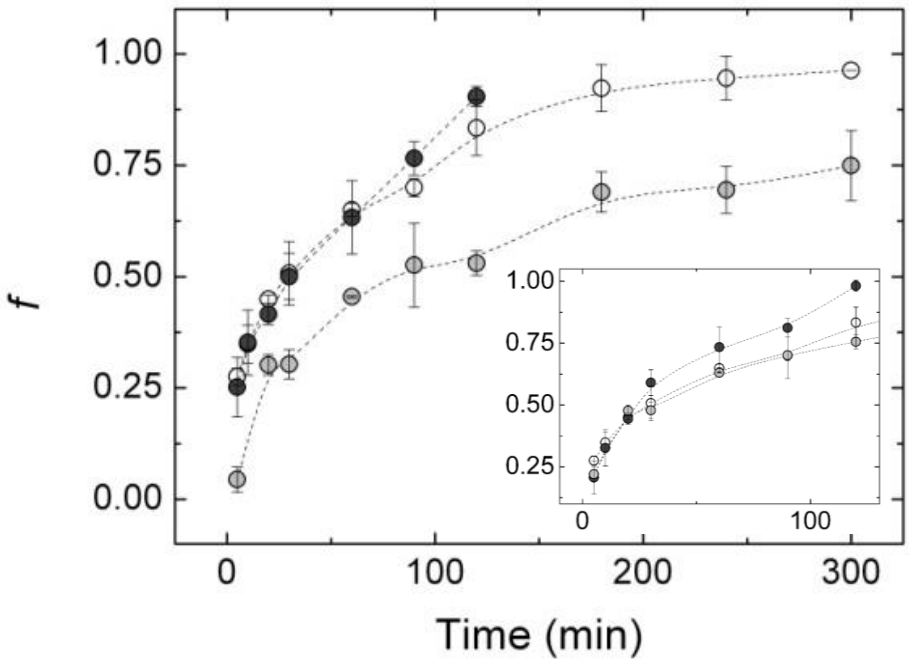

Figure 3.3 Fractional amount of fluorescein released in time from CWM in water (hollow circle), and simulated digestive fluids (black and grey circles for SGF and SIF respectively). Inset: Fractional release of fluorescein from CWM. The curves obtained in SGF (black circles) and SIF (grey circles) are vertically translated (+0.19 for SGF and +0.37 for SIF) in order to overlap the release kinetic obtained in water (hollow circles).

In the graph, the amount of released fluorescein normalized for the equilibrium value, *RReq*, is plotted as a function of the time. It should be evidenced that the release curve in SIF is reported after subtracting the final value of the kinetic in SGF. The **inset** of **figure 3.3** displays a focus of fluorescein release until 2 hours, where the release curve in SIF was vertically shifted until superposition with the release curve in water, with the aim to emphasize the similar shape with the one in water. Conversely, the release profile in SGF deviates immediately from the trend of the other two curves. As well-known from the literature (Crank, 1979), the type of curve of mass transport phenomena is strictly correlated with the mechanism involved in the process. The analysis of their shapes offers a useful tool to investigate which are the driving forces involved.

3.2.2 Mathematical modelling of the transport mechanism from CWM: empirical models

The mathematical modeling of experimental data provides a useful approach for the study of mass transport mechanism involved in the release phenomena, beyond allowing the prediction of the release behavior of the system. According to the literature (Crank, 1979; Peppas & Khare, 1993), the release process from hydrogel systems can be governed by diffusional phenomena, polymeric chain relaxation (case-II transport), or a combination of the two processes. In this section, empirical models were used to describe the release profile: each kinetic model refers to a different mechanism, and the determination of the best model was based on the comparison of the adjusted R^2 (adj-R^2), which express the goodness of fit. The fitting values of the most important parameters related to curves shape and kinetic are reported in **table 3.2**.

The zero-order kinetic model (**eq. 3.3**) describes a release process at a constant rate, independent on the encapsulated compound concentration, that corresponds to the case-II transport (Costa & Sousa Lobo, 2003). In this case the mechanism driving release is swelling or macromolecular relaxation of polymeric chains. None of the release profiles in **figure 3.3** has a linear trend, as highlighted by the adj-R^2 reported in **table 3.2**. Even, the fitting of the release curves according to the zero-order model display a regression coefficient lower than 0.80 in water and SIF. It means that CWM do not perform a sustained release over time but two stages (burst and slow release) can be identified in the process as already observed for more simple systems (Zandi, 2017).

The first-order model (**eq. 3.4**) describes a release process proportional to the amount of residual active agent in its interior. It is generally applied to soluble compounds incorporated in a porous matrix (Mulye & Turco, 2005; Fu & Kao, 2005), even though, it is difficult to conceptualise the driving mechanism in a theoretical basis. In our case, only the experimental release profile in SIF showed a good correspondence with the fitted function **eq. 3.4**, with a R^2 equal to 0.98. Instead R^2 displayed a value lower than 0.95 for the two other media, as reported in **table 3.2**. These results suggest that the release of fluorescein from CWM occurred with an initial burst-release phenomenon solely in simulated intestinal conditions (Zandi, 2017).

Higuchi's model is one of the most used mathematical equation to describe the release profile from planar geometries, and describes release process governed by Fickian diffusion. In our case, Baker-Lonsdale modification of Higuchi model (**eq. 3.5**) for a spherical geometry was considered, simplifying the system to spherical particles (Lopez-Sanchez *et al*., 2012). The correlation coefficients were higher than 0.98 for release kinetics performed in water and SIF, while a significant lower value was obtained for release in simulated gastric conditions. For this latter case, we can deduce that Fickian diffusion cannot be assumed to be the exclusive mechanism at the basis of the release behavior.

A better insight in release mechanism can be gained by studying the shape of the release profiles through the Weibull's model (**eq. 3.6**). It is a distribution function used to describe the phenomena and processes associated to a finite time. It has been demonstrated that the stretched exponential functional form arises due to the creation of a concentration gradient near the releasing boundaries (Kosmidis *et al*, 2003). The equation is an empirical model with no kinetic fundament, but it is really useful to describe the trend of the curves, which is classified according to the value of its exponential parameter (*b*). The fitting of the release profile in water ($b = 0.76$) indicates that the curve a parabolic shape, displaying high initial slope and a consistent exponential character ([B]ruschi, 2015). A similar result was determined for the release of fluorescein in SIF. On the contrary, the exponent value *b* reached a value of 1.15 in simulated gastric conditions, indicative of a sigmoid with a single point of inflection. This shape rules out trends typical for Fickian diffusion and indicates a complex mechanism driving the release process (Papadopoulou *et al.*, 2006, Macheras & Iliadis, 2016).

Table 3.2 Estimated kinetic parameters and R^2 values obtained from fitting release experimental data to empirical models.

		Water	**SGF**	**SIF**
Zero-order	k_0 (min^{-1})	$8.27 \cdot 10^3$	$15.87 \cdot 10^3$	$2.54 \cdot 10^3$
	R^2	0.797	0.910	0.783
First-order	k_1 (min^{-1})	$1.29 \cdot 10^{3}$	$5.16 \cdot 10^3$	0.45
	R^2	0.953	0.954	0.987
Baker-Lonsdale	k (min^{-1})	$8.12 \cdot 10^3$	$5.35 \cdot 10^3$	$1.17 \cdot 10^3$
	R^2	0.997	0.975	0.983
Weibull	d	0.77	1.15	0.31
	R^2	0.991	0.984	0.977

3.2.3 Mathematical modelling of the transport mechanism from CWM: semi-empirical models

Empirical models applied in the previous section are useful tools to predict the release behavior of the system but were not suitable to properly discriminate the mechanism driving fluorescein release. The use of semi-empirical models allowed to recognize the molecular mechanisms regulating the release kinetics.

Kormeyer-Peppas model (**eq. 3.7**) was used to fit experimental data with the objective of identifying the prevalent release mechanism. The shape of the release curve is described through the exponent parameter *n*, and the critical values are strongly affected by the geometrical features (Peppas & Sahlin, 1989). In our case, assuming a spherical shape for CWM particles (Lopez-Sanchez *et al.*, 2013), we can infer that the release is governed by Fickian diffusion when $n = 0.43$, while the case-II transport corresponds to a *n* value equal to 0.8 and is characterized by rearrangement of polymeric chains. An exponent parameter value between the reported extreme values ($0.43 < n < 0.85$) indicates an anomalous transport, given by the coexistence of both Fickian diffusion and case-II transport phenomena. The latter case was identified for the release profile in SGF, when *n* was calculated to be 0.56. Conversely, the fitting of release curves in both water and SIF determined an exponent value lower than 0.43 (0.34 and 0.30 respectively). Similar values ($0.30 < n < 0.43$), were found in different studies with biopolymeric systems, indicating a prevalence of Fickian diffusion, and such low values were justified by the polydispersity of systems and the heterogeneity of the gel layer (Ritger & Peppas, 1987; Saurì *et al.*, 2014). These

findings are coherent with the complexity of cell wall material structure, in terms of both composition and geometry. Thus, we can conclude that the release mechanism is mainly controlled by Fickian diffusion when water and SIF are used as dissolution media. It should be highlighted that Korsemeyer-Peppas model was found to be the most appropriate to describe and predict the trend of the curve compared to the previous ones, with a R^2 value higher than 0.99 in all three conditions.

Table 3.3 Estimated kinetic parameters and R^2 values obtained from fitting release experimental data to empirical models.

		Water	**SGF**	**SIF**
Korsemeyer-Peppas	*n*	0.34	0.56	0.30
	R^2	0.990	$R^2 = 0.992$	0.990
Peppas-Sahlin	K_D	0.14	0.12	0.66
	K_D	$5.01 \cdot 10^3$	0.02	0.09
	R^2	0.991	0.990	0.972

Peppas and Sahlin (1989) proposed a power law model (**eq. 3.8**) able to quantify the approximate contribution of the two mechanisms, diffusional and relaxational, in an anomalous release process. The ratio of the two contributions during the fluorescein release is calculated as:

$$\frac{R}{F} = \frac{K_D t^m}{K_R} \qquad \text{(eq. 3.11)}$$

where K_D and K_R are constants related to the diffusional and the case-II relaxational contribution respectively. **Figure 3.4** shows the ratio of the R/F versus fractional release (*f*). As clear from the fitting with the previous models, it is confirmed that pH is the most important condition affecting fluorescein transport mechanism. Indeed, the relaxational contribution was considerable in SGF compared to the curves obtained in water and simulated intestinal conditions. At more acidic pH values, it is hypothesized that the release mechanism is influenced by macromolecular chain rearrangement resulting from the increased binding between hemicelluloses (*i.e.* glucuronoarabinoxylan, GAX, and xyloglucan) and pectins. GAX and pectin were previously reported to bind to xyloglucan in a pH-dependent manner, with a maximum binding at pH values lower than 4 (Brett *et al.*, 1997; Rizk *et al.*, 2000). In this last case, the more crosslinked hydrogel structure (higher binding density) cold be accounted for the slower release rate, as evident from the values of the release velocity constant *k* in **table 3.3**, due to the smaller mesh size of the network.

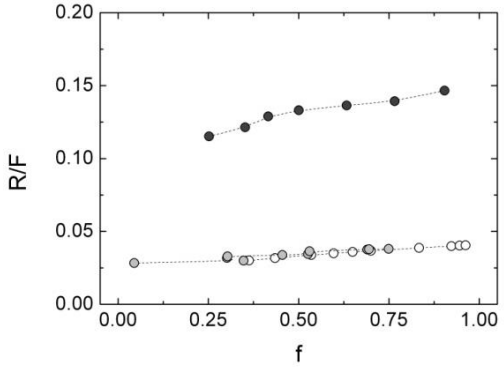

Figure 3.4 *R/F* ratio as a function of the fractional release from CWM in water (hollow circle), and simulated digestive fluids (black and grey circles for SGF and SIF respectively).

3.2.4 Mathematical modelling of the release kinetics

As discussed in the previous section paragraph (**3.2.2**) about the zero-order model, the release process is composed of two kinetic stages, at least. Thus, data obtained by the release kinetic studies were fitted to the early-time and late-time approximation equations (**eqs. 3.9** and **3.10**), and the corresponding diffusion coefficients D_E and D_L were calculated. The values reported in **table 3.4** show that diffusion coefficients obtained from late time approximation equation were always lower than those obtained from the early-time approximation equation, as expected since fluorescein release rates decreased with the release time. If we consider the release kinetic in water, it displayed the highest value among diffusion coefficients approximated for the early-time, about 10^{-8} cm^2/s, but the lowest value for the diffusion coefficient approximated for the late-time. Diffusion coefficient obtained from release experiments in SGF display an opposite trend. The different behavior can be ascribed to the tendency of the release process to get the equilibrium condition in water. It is translated in amore sustained release in simulated gastric fluid, and these findings are confirmed by the higher value of adj-R^2 of the zero-order model for SGF. In addition, the lower D_E values indicative of a lower mobility of the solute through the matrix; this finding agrees with the hypothesis discussed in the previous section of a higher binding density at lower pH values.

D_L values obtained from the release profile in SIF could not be accurately calculated, as the value adj-R^2 shows, due to the abrupt initial fluorescein release.

Table 3.4 Fluorescein diffusion coefficients calculated with the early-time and late-time approximation release equations (eq. 3.9 e 3.10) for different release media.

Coefficient/Medium	Water	SGF	SIF
D_E (cm^2/s)	$1.31\ 10^{-8}$	$2.08\ 10^{-9}$	$9.34\ 10^{-10}$
R^2	0.993	0.986	0.972
D_L (cm^2/s)	$2.22\ 10^{-12}$	$3.79\ 10^{-11}$	$9.25\ 10^{-12}$
R^2	0.986	0.969	0.915

The diffusion coefficients calculated for fluorescein released in water were normalized with respect to the to the fluorescein diffusion coefficient in water solution, which has a value of $4.25\ 10^{-6}$ cm^2/s (Culbertson *et al.*, 2002). It is evident how encapsulation of fluorescein into CWM effectively decrease of its diffusion coefficient, obtaining D_E *normalized* and D_L *normalized* equal to 0.31 and $5.22\ 10^{-5}$ respectively.

Conclusions

In conclusion, mathematical modelling confirmed to be an extremely useful tool to elucidate the mechanism underlying release of a water-soluble compound, fluorescein, from plant cell wall particles. Based on our results, different behaviours were discriminated as a function of the release medium. Release from CWM in water proved to be mainly driven by Fickian diffusion; similar results were found for release process in SIF, even though Fickian diffusion was forerun by an initial burst release event.

In the case of release from CWM in SGF, the process is an anomalous transport result of the contribution of both Fickian diffusion and polymeric chains relaxation. The last phenomenon may be related to the pH-dependent ability of hemicellulose and pectins to form linkages. The higher binding density effectively reduces the mobility of the solute trough the matrix (as highlighted by the early-time diffusional coefficient). This property is also reflected in the lower relative amount of released fluorescein at the equilibrium in simulated gastric conditions.

It should be highlighted that this study represents a premise to the application of these materials in food matrices as delivery devices, but the present results suggest a good ability of CWM to retain incorporated water soluble compounds in simulated gastric conditions.

Acknoledgments

I thank Giuliano Zanchetta (Dept. of Medical Biotechnology and Translational Medicine, UNIMI) for the micrograph by optical microscopy.

References

Alfrey, T., Gurnee, E. F., & Lloyd, W. G. (1966, January). Diffusion in glassy polymers. In *Journal of Polymer Science: Polymer Symposia* (Vol. 12, No. 1, pp. 249-261). Wiley Subscription Services, Inc., A Wiley Company

Baker, R. W., & Lonsdale, H. K. (1974). Controlled release: mechanisms and release. New York, Plenum Press, 1974.

Brett, C. T., Healy, S. A., McDonald, M. S., Macgregor, C., & Baydoun, E. H. (1997). Binding of nascent glucuronoxylan to the cell walls of pea seedlings. *International journal of biological macromolecules*, 21(1-2), 169-173.

Bruschi, M. L. (2015). Mathematical models of drug release. In: *Strategies to modify the drug release from pharmaceutical systems*. Woodhead Publishing.

Costa, P., & Sousa Lobo, J. M. (2003). Evaluation of mathematical models describing drug release from estradiol transdermal systems. *Drug development and industrial pharmacy*, *29*(1), 89-97.

Crank, J. (1979). *The mathematics of diffusion*. Oxford university press.

Culbertson, C. T., Jacobson, S. C., & Ramsey, J. M. (2002). Diffusion coefficient measurements in microfluidic devices. *Talanta*, *56*(2), 365-373.

Day, L., Xu, M., Øiseth, S. K., Lundin, L., & Hemar, Y. (2010). Dynamic rheological properties of plant cell-wall particle dispersions. *Colloids and Surfaces B: Biointerfaces*, *81*(2), 461-467.

Diehl, H., & Markuszewski, R. (1985). Studies on fluorescein—II22Part I—Talanta, 1980, 27, 937.: The solubility and acid dissociation constants of fluorescein in water solution. *Talanta*, *32*(2), 159-165.

Fang, Z., & Bhandari, B. (2010). Encapsulation of polyphenols–a review. *Trends in Food Science & Technology*, 21(10), 510-523.

Faulks, R. M., & Southon, S. (2008). Assessing the bioavailability of nutraceuticals. In Garti, N. (Ed.), *Delivery and controlled release of bioactives in foods and nutraceuticals* (p. 3). Elsevier.

Fu, Y., & Kao, W. J. (2010). Drug release kinetics and transport mechanisms of non-degradable and degradable polymeric delivery systems. *Expert opinion on drug delivery*, *7*(4), 429-444.

Korsmeyer, R. W., & Peppas, N. A. (1981). Effect of the morphology of hydrophilic polymeric matrices on the diffusion and release of water soluble drugs. *Journal of Membrane Science*, *9*(3), 211-227.

Kosmidis, K., Argyrakis, P., & Macheras, P. (2003). A reappraisal of drug release laws using Monte Carlo simulations: the prevalence of the Weibull function. *Pharmaceutical research*, *20*(7), 988-995.

Lopez-Sanchez, P., Chapara, V., Schumm, S., & Farr, R. (2012). Shear elastic deformation and particle packing in plant cell dispersions. *Food biophysics*,*7*(1), 1-14.

Macheras, P., & Iliadis, A. (2016). Modeling in biopharmaceutics, pharmacokinetics and pharmacodynamics: homogeneous and heterogeneous approaches (Vol. 30). Springer.

McClements, D. J., Decker, E. A., Park, Y., & Weiss, J. (2009). Structural design principles for delivery of bioactive components in nutraceuticals and functional foods. *Critical reviews in food science and nutrition*, 49(6), 577-606.

Mulye, N. V., & Turco, S. J. (1995). A simple model based on first order kinetics to explain release of highly water soluble drugs from porous dicalcium phosphate dihydrate matrices. *Drug development and industrial pharmacy*,*21*(8), 943-953.

Papadopoulou, V., Kosmidis, K., Vlachou, M., & Macheras, P. (2006). On the use of the Weibull function for the discernment of drug release mechanisms. *International journal of pharmaceutics*, 309(1-2), 44-50.

Paunov, V. N., Mackenzie, G., & Stoyanov, S. D. (2007). Sporopollenin micro-reactors for in-situ preparation, encapsulation and targeted delivery of active components. *Journal of Materials Chemistry*, *17*(7), 609-612.

Peppas, N. A., & Khare, A. R. (1993). Preparation, structure and diffusional behavior of hydrogels in controlled release. *Advanced drug delivery reviews*,*11*(1-2), 1-35.

Peppas, N. A., & Sahlin, J. J. (1989). A simple equation for the description of solute release. III. Coupling of diffusion and relaxation. *International journal of pharmaceutics*, *57*(2), 169-172.

Pizzolitto, R. P., Armando, M. R., Combina, M., Cavaglieri, L. R., Dalcero, A. M., & Salvano, M. A. (2012). Evaluation of Saccharomyces cerevisiae strains as probiotic agent with aflatoxin B1 adsorption ability for use in poultry feedstuffs. *Journal of Environmental Science and Health, Part B*, 47(10), 933-941.

Ritger, P. L., & Peppas, N. A. (1987). A simple equation for description of solute release I. Fickian and non-Fickian release from non-swellable devices in the form of slabs, spheres, cylinders or discs. *Journal of controlled release*,*5*(1), 23-36.

Rizk, S. E., Abdel-Massih, R. M., Baydoun, E. A. H., & Brett, C. T. (2000). Protein-and pH-dependent binding of nascent pectin and glucuronoarabinoxylan to xyloglucan in pea. *Planta*, *211*(3), 423-429.

Roversi, T., Ferrante, A., & Piazza, L. (2016). Mesoscale investigation of the structural properties of unrefined cell wall materials extracted from minimally processed salads during storage. *Journal of Food Engineering*, 168, 191-198.

Roversi, T., & Piazza, L. (2016). Changes in minimally processed apple tissue with storage time and temperature: mechanical–acoustic analysis and rheological investigation. *European Food Research and Technology*, 242(3), 421-429.

Saurí, J., Millán, D., Suñé-Negre, J. M., Colom, H., Ticó, J. R., Miñarro, M., ... & García-Montoya, E. (2014). Quality by design approach to understand the physicochemical phenomena involved in controlled release of captopril SR matrix tablets. *International journal of pharmaceutics*, *477*(1), 431-441.

Zandi, M. (2017). Evaluation of the Kinetics of Ascorbic Acid (AA) Release from Alginate-Whey Protein Concentrates (AL-WPC) Microspheres at the Simulated Gastro–Intestinal Condition. *Journal of Food Process Engineering*, *40*(1).

Brett, C. T., Healy, S. A., McDonald, M. S., Macgregor, C., & Baydoun, E. H. (1997). Binding of nascent glucuronoxylan to the cell walls of pea seedlings. *International journal of biological macromolecules*, 21(1-2), 169-173.

Rizk, S. E., Abdel-Massih, R. M., Baydoun, E. A. H., & Brett, C. T. (2000). Protein-and pH-dependent binding of nascent pectin and glucuronoarabinoxylan to xyloglucan in pea. *Planta*, *211*(3), 423-429.

Experiment 4:

Plant-derived supramolecular aggregates, intended as carrier of bioactive compounds: Encapsulation, Thermal Protection, and Release of Ascorbate

Ascorbic acid is a primary antioxidant present in biological systems to counter oxidative stress. It also acts as enzyme cofactor, and chemical reductant in the human metabolism, with a number of health benefits (Naidu, 2003). In the food industry, ascorbic acid is widely used as food additive (with the code E300 for the European legislation) acting as secondary antioxidant with multiple functions (e.g. oxygen scavenger, shifting the redox potential of food systems to the reducing range, synergic action with chelators, regenerator of primary antioxidants) (Reische *et al.*, 2008). Despite the evident positive properties of this bioactive molecules, it is highly prone to oxidative degradation and its stability varies markedly as a function of environmental conditions such temperature, pH, oxygen, light, and presence of metal ions (Tsao, 1997).

CWM could play a role as protective agent for ascorbate during the storage and processing of a formulated food product. This study explores the possibility of entrapping ascorbate into plant-derived structures in order to control its release in water medium and stabilize it during a pasteurization thermal treatment.

4.1 Materials and Methods

Fresh-cut rocket salad, *Eruca sativa*, (Bonduelle, Italy) was purchased at a local market in Milano (Italy) and stored at 4 °C prior to processing. All chemicals were supplied by Sigma-Aldrich.

4.1.1 CWM preparation

Cell wall material was obtained according to the procedure described by Roversi *et al*. (2016). Briefly, salad leaves were boiled in 95% (v/v) ethanol for 30 min to inactivate potential wall-modifying enzymes. After the homogenization at top speed in a Polytron (Brinkam Instruments) for 1 min, the dispersion was filtered under pressure with Glass Microfiber Filters (Whatman), pore size 125 μm. The resulting pellets were washed with a methanol-chloroform solution (1:1) until their complete discoloration. In the end, cell walls underwent acetone washing to remove loosely associated water. Final samples were dried at room temperature overnight, and particles with a diameter between 125 and 250 μm, corresponding to small clusters of cells (Day *et al.*, 2010), were selected by sieving.

Sodium ascorbate was precipitated into CWM according to the industrial procedure described by Holland (1948), with slight modifications. In our case, 0.4 g of CWM was poured into 60 ml of L-ascorbate 1.14 mM under magnetic stirring for 30 minutes. At the end of the waiting time, the imbibed material was filtered under pressure with Glass Microfiber Filters (Whatman), without any washing. Subsequently, the CWM was deepened into 60 ml of aqueous solution of $NaHCO_3$ 1.19 mM, which reacts with the ascorbate forming sodium ascorbate and carbon dioxide. CWM particles were filtered as previously described for ascorbate and washed with 50 ml of water.

The amount of adsorbed ascorbate was quantified after enzymatic degradation of the CWM. CWM loaded with ascorbate (0.4 g) was hydrolysed with cellulase from *Aspergillus niger*, 0.8 U/mg (Sigma, Germany), and pectinase from *Aspergillus niger*, 1 U/mg (Sigma, Germany). The amount of ascorbate released was measured according to the colorimetric method described in the following paragraph (**4.1.2**). The loading yield was calculated by subtracting the adsorbed amount of ascorbate to the initial amount used in the loading procedure.

In order to prevent vitamin oxidation due to its light-sensitivity, all the operations previously described and the following release procedure were performed in dark conditions by covering the containers with aluminium foils.

4.1.2 Release kinetic study

The release studies were conducted in sink conditions, dispersing 0.2 g of CWM, loaded with sodium ascorbate, in 50 ml of water. Aliquots (0.2 ml) were periodically withdrawn from the dissolution medium and the concentration of ascorbate was quantified with an ascorbic acid assay kit (Sigma Aldrich MAK075). In this assay, ascorbic acid concentration is determined using the Ferric Reducing/Antioxidant and Ascorbic Acid (FRASC) assay; Fe3+ is reduced to Fe2+ by antioxidants present in the sample, which results in a colorimetric (593 nm) product. The absorbance of the coloured samples was measured using a UV-VIS spectrophotometer (Jasco V-650, Japan).

The results were expressed as relative release (*RR%*) or fractional release (*f*):

$$RR\% = \frac{M_t}{M_{CWM}} \qquad \text{(eq. 4.1)}$$

$$f = \frac{M_t}{M_\infty} \qquad \text{(eq. 4.2)}$$

where M_t is the amount of ascorbate release at time *t*, M_{CWM} the amount of ascorbate loaded in CWM, and M_∞ is the amount of ascorbate released at the equilibrium (after 6 hours).

4.1.4 Thermal degradation

The ability of CWM to protect ascorbate from thermal damage was evaluated by comparing the degree of vitamin degradation for free ascorbate in water and CWM-entrapped ascorbate. Both systems contained 2.25% of vitamin and were subjected to a pasteurization treatment at 65 °C for 15 minutes (Rodriguez-Gonzalez *et al.*, 2010) using a Peltier system to control the temperature. A parallel set of samples was subjected to the same treatment but at room temperature (23 °C) for the same test time. The amount of non-oxidized ascorbate was measured with the colorimetric method described in the previous paragraph (**4.1.3**). In order to access the CWM-entrapped ascorbate, an enzymatic pre-treatment as previously described (**paragraph 4.1.1**) was applied to the samples to free the vitamin molecules. The degree of degradation was expressed as the percentage ratio between the measured concentration of ascorbate after treating at 65 °C and 23 °C.

4.2 Results and Discussion

4.2.1 Loading Efficiency of Ascorbate in CWM particles

CWM cavities were used as reaction sites for the precipitation of the sodium ascorbate. In order to evaluate the efficiency of this procedure, the loading yield into CWM was quantified and resulted equal to 1.65%. The value is slightly lower than results obtained with other encapsulation systems for vesicular delivery, for example internal gelation and liposome inclusion (Zandi, 2017; Kirbi, Whittle *et al*, 1991). It should be also highlighted that each gram of CWM was able to hold back 0.45 g of ascorbate, as quantified after enzymatic degradation of CWM as described in **paragraph 4.1.1**.

4.2.2 Release kinetic of ascorbate from cell wall materials in water medium

The relative release of ascorbate through the cell walls into water medium was monitored for 5 hours and the release curve is reported in **figure 4.1**. The transport of the bioactive is really fast and more than half of the release phenomenon occurred within the first 5 minutes. Furthermore, the maximum amount of released ascorbate was reached in 30 minutes and corresponded to the 24.45% of the ascorbate initially entrapped. To have a better insight of the mechanisms driving the mass transport phenomena, the shape of the fractional release curve (**inset** in **fig. 4.1**) was analysed through mathematical modelling.

In swellable release systems, the prevailing molecular mechanism involved in release is a coupling of diffusion and macromolecular relaxation as a result of which the entrapped bioactive diffuses. Modelling of release from swellable polymeric systems belongs to a category of diffusion problems known as moving-boundary (Lee, 1980; Peppas, 1984). Crank (1987) has pointed out that the required equations for fitting of data in this case are significantly different and more complicated than those used for non-swellable systems. In fact, since the constitutive equation for drug transport in the presence of both diffusional and relaxational phenomena is highly non-linear, exact analytical solutions are not available. Instead, empirical mathematical solutions can be used as predictive tools.

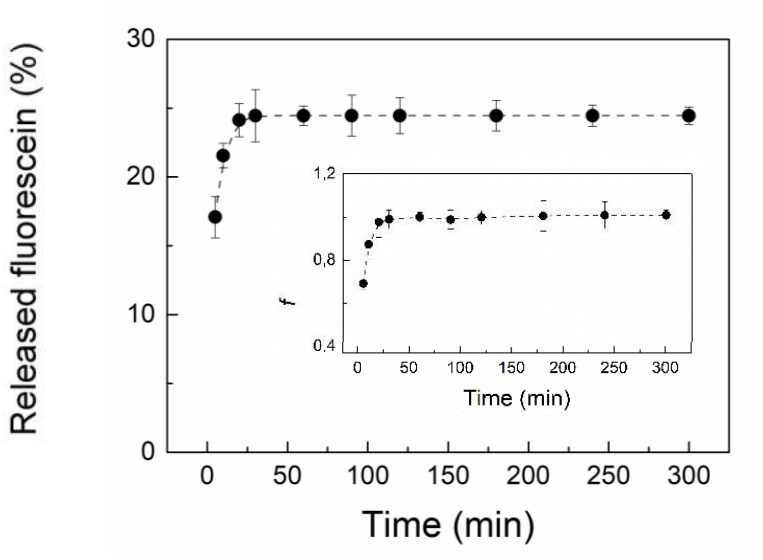

Figure 4.1 Release profile of ascorbate from CWM in water monitored for 5 hours. Inset: Fractional amount of ascorbate released in time from CWM in water monitored for 5 hours.

According to the traditional mathematical kinetic description, ascorbate release from CWM to water followed a first-order kinetics. Indeed, data were successfully fitted exponential model:

$$f = 1 - e^{k \cdot time} \quad \text{(eq. 4.3)}$$

with a R^2 = 0.99 and a rate constant *k* of 0.57 min^{-1}. These results suggest that the process is characterized by an initial burst-release phenomenon (Zandi, 2017; Huang & Brazel, 2001).

The high solubility of ascorbate in water played a role in facilitating its diffusion, but the small molecular size of the bioactive and the porous architecture of CWM matrix were supposed to be the decisive factors causing a fast migration of ascorbate toward the medium bulk. Indeed, in anomalous release, the polymer dissolution is modeled to follow first-order kinetics at the interface with surrounding medium, whereas the bioactive transport through a polymeric matrix is commonly described with more complex models when the diffusion coefficient depends strongly on polymer concentration since polymer swelling and relaxation enhance the drug mobility (Arifin *et al.*, 2006). For this reason, first-order models are traditionally used to explain release of highly water-soluble drugs from porous matrices (Mulye & Turco, 1995, Wang *at al.*, 2002). In this case, dissolution is the driving process despite the swelling features of the carrier system, that should lower the ascorbate diffusivity in the matrix (Lee & Peppas, 1987). We can hypothesize that the molecular size is too small compared to the pore size to be retained.

4.2.3 Fickian and Relaxational Contribution Quantification of Ascorbic Acid Release from Cell Wall Materials

Since CWM can be defined hydrogel-based delivery systems, the release mechanism can be ascribed to two main contributions: the Fickian diffusion and the biopolymers rearrangement (case-II transport). Kormeyer-Peppas model (**eq. 4.4**) allowed to identify the predominant release mechanism through the analysis of its exponential parameter (*n*), which reflects the shape of the release profile curve:

$$f = kt^n \quad \text{(eq. 4.4)}$$

where *k* is the release velocity constant and *n* is the exponent related to the release mechanism (Korsmeyer & Peppas, 1981).

For the curve in **inset** in **figure 4.1**, *n* was calculated to be 0.32, confirming that swelling and relaxation phenomena have a minor role in the control of the bioactive release. Indeed, Peppas and Sahlin (1989) identified two critical value for the diffusion exponent *n*, corresponding to the main mechanism involved in the release phenomenon (n = 0.43 for Fickian diffusion, *n* = 0.85 for Case-II transport). The value obtained for the present system indicated a prevalence of the diffusion mechanism with a negligible effect of the matrix biopolymers. In order to quantify the relative importance of diffusional and relaxational contribution, data were modelled using Peppas-Sahlin equation (**eq. 4.5**).

Since diffusion and relaxation of polymeric chains can be considered as additives mechanism (Alfrey *et al.*, 1966), Peppas and Sahlin (1989) developed a release kinetic model constituted by the sum of two power laws:

$$f = K_D t^m + K_R t^{2m} \quad \text{(eq. 4.4)}$$

In this equation, K_D is the release kinetic constant for diffusion, K_R is the release kinetic constant for polymers relaxation, and *m* is a constant coefficient.

The front parameters *k1* and *k2*, belonging to the diffusional and relaxational contribution terms, were determined to be $4.07 \cdot 10^2$ and $4.16 \cdot 10^3$ min^{-1}, respectively. But it is not possible to give an exact answer as to the importance of the Fickian or Case-II mechanism from measurement of K_1 and K_2. For these reasons, the percentage of bioactive release due to the Fickian diffusion mechanism must be calculating the following equation obtained from Peppas-Sahlin model:

$$F = \frac{1}{1+\frac{k_2}{k_1}t^m} \quad \text{(eq. 4.4)}$$

consequently, the relaxational relative contribution is calculated by subtraction, R = 1 - F. The evolution of *F* and *R* during release time is reported in **figure 4.2**, where than 95% of the ascorbate release could be ascribed to the Fickian diffusion. In conclusion, the idea of using a swelling polymer to provide more control over the release of drug was not successful since it was not efficient in slowing down the bioactive migration in the water medium.

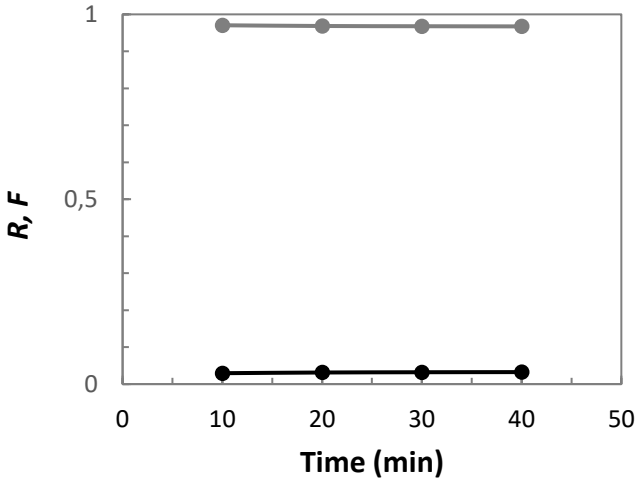

Figure 4.2 Diffusion (*F*, black) and relaxational (*R*, grey) contribution to ascorbate release from CWM in water.

4.2.4 Protective Effect of CWM against Ascorbate Thermal Degradation

To evaluate the protective effect of CWM against ascorbate thermal degradation. The bioactive was subjected to a pasteurization treatment (65 °C for 15 min) as it is and in CWM. The level of degradation was quantified by normalizing the degraded amount of ascorbate after pasteurization to the amount determined applying the same procedure at room temperature, with no heating.

Figure 4.3 displays the results obtained for the two systems. The presence of the CWM had a protective effect and the amount of degraded bioactive was about one third than the value obtained for ascorbate alone. The degree of degradation is lower also if compared with ascorbate reduction in more complex systems (e.g. pasteurized juice) which underwent an ascorbate reduction ~15% (Saeeduddin *et al.* 2015; Terragrosa *et al.*, 2006).

Even though there are no information about the mechanisms underlying ascorbate stabilization to thermal degradation in the presence of cell wall materials, other biopolymers had already proved to have protective effect. In particular Dai-Dong *et al.* (1990) described the stabilization effect of vitamin C by β-lactoglobulin during heat treatment. Pauyol *et al*. (1994) also suggested that the antioxidant effect of reductive thiols in β-lactoglobulin may have a positive effect. On the other hand, Herbig and her group (2017) compared the kinetic of ascorbate in simple water media and complex food system (i.e. fruit purées). They correlated the degradation rate to the different oxygen accessibility, which was reduced in the case of fruit samples.
The tremendous complexity of the multicomposite system considered multiplies the possible mechanisms (reactives accessibility, internal redox reactions...) that can affect the oxidative reaction of ascorbate. For this reason, the CWM entrapping of ascorbate for thermal protection is a promising approach, but it still needs further and more specific investigations.

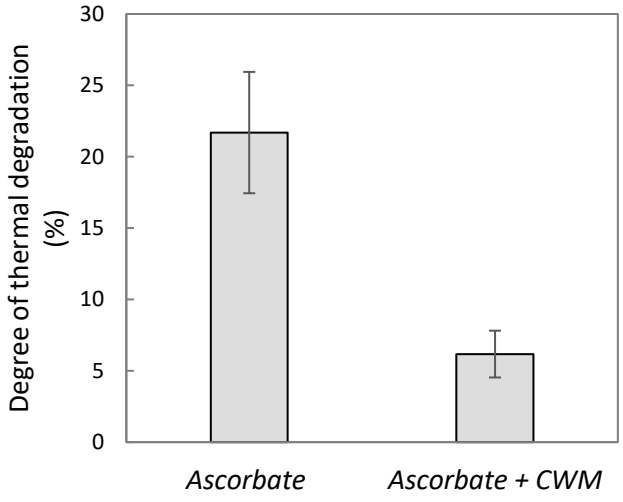

Figure 4.3 Thermal degradation degree of ascorbate in water solution or in the presence of CWM after pasteurization.

Conclusions

The ascorbate displayed a very fast release kinetic, indicating that the permeable structure of CWM matrix was not suitable to control the bioactive migration in the medium in favour of a more sustained release. On the contrary, CWM was successful in reducing ascorbate thermal oxidation during thermal treating, even though the mechanisms involved are not still clear.

References

Arifin, D. Y., Lee, L. Y., & Wang, C. H. (2006). Mathematical modeling and simulation of drug release from microspheres: Implications to drug delivery systems. *Advanced drug delivery reviews*, 58(12-13), 1274-1325.

Crank, J. (1987). Free and moving boundary problems. Oxford University Press.

Dai-Dong, J. X., Novak, G., & Hardy, J. (1990). Stabilization of vitamin C by β-lactoglobulin during heat treatment. *Sciences des Aliments*, 10(2), 393-401.

Herbig, A. L., Maingonnat, J. F., & Renard, C. M. (2017). Oxygen availability in model solutions and purées during heat treatment and the impact on vitamin C degradation. *LWT-Food Science and Technology*, 85, 493-499.

Holland, W. A. (1948). *U.S. Patent No. 2,442,005*. Washington, DC: U.S. Patent and Trademark Office.

Huang, X., & Brazel, C. S. (2001). On the importance and mechanisms of burst release in matrix-controlled drug delivery systems. *Journal of controlled release*, 73(2-3), 121-136.

Kirby, C. J., Whittle, C. J., Rigby, N., Coxon, D. T., & Law, B. A. (1991). Stabilization of ascorbic acid by microencapsulation in liposomes. International journal of food science & technology, 26(5), 437-449.

Lee, P. I. (1980). Diffusional release of a solute from a polymeric matrix—approximate analytical solutions. *Journal of membrane science*, 7(3), 255-275.

Lee, P. I., & Peppas, N. A. (1987). Prediction of polymer dissolution in swellable controlled-release systems. Journal of Controlled Release, 6(1), 207-215.

Mulye, N. V., & Turco, S. J. (1995). A simple model based on first order kinetics to explain release of highly water soluble drugs from porous dicalcium phosphate dihydrate matrices. *Drug development and industrial pharmacy*, 21(8), 943-953.

Naidu, K. A. (2003). Vitamin C in human health and disease is still a mystery? An overview. *Nutrition Journal*, 2(1), 7.

Peppas, N. A. (1984). Release of bioactive agents from swellable polymers: theory and experiments. In *Recent Advances in Drug Delivery Systems* (pp. 279-289). Springer, Boston, MA.

Peppas, N. A., & Sahlin, J. J. (1989). A simple equation for the description of solute release. III. Coupling of diffusion and relaxation. *International journal of pharmaceutics*, 57(2), 169-172.

Reische, D. W., Lillard, D. A., & Eitenmiller, R. R. (2008). Antioxidants. In Akoh, C.C. (Ed.), *Food lipids: chemistry, nutrition, and biotechnology* (p. 422). CRC press.

Rodriguez-Gonzalez, V. M., Femenia, A., Gonzalez-Laredo, R. F., Rocha-Guzman, N. E., Gallegos-Infante, J. A., Candelas-Cadillo, M. G., ... & Rossello, C. (2011). Effects of pasteurization on bioactive polysaccharide acemannan and cell wall polymers from Aloe barbadensis Miller. *Carbohydrate Polymers*, 86(4), 1675-1683.

Saeeduddin, M., Abid, M., Jabbar, S., Wu, T., Hashim, M. M., Awad, F. N., ... & Zeng, X. (2015). Quality assessment of pear juice under ultrasound and commercial pasteurization processing conditions. *LWT-Food Science and Technology*, 64(1), 452-458.

Torregrosa, F., Esteve, M. J., Frígola, A., & Cortés, C. (2006). Ascorbic acid stability during refrigerated storage of orange–carrot juice treated by high pulsed electric field and comparison with pasteurized juice. *Journal of Food Engineering*, 73(4), 339-345.

Tsao, C. S. (1997). An overview of ascorbic acid chemistry and biochemistry. In Bartosz, G. (Ed.), *Food oxidants and antioxidants: chemical, biological, and functional properties* (p. 28). CRC press.

Wang, J., Wang, B. M., & Schwendeman, S. P. (2002). Characterization of the initial burst release of a model peptide from poly (D, L-lactide-co-glycolide) microspheres. *Journal of controlled release*, 82(2-3), 289-307.

Zandi, M. (2017). Evaluation of the Kinetics of Ascorbic Acid (AA) Release from Alginate-Whey Protein Concentrates (AL-WPC) Microspheres at the Simulated Gastro–Intestinal Condition. *Journal of Food Process Engineering*, *40*(1).

Experiment 5:

Release Behavior of Plant-Derived Unrefined Ingredients: Structural Modification for a Sustained Release

A less selective extraction of polysaccharide-based materials from rocket salad was performed with the aim to limit the impact of chemical solvents (i.e. methanol, chloroform, acetone) compared to the traditional process (Roversi *et a.*, 2016), both in terms of chemical management and residual solvent traces. This approach is based on the ability of ethanol to destabilize and disrupt the physical structure of cellular membranes (Gurtovenko & Anwar, 2009; Golstein, 1986), without the harsh extraction operated by methanol and chloroform. For this reason, the final product is expected to be less refined that CWM.

The aim of this work is investigating if the use a more complex polymeric matrix as delivery system for bioactive compounds (i.e. folic acid) is benefiacial for the final performance. In addition, calcium is used to increase interaction within biopolymers in the cell wall, lowering permeability, and obtain amore sustained release.

5.1 Material and methods

5.1.1 Materials

Fresh-cut rocket salad, *Eruca sativa*, (Bonduelle, Italy) was purchased at a local market in Milano (Italy) and stored at 4 °C prior to processing. All the chemicals were supplied by Sigma-Aldrich at analytic grade.

5.1.2 Unrefined Materials Extraction and Loading

Cell Wall Material (CWM)

Cell wall material was obtained according to the procedure described by Roversi *et al*. (2016) with slight modifications. Briefly, salad leaves were boiled in 95% (v/v) ethanol for 30 min to inactivate potential wall-modifying enzymes. After the grinding with a heavy-duty blender (Waring Laboratory, Torrington, CT) for 30 s at 18500 rpm, the dispersion was filtered under vacuum through four layers of nylon tulle. The resulting pellets were washed with a methanol-chloroform solution (1:1) until their complete discoloration. In the end, cell walls underwent acetone washing to remove loosely associated water. Final samples were dried at room temperature overnight, and particles with a diameter between 125 and 250 μm, corresponding to small clusters of cells (Day *et al.*, 2010), were selected by sieving.

Sodium fluorescein and methylene blue were selected as model molecules to easily trace the release behaviour during the kinetic study. According to the procedure proposed by Paunov and his group (2007), 0.5 g of CWM was poured into 60 ml of alcoholic solution of methylene blue (0.46 g/100 ml) for two hours. The imbibed material was filtered under pressure with Glass Microfiber Filters (Whatman) washing with water until removing the excess of dye. Subsequently, the CWM was deepened into 60 ml of aqueous solution of sodium fluorescein (0.46 g/100 ml), which interacts with the methylene blue leading to the formation of a less soluble complex. The reduced solubility of the product compound was exploited to load particles. CWM particles were filtered as previously described for methylene blue and washed exceeding water to remove every excess of free fluorescein. The amount of adsorbed fluorescein was quantified by subtracting the amount of fluorescein contained into the water used for the washing operations to the amount of fluorescein of the initial loading solution.

Alcohol Insoluble Residues (AIR)

Firstly, salad leaves (80 g) were boiled in 95% (v/v) ethanol (200 ml) for 30 min to dehydrate the system, destabilize cell membranes (Goldstein, 1986; Patra *et al.*, 2006) and inactivate potential wall-modifying enzyme. The material was grounded by means of a heavy-duty blender (Waring Laboratory, Torrington, CT) for 30 s at 18500 rpm, and filtered under pressure through four layers of nylon tulle. Subsequently, the sample was dispersed in water (100 m) and filtered as described before, after 10 minutes at rest, to remove water-soluble components. The resulting insoluble material was washed with 100 ml of water and finally with 300 ml of ethanol to dehydrate the cell wall structure and accelerate the following drying operation avoiding its collapse. The solvent was removed in a vacuum oven at 30 °C overnight.

AIR was loaded with dye tracers (sodium fluorescein and methylene blue) as previously described for CWM. While folic acid was entrapped by acidic precipitation (Kéki *et al*., 1998; Wu *et al.*, 2010). AIR (5 g) were let hydrate in water (50 ml) for 3 hours under magnetic stirring, and subsequently 0.2 g of folic acid were added. After 30 minutes, to guarantee a homogeneous

distribution of the vitamin into the AIR, the system pH was lowered with 1 M HCl until 4.7. AIR particles were filtered as previously described for fluorescein and washed with 50 ml of water.

In order to prevent vitamin oxidation due to its light-sensitivity, all the operations previously described and the following release procedure were performed in dark conditions by covering the containers with aluminium foils.

Alcohol Insoluble Residues with Calcium Treatment
In this case the material was extracted as described for AIR, with the exception that a solution of calcium lactate (2.55 w/v) was used for the washing operation instead of deionized water.

Loading Capacity
The amount of loaded compound was quantified after enzymatic degradation of the CWM. loaded CWM was hydrolysed with cellulase from *Aspergillus niger*, 0.8 U/mg (Sigma, Germany), and pectinase from *Aspergillus niger*, 1 U/mg (Sigma, Germany). The amount of folate released was measured according to the spectrophotometric method described in the following paragraph (**5.1.3**).

5.1.3 Release Kinetic Study
The release tests were performed in two different digestive simulated conditions, which were reproduced according to the indications of U.S. Pharmacopeia. Simulated gastric fluid (SGF) was obtained dissolving 2 g of NaCl and 3.2 g of pepsin form porcine gastric mucosa, 4000 units/mg (Sigma-Aldrich), in 1000 ml of hydrochloridric acid solution (7 % v/v). Simulated intestinal fluid (SIF) was produced dissolving 6.8 g of KH_2PO_4 and 0.9 g of NaOH in 1000 ml of deionized water. The solution was added with 10 g of pancreatin from porcine pancreas (Sigma-Aldrich), and adjusted with 0.1 M NaOH or 0.1 M HCL until reaching pH 6.8.

The kinetic study was conducted in sink conditions, dispersing 0.2 g of loaded material (CWM or AIR) in 50 ml of SGF. After 120 minutes, the material was quickly filtered with a folded nylon tulle and then was immersed in 50 ml of SIF. Aliquots (0.2 ml) were periodically withdrawn from the dissolution medium and the concentration of folate was quantified using a UV-VIS spectrophotometer (Jasco V-650, Japan). The wavelength of maximal absorbance considered were 440 and 495 for fluorescein in SGFand SIF, and 377 nm for folate.
The results are expressed as relative release (*RR%*) or fractional release (*f*):

$$RR\% = \frac{M_t}{M_{CWM}} \qquad \text{(eq. 5.1)}$$

$$f = \frac{M_t}{M_\infty} \qquad \text{(eq. 5.2)}$$

where M_t is the amount of released compound at time *t*, M_{CWM} the amount of compound loaded in the sample, and M_∞ is the release at the equilibrium (after 24 hours).

5.1.4 Physico-chemical characterization
Water binding capacity (WBC) was evaluated using a centrifuge procedure. An aliquot of 0.2 g of CWM or AIR was dispersed in 10 mL distilled water in a 15 ml preweighed centrifuge tube. The dispersions were allowed to stand for 24 hours to guarantee a complete hydration and then centrifuged at 10000 g for 25 min at room temperature. The supernatant was decanted, and the tube containing the precipitate was weighed again to determine amount of water retained per gram of sample.

The viscoelastic behavior of aqueous suspensions of AIR (5% w/v) was studied by using a CMT rheometer (DHR-2, TA Instruments, USA) equipped with a 40 mm diameter plate-plate geometry, with a gap of 1 mm. A solvent trap provided by the manufacturer for liquid samples was used to prevent loss of solvent. First, oscillatory strain sweeps were performed to determine the linear viscoelastic region for each sample. Frequency sweep experiments were then performed at low amplitude of strain (0.2%, in linear regime) in the frequency range of 0.1–100 rad/s.

5.1.5 Mathematical Modelling

For all the curves, the fitting was performed with OriginLab Version 9.1 software. The error of the calculated parameters is expressed as standard error.

5.2 Results and discussion

5.2.1 Loading Capacity

AIR extracted from rocket salad were assessed as delivery systems and fluorescein complex with methylene blue was firstly considered as treacer molecule to monitor the release process. After the loading procedure, each gram of AIR was found to contain 0.49 g of fluorescein, that is almost 3-folds more than the value obtained for CWM extracted from the same type of product (as reported in the **paragraph 3.2**). The increased loading of fluorescein of AIR compared to CWM can be related to their higher ability of entrapping and retaining small molecules, like the water as proved through WBC measurements (**figure 5.1**).

It can be hypothesized that the application of a less selective extraction procedure results in a more complex wall matrix, especially in terms of composition, which have been reported to constitute a less permeable cell wall network, reflected in higher WBC values (Ramaswamy *et al.*, 2013).

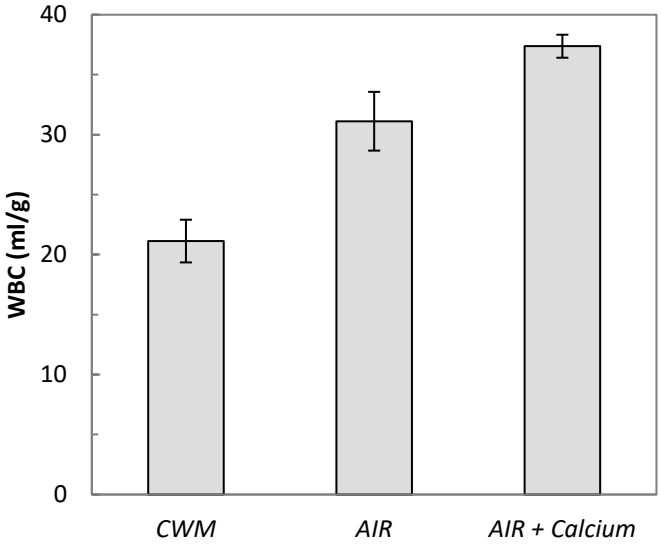

Figure 5.1 Comparison of water binding capacity for CWM and AIR materials, and AIR with the addition of calcium.

AIR was then use as delivery system for the vehiculation of folic acid, and it demonstrated a good loading capacity, equal to 0.95 g of folate for each gram of CWM. In a second step, AIR extraction procedure was modified with the addition of calcium lactate during the washing operation in order to modify the cell wall structure. The loading capacity was almost doubled in the presence of calcium, with a final value of 1.64 g_{folate}/g_{AIR}. It was widely reported that calcium ions act by

complexing with cell wall and middle lamella pectin (Martin-Diana *et al.*, 2005). Studying vegetables and fruits shelf-life, the addition of calcium is generally associated to firmness preservation by cross-linking with both cell wall and middle lamella pectin (Grant *et al.*, 1973; Van-Buren, 1979). This stronger organization of the matrix was also reflected in higher WBC values, as evident in **figure 5.1**. We can assume that a more compact structure is able to reduce losses of folate during the washing operations, increasing the final ability of the AIR material to retain it.

5.2.2 Release Behaviour of Alcohol Insoluble Residues: A Model System

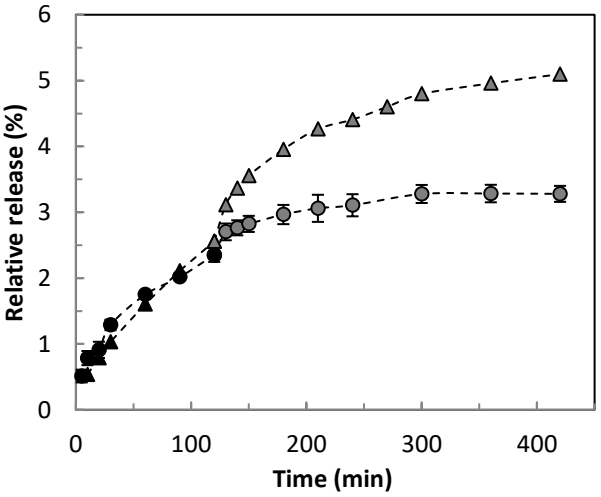

Figure 5.2 Profile of fluorescein release in SGF (black) and SIF (grey) from AIR (triangles) and CWM (circles).

Figure 5.2 shows the release profile of fluorescein from AIR and CWM in gastric (SGF) and intestinal (SIF) simulated conditions. It is evident that the curve obtained for AIR reached a value equal to 4.50% at the end of test period, that is almost 1.5-fold more than the final release observed from CWM (3.36%).

Despite the risen relative release of fluorescein from AIR compared to CWM final release, the extent of the increase was not proportional to the higher loading yield (discussed in the previous paragraph). However, it should be highlighted that release from AIR in did not reach a plateau value in both fluids, conversely to the behaviour observed for CWM in SIF, and thus the overall fluorescein released at the end of the test did not correspond to the whole amount of dye molecules available for the release. In order to better understand the influence of different extraction process on the release behaviour in time, the release profiles were described with a first order kinetic model:

$$RR = 1 - RR_{\infty}e^{kt} \qquad \text{(eq. 5.3)}$$

where RR_{∞} is the relative release plateau value at equilibrium, t is the release time, and k is the constant rate of the phenomenon. It should be evidenced that the release curve in SIF is reported after subtracting the final value of the kinetic in SGF.

The kinetic rate values obtained for AIR and CWM in simulated gastric and intestinal conditions are reported in **table 5.1**. Both in SGF and SIF, fluorescein release is significantly slower from AIR than from CWM, as expressed by k values that are almost halved. These results suggest that AIR represented a more effective barrier to fluorescein migration than CWM.

Table 5.1 Kinetic rate constant for fluorescein release in simulated digestive fluids from AIR and CWM.

	$k\ 10^{-2}$ (min^{-1})	
	SGF	SIF
AIR	1.06±0.07	2.41±0.16
CWM	2.25±0.29	4.62±0.38

The error is expressed as standard error of the fitting.

In order to confirm this hypothesis, the release was expressed in fractional terms by dividing the relative release to the measured equilibrium value (RR_∞). The new graph, shown in **figure 5.3**, highlights the differences in shape between curves. All curves tended toward the value maximum value 1, representative of the maximum release at equilibrium, but the plateau value was reached only in the case of fluorescein released in SIF from CWM (**figure 5.3b**). In general, comparing the release behaviour in the same conditions from different materials, we can recognize different curves shapes which are correlated to the mechanisms involved in mass transport trough the polymeric matrix (Crank, 1979).

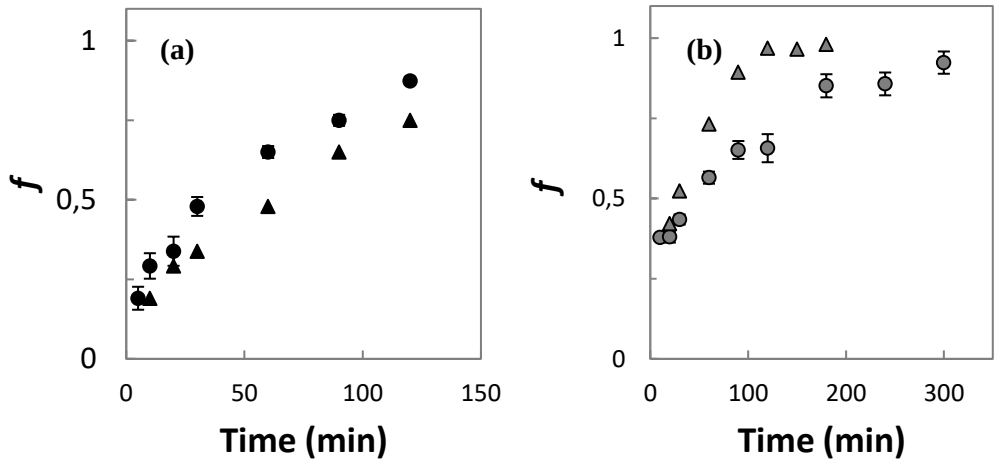

Figure 5.3 Fractional amount of released fluorescein in time from CWM (circles) and AIR (triangles) in SGF (a), and SIF (b).

Thus, the fractional release kinetics were modelled according to Kosmeyer equation (Korsmeyer & Peppas, 1981):

$$f = kt^n \qquad \text{(eq. 5.4)}$$

where k is the release velocity constant, incorporating structural modifications and geometrical characteristics of the system, and n is the exponent related to the release mechanism (Korsmeyer & Peppas, 1981). The power law exponent n characterizes the mechanism driving the release of encapsulated molecules, discriminating Fickian diffusion (n = 0.43), swelling controlled release (n = 0.85) and the anomalous transport (n = 0.43-0.85) resulting by the coexistence of the other two mechanisms (Peppas & Khare, 1993; Peppas & Sahlin, 1989). The release in SIF showed similar n values, 0.35±0.02 and 0.30±0.01 for AIR and CWM respectively, below the critical value for Fickian diffusion. Similar values ($0.30 < n < 0.43$), were found in different studies with biopolymeric systems, indicating a prevalence of Fickian diffusion, and such low values were justified by the polydispersity of systems and the heterogeneity of the gel layer (Ritger & Peppas, 1987; Saurì *et al.*, 2014). The Korsmeyer-Peppas exponent for release curves in SGF is slightly

increased from 0.55±0.01 for CWM to 0.59±0.03 for AIR, suggesting an increased importance of relaxational mechanisms during fluorescein release.

The application of Peppas-Sahlin model allowed to quantify the relative contribution of the two main mechanisms driving the release from CWM and AIR (Peppas & Sahlin, 1989). The fractional release curves were fitted using the following equation:

$$f = K_D t^m + K_R t^{2m} \quad \text{(eq. 5.5)}$$

where, K_D is the release kinetic constant for diffusion, K_R is the release kinetic constant for polymers relaxation, and *m* is a constant coefficient.

Since the less selective extractive procedure was hypothesised to produce materials acting as more effective barriers to fluorescein migration, it is supposed that the polymeric chains relaxation gains a more important role the release phenomena. For this reason, the relative contribution of case-II mechanism (*R*) was calculated using the following equation obtained from Peppas-Sahlin model:

$$R = \frac{1}{1+\frac{K_D}{K_R}t^m} \quad \text{(eq. 5.6)}$$

The evolution of *R* during release time is reported in **figure 5.4**. The release in SIF did not show significant differences for AIR and CWM, with a difference in *R* values lower than 5%. On the contrary the relaxational contribution in SGF increase more than 15% in the initial phase. The predominant contribution of polymeric chains reorganization in simulated gastric conditions for AIR can be explained by the enhancement of interactions due to the more complex matrix (Ramaswamy *et al.*, 2013).

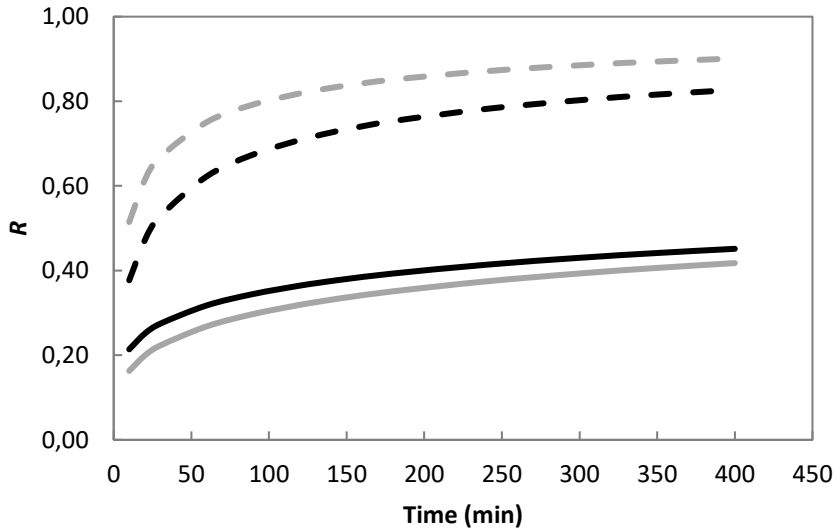

Figure 5.4 Relaxational contribution (*R)* as a function of time for CWM (clack) and AIR (grey) in simulated digestive fluids (dashed and straight lines for SGF and SIF respectively).

5.2.3 Release of Folate from Alcohol Insoluble Residues: Effect of Calcium

The folate release profiles from AIR produced with different washing solutions are reported in **figure 5.5**. The presence of calcium lowered the final value of folate release from 8.46% for AIR to 5.53% for AIR with calcium, and the main divergence occurred during the release in SIF. In order to understand if the differences were due to a different kinetic behavior, the profiles were modeled using a first-order equation (**eq. 5.3**) and the rate constants (*k*) and the measured plateau

relative release values (RR_∞) are provided in **table 5.2**. The results suggested that the presence of calcium did not affected significantly the folate release in SGF both in terms of amount released and kinetic behavior. It could be hypothesized that the effect of enhanced binding between matrix biopolymers at pH < 4 (Brett *et al.*, 1997; Rizk *et al.*, 2000) is predominant compared to the effect of calcium ions. On the contrary, the treatment with calcium seems not only to retain folate more effectively, but it significantly slowed down the release kinetic.

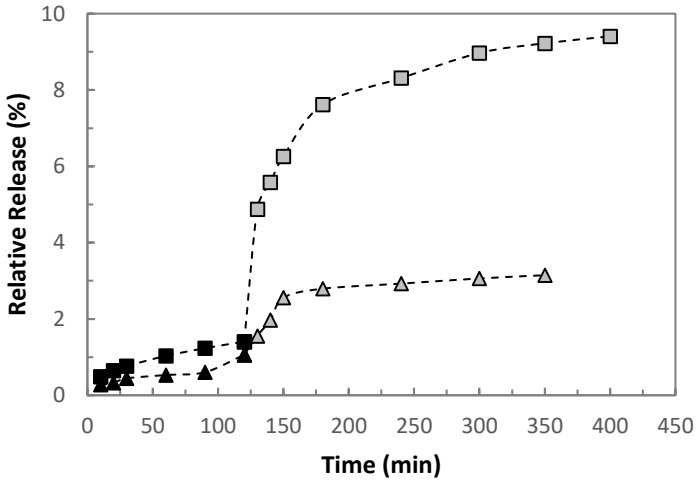

Figure 5.5 Profile of folate release in SGF (black) and SIF (grey) from AIR with (triangles) and without (squares) the treatment with calcium lactate.

Table 5.2 Releative release at equilibrium and kinetic rate constant for folate release in simulated digestive fluids from AIR treated with different washing solutions.

	SGF		***SIF***	
	RR_∞ **(%)**	k **10^{-2} (min^{-1})**	RR_∞ **(%)**	k **10^{-2} (min^{-1})**
AIR	1.31	2.56±0.25	6.75	3.28±0.22
AIR + Calcium	1.77	2.59±0.34	4.17	1.67±0.12

The error is expressed as standard error of the fitting.

Figure 5.6 shows the fractional profiles (**eq. 5.2**) of folate from the two materials in different simulated digestive conditions. As observed before, the folate release curves from AIR in presence or in absence of the calcium treatment in SGF had a similar behaviour, and at the end of the first phase of the test (120 min) none of the materials reached the equilibrium state. In the case of the release in SIF, both the profiles approached the equilibrium release (corresponding to f = 1) by reaching fractional release values higher than 0.95 but with a different shape.

The use of the Korsmeyer-Peppas model (**eq. 5.4**) allowed to investigate if the changes in cell wall structure induced by calcium ions modified the mechanisms driving the folate release. In particular, it is expected that the formation of cross-linked calcium pectate reduced the contribution of Fickian release in favour of a prevalent role of biopolymers. This hypothesis was confirmed by the values obtained for the power law exponent n, correlated to the type of phenomenon driving release, which are reported in **table 5.3**.

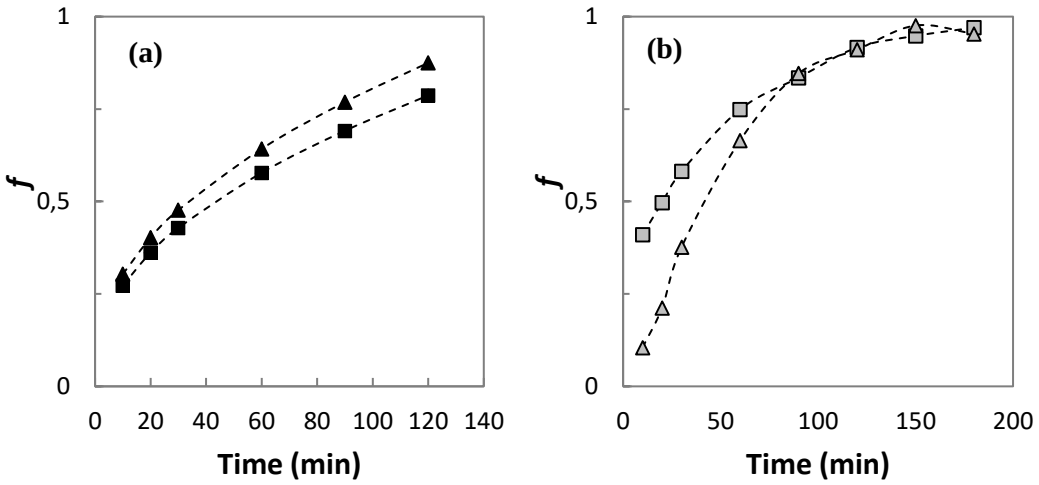

Figure 5.6 Fractional amount of released fluorescein in time from AIR without (triangles) and with calcium ions (squares) in SGF (a), and SIF (b).

In SGF, the behaviour of both materials was characterized by an anomalous release, result of the coexistence of both diffusion and relaxational mechanisms. Regarding the release in SIF, we can distinguish two opposite behaviours for the two materials. The release of folate from AIR could be mainly explained by Fickian diffusion phenomena, since n = 0.402 that is quite close to the critical value (0.43) defined for diffusion driven release from spherical particles (Ritger & Peppas, 1987). Considering AIR modified with calcium, the kinetic behaviour was typical of Case-II release, with the main contribution of chains relaxation phenomena in folate release. Indeed, the power law exponent (n = 0.847) corresponded to the value characteristic for Case-II release from spherical particles (Ritger & Peppas, 1987). It means that the presence of calcium ions modified significantly the cell wall structure producing a more sustained release mainly driven by the matrix swelling and relaxation mechanisms.

Table 5.3 Power law exponent (n) for folate release in simulated digestive fluids from AIR treated with different washing solutions.

	n	
	SGF	*SIF*
AIR	0.533±0.003	0.402±0.014
AIR + Calcium	0.531±0.004	0.847±0.008

In the end, AIR aqueous dispersions (5% w/v) were subjected to rheological analysis in frequency sweep and the results are reported in **figure 5.7**.

According to the cooperative flow theory presented by Bohlin (1980), in dynamic experiments, the complex modulus and the frequency are related by the following expression:

$$G^*(\omega)=A_f\,\omega^{1/z} \qquad \text{(eq. 5.7)}$$

where $G^*(\omega)$ is the complex modulus, ω the frequency, A_f represents the interaction strength between the flow units inside the gel, and z is the coordination number of cooperative flow units in the structure, a reticulation factor correlated to the number of interactions the substance microstructure.

AIR treated with calcium displayed a higher coordination number (around 12.5 rad/Pa s) compared to simple AIR (z = 0.7 rad/Pa s), and this should correspond to a more packed

arrangement of the structure (Roversi & Piazza, 2016; Luna-Guzmán & Barrett, 2000), confirming the previous results.

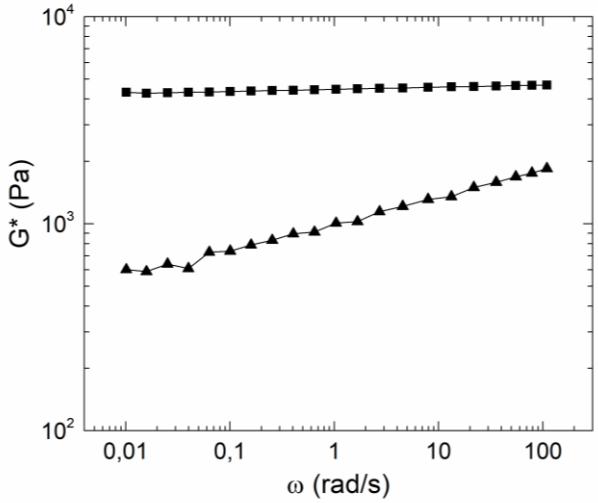

Figure 5.7 Complex modulus (*G**) as a function of the frequency for aqueous dispersion (5% w/v) of AIR obtained without (triangles) and with calcium treatment (squares).

Conclusions

The application of a less selective extraction procedure was reflected in a more sustained release, suggesting that AIR present a more complex matrix (compared to CWM,) and able to slow down the release of bioactive compounds.

The addition of calcium ions to the cell walls was reported to induce the formation of a more compact architecture duet to the cross-linked calcium pectate. This structural modification was reflected in a decrease in folate release kinetic, but only in simulated intestinal conditions.

The information obtained constitute the basis for a rational optimization of the system to gain a better control on release performance

References

Bohlin, L. (1980). A theory of flow as a cooperative phenomenon. *Journal of Colloid and Interface Science*, 74(2), 423-434.

Brett, C. T., Healy, S. A., McDonald, M. S., Macgregor, C., & Baydoun, E. H. (1997). Binding of nascent glucuronoxylan to the cell walls of pea seedlings. *International journal of biological macromolecules*, 21(1-2), 169-173.

Crank, J. (1979). *The mathematics of diffusion*. Oxford university press.

Grant, G. T., Morris, E. R., Rees, D. A., Smith, P. J., & Thom, D. (1973). Biological interactions between polysaccharides and divalent cations: the egg-box model. *FEBS letters*, 32(1), 195-198.

Goldstein, D. B. (1986). Effect of alcohol on cellular membranes. *Annals of emergency medicine*, 15(9), 1013-1018.

Gurtovenko, A. A., & Anwar, J. (2009). Interaction of ethanol with biological membranes: the formation of non-bilayer structures within the membrane interior and their significance. *The Journal of Physical Chemistry B*, 113(7), 1983-1992.

Kéki, S., Sipos, T., DEAK, G., Mezey, G., & Zsuga, M. (1998). Investigation of the microprecipitation of folic acid from slightly acidic injection solutions using dynamic light scattering. *Chemical and pharmaceutical bulletin*, 46(8), 1333-1334.

Korsmeyer, R. W., & Peppas, N. A. (1981). Effect of the morphology of hydrophilic polymeric matrices on the diffusion and release of water soluble drugs. *Journal of Membrane Science*, *9*(3), 211-227.

Luna-Guzmán, I., & Barrett, D. M. (2000). Comparison of calcium chloride and calcium lactate effectiveness in maintaining shelf stability and quality of fresh-cut cantaloupes. *Postharvest Biology and Technology*, 19(1), 61-72.

Martin-Diana, A. B., Rico, D., Barry-Ryan, C., Frias, J. M., Mulcahy, J., & Henehan, G. T. (2005). Calcium lactate washing treatments for salad-cut Iceberg lettuce: Effect of temperature and concentration on quality retention parameters. *Food Research International*, 38(7), 729-740.

Patra, M., Salonen, E., Terama, E., Vattulainen, I., Faller, R., Lee, B. W., ... & Karttunen, M. (2006). Under the influence of alcohol: the effect of ethanol and methanol on lipid bilayers. *Biophysical journal*, 90(4), 1121-1135.

Peppas, N. A., & Khare, A. R. (1993). Preparation, structure and diffusional behavior of hydrogels in controlled release. *Advanced drug delivery reviews*,*11*(1-2), 1-35.

Peppas, N. A., & Sahlin, J. J. (1989). A simple equation for the description of solute release. III. Coupling of diffusion and relaxation. *International journal of pharmaceutics*, *57*(2), 169-172

Ramaswamy, U. R., Kabel, M. A., Schols, H. A., & Gruppen, H. (2013). Structural features and water holding capacities of pressed potato fibre polysaccharides. *Carbohydrate polymers*, 93(2), 589-596.

Ritger, P. L., & Peppas, N. A. (1987). A simple equation for description of solute release I. Fickian and non-Fickian release from non-swellable devices in the form of slabs, spheres, cylinders or discs. *Journal of controlled release*,*5*(1), 23-36.

Rizk, S. E., Abdel-Massih, R. M., Baydoun, E. A. H., & Brett, C. T. (2000). Protein-and pH-dependent binding of nascent pectin and glucuronoarabinoxylan to xyloglucan in pea. *Planta*, *211*(3), 423-429.

Roversi, T., Ferrante, A., & Piazza, L. (2016). Mesoscale investigation of the structural properties of unrefined cell wall materials extracted from minimally processed salads during storage. *Journal of Food Engineering*, 168, 191-198.

Roversi, T., & Piazza, L. (2016). Changes in minimally processed apple tissue with storage time and temperature: mechanical–acoustic analysis and rheological investigation. *European Food Research and Technology*, 242(3), 421-429.

Saurí, J., Millán, D., Suñé-Negre, J. M., Colom, H., Ticó, J. R., Miñarro, M., ... & García-Montoya, E. (2014). Quality by design approach to understand the physicochemical phenomena involved in controlled release of captopril SR matrix tablets. *International journal of pharmaceutics*, *477*(1), 431-441.

Van Buren, J. P. (1979). The chemistry of texture in fruits and vegetables. *Journal of Texture Studies*, 10(1), 1-23.

Wu, Z., Li, X., Hou, C., & Qian, Y. (2010). Solubility of Folic Acid in Water at pH Values between 0 and 7 at Temperatures (298.15, 303.15, and 313.15) K. *Journal of Chemical & Engineering Data*, 55(9), 3958-3961.

Topic 3

FUNCTIONAL-DRIVEN FRACTIONATION: UNREFINED INGREDIENTS

Mild fractionation processes have recently proved to be a suitable technique to valorize residues from agro-food manufacturing, producing enriched fractions with improved technical properties compared to the purified ingredients thanks to their more complex composition and the conservation of natural structures (van der Goot *et al.*, 2016).

Functional-driven mild fractionation intends to concentrate valuable components by means of mild physical techniques and relies on the morphological characteristics of the raw materials. The distribution of the various components in the tissues constituting the food matrix is exploited to concentrate desirable components by removing parts rich in contaminants and undesirable compounds. The final products are unrefined materials, with a different composition compared to the raw material from a quantitative point of view, but not so qualitatively diverse.

The mild-fractionation is able to preserve the variety of both macro- and micro-components and the cooperation phenomena between them. For example, in fibers-enrich products it is widely recognized also the role of minor associated compounds to the health benefits of their consumption (Jacobs & Tapsell, 2007; Vitaglione *et al.*, 2008). But the interactions between components inside the matrix have been proved to be advantageous also in a technological perspective (Wang *et al.*, 2004; Ozdal *et al*., 2013). In addition, we should not forget the increased sustainability of the extractive process compared to traditional fractionation.

The purification to highly refined ingredients requires large amounts of water and chemicals (e.g. solvents, acids, bases) to remove some components (such as oil, whey proteins, sugars, fibers, etc.) and to precipitate and neutralize the desired components (Wright & Bumstead, 1994; Schutyser et al. 2015). Once the compounds of interest are isolated, water removal is necessary to improve the stability and handling of the products, but it is an energy-intensive process (Atuonwu *et al*., 2011; Motevali *et al*., 2011). Moreover, the focus on target components results in the production of by-products of a lower quality (Raak *et al*. 2017). The current trends indicate that ingredient production is always more focused on functionality rather than purity.

Milling of grains can be presented as a traditional example of concentration of desirable components with the aim of removing poorly digested compounds (Slavin *et al*, 2000), especially suitable for cereals and *Leguminosae* (Malleshi *et al.*, 2001; Charalampopoulos *et al.*, 2002).
Protein-enriched fractions represents an important class of functional ingredients, that is becoming really popular in the last years. The interest in the production of gluten-free products triggered the research of alternative sources of structuring polymers to substitute the mechanical function of gluten network in food products (Melini *et al.*, 2017; Anton & Artfield, 2008). More recently, increasing attention has been paid to the substitution of animal proteins with more economically and environmentally sustainable sources, and plants were considered a major potential source of novel food proteins for long (Multari *et al*., 2015; Day, 2013). In the past decades, leguminous flours have been extensively investigated as source of macronutrients and technological (structure- and texture-forming) agents (Guillon & Champ, 2002; Doxastakis *et al.*, 2002), but the production of these ingredient still requires a dedicated cultivation. More recently, scientific research addressed cakes residues from seed (e.g. mustard, sesame, linseed, seed) oil extraction (Ramachandran *et al.*, 2007). Indeed, seeds are structures characterized by abundant storage reserves rich in nutrients necessary to support germination (Shewry & Casey, 1999) and it makes oil cakes materials with high nutritional value, especially in terms of protein content

ranging from 15% to 50% (Ramachandran *et al.,* 2007). Most efforts are focused on the optimization of the extraction processes in view of an industrial scale-up. At the present, studies are focused on protein-enriched fractions less pure but containing also insoluble proteins, which are lost with traditional aqueous extraction methods (Tenorio *et al.*, 2016).

Hemp Seed Meal

Cannabis sativa L., commonly referred to as hemp, is a widely cultivated plant of industrial importance, as an important source of food, fiber, and medicine (Finell *et al., 2006*). The availability of non-drug varieties possessing low δ-9-tetrahydrocannabinol (Regulation 2013/1307/EU) contents has increased industrial utilization in the last years. In particular hemp seeds have been largely exploited to obtain an excellent dietary oil, rich in polyunsaturated and essential fatty acids (Parker *et al., 2003*). Hemp seed meal (HSM) is the residue of oil extraction by cold-pressing and represents a rich source of high nutritional quality protein (about 25%), in addition to considerable amounts of vitamins and useful minerals (Callaway, 2004). The protein fraction (contained in HSM is expected to play an important role in making such ingredients useful for novel food formulations, as already reported for other protein-rich products (Mundi and Aluko, 2013, Yin et al., 2011). Despite the growing interest in this emerging material, most of recent studies are focused on nutritional and nutraceutical aspects (House et al., 2010; Wang et al., 2008), whereas little attention has been paid to the structural role of its macro-components. The protein fraction, constituted mainly by albumin and edestin, has been extensively investigated in a refined form (Malomo *et al*., 2014; Malomo & Aluko, 2015), while few information is available for the whole meal in the presence of the fiber fraction. But, it is well known that macromolecules (polysaccharides, lipids, and proteins) are inherently functional by virtue, not only of their individual molecular structures, but also of their ability to interact to form complexes with each other or with other molecules. (Aryee *et al.*, 2017).

Recently, commercial products with the addition of HSM are available as protein supplements, but its integration into food formulated products is quantitatively limited to maintain manufactures qualitative standards. Thus, the effective utilization of HSM in food formulations still requires a deeper knowledge of mechanisms driving and affecting its technological performance.

Anton, A. A., & Artfield, S. D. (2008). Hydrocolloids in gluten-free breads: a review. *International journal of food sciences and nutrition*, 59(1), 11-23.

Aryee, A. N. A., Agyei, D., & Udenigwe, C. C. (2017). Impact of processing on the chemistry and functionality of food proteins. In: Yada, R. Y. (Ed.), *Proteins in food processing* (pp 27-45). Woodhead Publishing.

Atuonwu, J. C., Jin, X., van Straten, G., van Deventer Antonius, H. C., & Van Boxtel, J. B. (2011). Reducing energy consumption in food drying: Opportunities in desiccant adsorption and other dehumidification strategies. *Procedia Food Science*, 1, 1799-1805.

Callaway, J. C. (2004). Hempseed as a nutritional resource: an overview. *Euphytica*, 140(1-2): 65-72.

Charalampopoulos, D., Wang, R., Pandiella, S. S., & Webb, C. (2002). Application of cereals and cereal components in functional foods: a review. *International journal of food microbiology*, 79(1-2), 131-141.

Day, L. (2013). Proteins from land plants–potential resources for human nutrition and food security. *Trends in Food Science & Technology*, 32(1), 25-42.

Doxastakis, G., Zafiriadis, I., Irakli, M., Marlani, H., & Tananaki, C. (2002). Lupin, soya and triticale addition to wheat flour doughs and their effect on rheological properties. *Food Chemistry*, 77(2), 219-227.

Finell, M., Xiong, S., & Olsson, R. (2006). Multifunctional industrial hemp for Northern Sweden. *Umeå: SLU e Swedish University of Agricultural Sciences, BTC e Unit for Biomass Technology and Chemistry*.

Guillon, F., & Champ, M. J. (2002). Carbohydrate fractions of legumes: uses in human nutrition and potential for health. British Journal of Nutrition, 88(S3), 293-306.

House, J. D., Neufeld, J., & Leson, G. (2010). Evaluating the quality of protein from hemp seed (*Cannabis sativa* L.) products through the use of the protein digestibility-corrected amino acid score method. *Journal of agricultural and food chemistry*, 58(22), 11801-11807.

Jacobs, D. R., & Tapsell, L. C. (2007). Food, not nutrients, is the fundamental unit in nutrition. *Nutrition reviews*, 65(10), 439-450.

Malleshi, N. G., Daodu, M. A., & Chandrasekhar, A. (1989). Development of weaning food formulations based on malting and roller drying of sorghum and cowpea. International Journal of Food Science & Technology, 24(5), 511-519.

Malomo, S. A., He, R., & Aluko, R. E. (2014). Structural and functional properties of hemp seed protein products. *Journal of food science*, 79(8), C1512-C1521.

Malomo, S. A., & Aluko, R. E. (2015). Conversion of a low protein hemp seed meal into a functional protein concentrate through enzymatic digestion of fibre coupled with membrane ultrafiltration. *Innovative Food Science & Emerging Technologies*, 31, 151-159.

Melini, F., Melini, V., Luziatelli, F., & Ruzzi, M. (2017). Current and Forward-Looking Approaches to Technological and Nutritional Improvements of Gluten-Free Bread with Legume Flours: A Critical Review. *Comprehensive Reviews in Food Science and Food Safety*, 16(5), 1101-1122.

Motevali, A., Minaei, S., & Khoshtagaza, M. H. (2011). Evaluation of energy consumption in different drying methods. *Energy Conversion and Management*, 52(2), 1192-1199.

Multari, S., Stewart, D., & Russell, W. R. (2015). Potential of fava bean as future protein supply to partially replace meat intake in the human diet. *Comprehensive Reviews in Food Science and Food Safety*, 14(5), 511-522.

Mundi, S., & Aluko, R. E. (2012). Physicochemical and functional properties of kidney bean albumin and globulin protein fractions. *Food Research International*, 48(1), 299-306.

Ozdal, T., Capanoglu, E., & Altay, F. (2013). A review on protein–phenolic interactions and associated changes. *Food Research International*, 51(2), 954-970.

Parker, T. D., Adams, D. A., Zhou, K., Harris, M., & Yu, L. (2003). Fatty acid composition and oxidative stability of cold-pressed edible seed oils. *Journal of food science*, 68(4), 1240-1243.

Raak, N., Symmank, C., Zahn, S., Aschemann-Witzel, J., & Rohm, H. (2017). Processing-and product-related causes for food waste and implications for the food supply chain. *Waste management*, 61, 461-472.

Ramachandran, S., Singh, S. K., Larroche, C., Soccol, C. R., & Pandey, A. (2007). Oil cakes and their biotechnological applications–A review. *Bioresource technology*, 98(10), 2000-2009.

Schutyser, M. A. I., & Van der Goot, A. J. (2011). The potential of dry fractionation processes for sustainable plant protein production. *Trends in food science & technology*, 22(4), 154-164.

Schutyser, M. A. I., Pelgrom, P. J. M., Van der Goot, A. J., & Boom, R. M. (2015). Dry fractionation for sustainable production of functional legume protein concentrates. *Trends in Food Science & Technology*, 45(2), 327-335.

Shewry, P. R., & Casey, R. (1999). Seed proteins. In Seed proteins (pp. 1-10). Springer, Dordrecht.

Slavin, J. L., Jacobs, D., & Marquart, L. (2000). Grain processing and nutrition. *Critical Reviews in Food Science and Nutrition*., 40(4), 309-326.

Tenorio, A. T., Gieteling, J., De Jong, G. A., Boom, R. M., & Van Der Goot, A. J. (2016). Recovery of protein from green leaves: Overview of crucial steps for utilisation. *Food chemistry*, 203, 402-408.

Thorpe, J., & Beal, J. D. (2001). Vegetable protein meals and the effects of enzymes. BEDFORD, MR; PARTRIDGE, GG Enzymes in farm nutrition. Londres: Cab International, 125-143.

Vitaglione, P., Napolitano, A., & Fogliano, V. (2008). Cereal dietary fibre: a natural functional ingredient to deliver phenolic compounds into the gut. *Trends in Food Science & Technology*, 19(9), 451-463.

van der Goot, A. J., Pelgrom, P. J., Berghout, J. A., Geerts, M. E., Jankowiak, L., Hardt, N. A., ... & Boom, R. M. (2016). Concepts for further sustainable production of foods. *Journal of Food Engineering*, 168, 42-51.

Wang, M., van Vliet, T., & Hamer, R. J. (2004). How gluten properties are affected by pentosans. *Journal of Cereal Science*, 39(3), 395-402.

Wang, X. S., Tang, C. H., Yang, X. Q., & Gao, W. R. (2008). Characterization, amino acid composition and in vitro digestibility of hemp (*Cannabis sativa* L.) proteins. *Food Chemistry*, 107(1), 11-18.

Wright, D. J., & Bumstead, M. R. (1984). Legume proteins in food technology. *Phil. Trans. R. Soc. Lond. B*, 304(1120), 381-393.

Yin, S. W., Tang, C. H., Cao, J. S., Hu, E. K., Wen, Q. B., & Yang, X. Q. (2008). Effects of limited enzymatic hydrolysis with trypsin on the functional properties of hemp (*Cannabis sativa* L.) protein isolate. *Food chemistry*, 106(3), 1004-1013.

Experiment 6:

Evaluation of the technological properties of unrefined ingredients from *Cannabis sativa* L. hemp seeds, intended for food formulations

Cannabis sativa L. is subjected to a renewed interest as important source of food, fiber, and medicine. Although it is one of the oldest crops, the availability of non-drug varieties of hemp seed possessing low δ-9-tetrahydrocannabinol contents has increased industrial utilization in the last years. Regarding food manufacture, hemp seed processing primarily involves cold-pressing to recover oil and leave behind a high protein meal (HSM), containing about 25% protein of high nutritional quality. But the effective utilization of this by-product in food formulations still requires a deeper knowledge of mechanisms driving and affecting its technological performance. This works aimed to explore HSM functional properties, and how they are influenced by different factors (i.e. cultivar, granulometry, pH).

6.1 Materials and methods

The HSM used in this work were kindly provided by two different suppliers, Erba Voglio (Brescia, Italy) and Le Canapaie (Nocera Umbra, Italy), and were obtained from Finola and Carmagnola variety respectively. All the chemicals were supplied by Sigma-Aldrich S.r.l. (Germany) at analytical grade.

6.1.1 Sample pre-treatment

The fat was removed through solvent extraction using hexan 1:20 ratio w/v in agitated condition with a magnetic stirrer for 5 hours. Later, hexan/oil mixture was filtered with filter paper n. 113v (Whatman International LDT, UK) and the solid residue was dried overnight. The defatted sample was sieved by means of the analytical sieve shaker Octagon Digital (Endecotts Ltd., England), by using 3 certified sieves with pore size of 90, 125 and 250 μm.

For the technological characterization, five different samples were compared/considered: HSM as it is (HSM), defatted HSM (d-HSM), defatted HSM with particles size < 90 μm (S-HSM), < 125 μm (M-HSM) and > 125 μm (L-HSM).

6.1.2 Chemical characterization

Proximate analysis

Moisture was determined gravimetrically at 103 °C according to the Regulation 2009/152/EU. Ash content was measured with a gravimetric method by means of a muffle furnace at 550°C, AOAC 942.05 (Thiex *et al.*, 2012). The total nitrogen content was quantified according to the Kjeldahl method; the protein content (g/100 g db) was then calculated adopting 6.25 as conversion factor (AOAC 2011.11). Lipid content was determined by weighting the dry residue obtained after extraction with petroleum ether ccording to Italian D.M. 21/12/1998 – GU no. 31 8/2/1999 suppl. no. 13 (Decreto Ministeriale, 1999). Raw fiber was quantified as organic residue subsequent to chemical digestion with H_2SO_4 0.255 N and NaOH 0.313 N, AOCS Approved Procedure Ba 6a-05 (ANKOM, 2008).

For the quantitative analysis of cannabinoids, 50 mg of each product were macerated in 5 mL methanol; after centrifugation (5 min at 4000 rpm), 50 μL of the supernatant were decanted, filtered and analyzed by GC/FID for the quantitative determination of the active principles. GC/MS analyses were performed using an Agilent 6890/5973 GC-MS instrument (Santa Clara, CA, US) equipped with aN Agilent DB-5MS capillary column (30 m × 0.25 mm i.d., 0.25 μm film thickness).

6.1.3 Protein profile assessment

Protein extraction

All the samples evaluated were previously defatted as described in **paragraph 6.1.1**. Proteins were extracted from defatted hemp seed meal immersed in 100 mM Tris–HCl/0.5 M NaCl buffer (1:10 w/v), pH 8, at 4 °C under magnetic stirring overnight. After centrifugation at 6500 g, for 30 min at 4 °C, the supernatant was dialyzed against 100 mM Tris–HCl buffer pH 8.2 for 36 h at 4 °C. At the end, the hemp seed protein extract was recovered by centrifugation at 6500 g, for 30 min at 4 °C.

Bradford assay

The protein concentration of the protein extract was determined using the Bradford assay reagent with bovine serum albumin as the standard. The absorbance of the standards and unknown sample was determined at 595 nm.

SDS-PAGE electrophoresis

The hemp seed protein extract was loaded onto the SDS-PAGE gel in a specific volume for each sample in order to have the same protein content, as deduced by Bradford assay. The gel was composed of a 4% polyacrylamide stacking gel over a 12% resolving polyacrylamide gel. The cathodic and anodic compartments were filled with Tris–glycine buffer, pH 8.3, containing 0.1%, m/v, SDS. The electrophoresis was conducted at 100 V until the dye front reached the gel bottom. Staining was performed with colloidal Coomassie Blue and destaining with 7% (v/v) acetic acid in water. The image was acquired by means of a scanner.

6.1.4 Physical and technological characterization

The distribution of the particle size according to granulometry classes was performed by gravimetric method after sieving the material with the analytical sieve shaker Octagon Digital (Endecotts Ltd., England), by using 5 certified sieves with pore size of 40, 90, 125, 250 and 250 μm.

The water binding capacity (*WBC*) and oil binding capacity (*OBC*) were assessed according to the method described by Malomo *et al*. (2014) with slight modifications. Protein sample (2 g) was dispersed in 10 mL distilled water (or sunflower oil) in a 15 mL preweighed centrifuge tube. The dispersions were allowed to stand for 30 min and then centrifuged at 7000 × g for 25 min at room temperature. The supernatant was decanted, and the tube containing the precipitate was weighed again to determine amount of water or oil retained per gram of sample.

For foaming capacity (*FC*) determination, the sample was suspended in aqueous media (acetate buffer pH 4, phosphate buffer pH 7 and pH 10) at 2% (w/v) in order to investigate the effect of the pH on this parameter. The suspension was homogenized at 20000 rpm for 1 min using an Ultra-Turrax (Ika, Germany) homogenizer (shaft S-25N-10G). The capacity of the continuous phase to include air (*FC*) was determined as follows:

$$FC = \frac{V_f - V_i}{V_i} \qquad \textbf{(eq. 6.1)}.$$

Where V_f is the volume of the suspension after homogenization and V_i is the volume of the suspension before homogenization. The ability to retain air for a certain period of time (foam stability, *FS*) was calculated by measuring the foam volume after storage at room temperature 60 min and expressed as percentage of the original volume.

Emulsions were prepared by suspending the sample in aqueous media (10% w/v) and adding sunflower oil in a ratio 1:5 (oil:suspension). The mixture was homogenized at 20000 rpm for 1 min using Ultra-Turrax (Ika, Germany) homogenizer (shaft S-25N-10G). For each sample three different pH conditions were considered using three different dispersion media (acetate buffer at pH 4, and phosphate buffer at pH 10). Emulsion stability was evaluated using a Turbiscan Tower instrument (Formulaction, France). The principles underlying the operativity of this instrument was detailed by Lemarchand *et al.* (2003). Briefly, the emulsion sample was transferred to a cylindrical glass cell and analyzed by a light beam emitted in near infrared (850 nm) wavelength which scanned the sample cell from the bottom to the top. Two synchronous optical sensors received respectively the light transmitted through the sample and the light backscattered by the sample. By scanning the sample at preset intervals, a pattern of the light flux backscattering as a function of the sample height was obtained, giving a macroscopic fingerprint of the sample at a given time. The changes in the emulsion stability were monitored for 18000 s.

6.1.5 Rheological analysis

The viscoelastic behavior of aqueous suspensions of HSM was studied by using a CMT rheometer (DHR-2, TA Instruments, USA) equipped with a 40 mm diameter plate-plate geometry, with a gap of 1 mm. A solvent trap provided by the manufacturer for liquid samples was used to prevent loss of solvent. Aqueous suspensions of HSM were studied at different concentrations (10%, 20%, 30% w/v), using two different materials with particle size < 90 μm and <125 μm (S-HSM and M-HSM).

First, oscillatory strain sweeps were performed to determine the linear viscoelastic region for each sample. Frequency sweep experiments were then performed at low amplitude of strain (0.2%, in linear regime) in the frequency range of 0.1–100 rad/s. The tests were performed at different time after water addition (5-240 min), at constant concentration 25% (w/v), to identify the time required to get a complete hydration of the components.

6.1.6 Statistical analysis and mathematical fitting

Data were processed by Origin for Windows v. 9.1 (OriginLab Corporation, USA) for both statistical analysis and mathematical modelling. Statistical significance was found by One-Way ANOVA, Fisher's LSD *post hoc* test was used to analyze differences. The presented data (arithmetic mean value ± standard deviation) resulted from at least three independent experiments ($n \geq 3$), the value of $p \leq 0.05$ was considered as significant.

6.2. Results and discussion

6.2.1 Particle size distribution

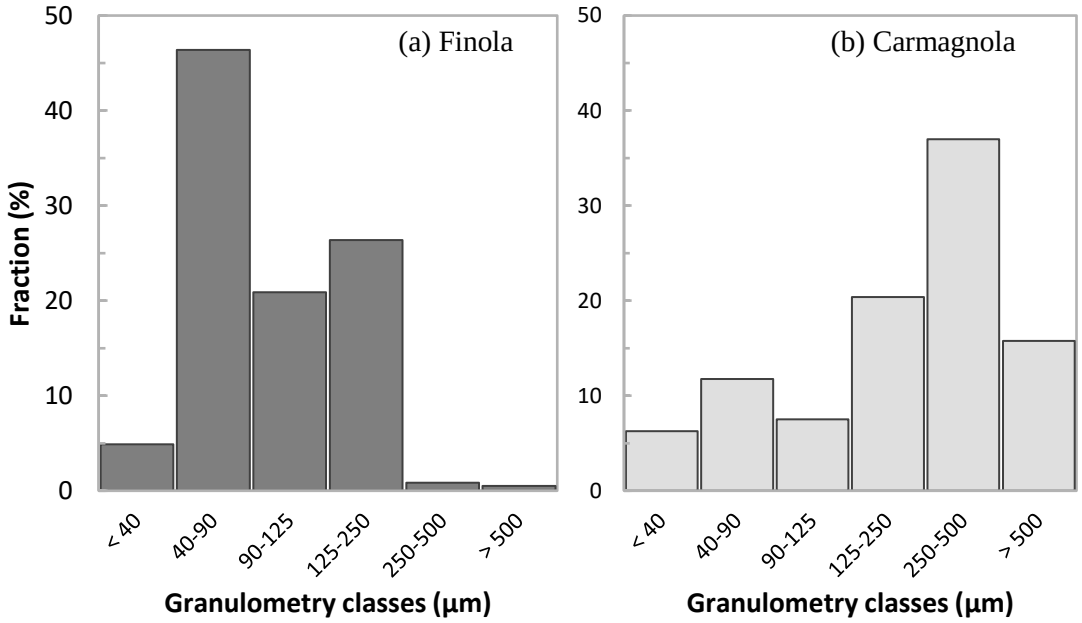

Figure 6.1 Mass distribution of the two HSM (a: Finola; b: Carmagnola) in granulometry classes.

In **figure 6.1**, it is reported the relative mass distribution in granulometry classes of HSM obtained from Finola and Carmagnola cultivars based on their particle size. For Finola HSM, more than half of the sample mass (51.27%) display a granulometry lower than 90 μm, while negligible fraction (1.37%) was detected for particle size > 250 μm. Carmagnola HSM is characterized by a greater granulometry, with 52.75% of the mass fraction belonging to classes with particle size > 250 μm. If we consider 125 μm as critical particle size, Finola HSM presents 72.15% of mass fraction below this limit while Carmagnola HSM presents 73.12% of its mass fraction with a

granulometry greater than this critical size. Considered the net asymmetry of the distribution of Finola HSM, the different granulometry could be ascribed to a sieving step applied to the material by the producer before commercialization with the aim of reducing fiber content and concentrating proteins.

6.2.2 Proximate analysis

The proximate composition and cannabinoid content of the two meals (namely, Finola and Carmagnola) is reported in **table 6.1**. The values obtained for moisture, total fat and ash are comparable for the two cultivars, and agree with other results from literature (House *et al.*, 2010; Pojić *et al.*, 2014). On the contrary, protein content showed values significantly higher for HSM Finola (53.82%) compared to HSM Carmagnola (26.64%). From the literature, crude protein content is generally ranged between 25-33% (Vonapartis *et al.*, 2015; Latif & Anwar, 2009; Russo & Reggiani, 2015). The increase in protein content in Finola sample can be justified by the manufacture pre-treatment, which has been hypothesized to include a sieving step (**paragraph 6.2.1**) for the partial removal of fiber.

Cannabinoids are not explicitly produced within the seed, but traces of contamination have been reported to result from the pressing of the oil (Grotenhermen *et al.*, 1998). They are widely reported to exert many health benefits (anticonvulsive, anti-epileptic, and antimicrobial properties) may still be gained from its presence (Ashton, 1999; Leizer *et al.*, 2000).
The CBD content was quantified to be 2.9 and 3.9 μg/g for Finola and Carmagnola HSM, in agreement with results previously reported (Food Standards Australia New Zealand, 2017) ranging between 0.1 and 5 μg/g. The higher cannabinoids content in Finola HSM was reflected also in its acidic precursor (CBD-A) concentration that is almost six-fold higher than for Carmagnola HSM. The main cause of the different cannabinoid concentration can be identified in the diverse cultivar, but also the sieving applied to Finola HSM has been reported to have a positive effect on phenols concentration (Pojić et al., 2014).
The THC concentration was not detectable and thus it is considered under the legal limit (0.2%) for food application set by European Recommendation (EU) 2016/2115.

Table 6.1 Comparison of proximate composition and cannabinoid content between hemp seed meal obtain from two different cultivars (*Finola* and *Carmagnola*).

	HSM Finola	HSM Carmagnola
Moisture (%)	4.02	4.32
Crude protein (%)	53.82*	26.64*
Total fat (%)	10.82	10.79
Crude fiber (%)	9.16*	32.68*
Ash (%)	8.14	6.75
CBD (mg/g)	0.0039±0.009	0.0029±0.003
CBD-A (mg/g)	0.1805±0.034	0.0336±0.067
THC (mg/g)	n.d.	n.d.

6.2.3 Protein profile

In **table 6.2**, the protein concentration of protein extracts from HSM differing for cultivar and particle size. The samples obtained from Finola HSM showed a double protein concentration compared to those obtained from Carmagnola HSM, confirming the results in **table 6.1**. The particle size did not have the same effect on protein concentration for the two cultivars. Carmagnola extracts underwent a reduction in protein concentration from 1.288 to 0.802 μg/μL

after selecting the fraction with particle size > 125 μm, and this last value is almost the half if compared with the fraction with particle size < 90 μm. This behavior suggests that physical fractionation could represent an efficient method for concentrating protein components in hemp seed meal. Differently, a similar trend was not observed for Finola extracts but it can be hypothesized that, in this case, the removal of fiber excess in favor of protein concentration had already occurred during sieving pretreatment.

Table 6.2 Protein concentration in hemp seed protein extracts from defatted meal as it is (d-HSM) and after sieving (S-HSM, M-HSM, L-HSM), according to Bradford method**.**

	Protein concentration (μg/μL)	
	Finola	*Carmagnola*
d-HSM	2.769±0.097	1.288±0.177
S-HSM	2.818±0.077	1.633±0.071
M-HSM	2.682±0.084	1.714±0.239
L-HSM	2.771±0.139	0.802±0.052

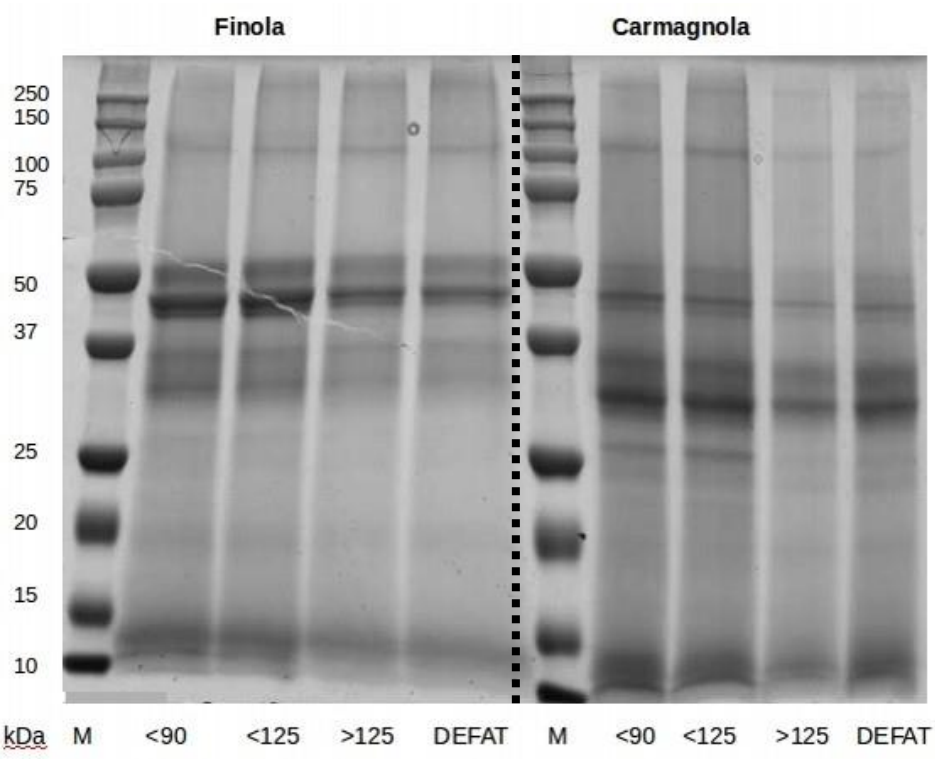

Figure 6.2 SDS-PAGE profiles of the hemp seed protein extract obtained from the two cultivars with different granulometry (< 90 μm, < 125 μm and > 125 μm) and defatted HSM. M: molecular mass ladder. Staining with micellar Coomassie blue.

Figure 6.2 shows the SDS-PAGE electrophoretic profile of hemp seed protein extract from defatted meal as it is (d-HSM) and after sieving (S-HSM, M-HSM, L-HSM) for the two cultivars. The miscellaneous bands of about 50-47 kDa, more evident for Finola, contains the main polypeptide in the HSM products and was attributed to edestin (Wang *et al.*, 2008; Malomo & Aluko, 2015). Other polypeptides are apparent in the 14, 25, and 34 kDa bands, in accordance with previous studies (Aiello *et al.*, 2016; Malomo et al., 2014), and are more evident for Carmagnola. From the comparison of the profile of d-HMS extract from the two cultivars, it emerges that the protein fraction presented significant differences in terms of relative composition. The cultivar was found to be a main factor determining variability of protein profile

also by other authors, when comparing results obtained by the analysis of different varieties (Malomo & Aluko, 2015). On the contrary, sieving did not affect the protein profile from a qualitative point of view.
Thus, as expected, seed cultivar significantly influences protein expression, both in terms of quantity and composition, that is assumed to induce a different functional and technological performance of the material.

6.2.4 Rheological Analysis

Kinetic Evolution of Viscoelastic Properties
The rheological behavior of aqueous dispersions (25% w/v) of defatted HSM fraction with a particle size < 125 µm is studied. Frequency sweep test were performed at different time and the complex modulus (*G**), related to the strength of interactions between units (Phillips & Williams, 2009), was monitored as reported in **figure 6.3** for both cultivars.

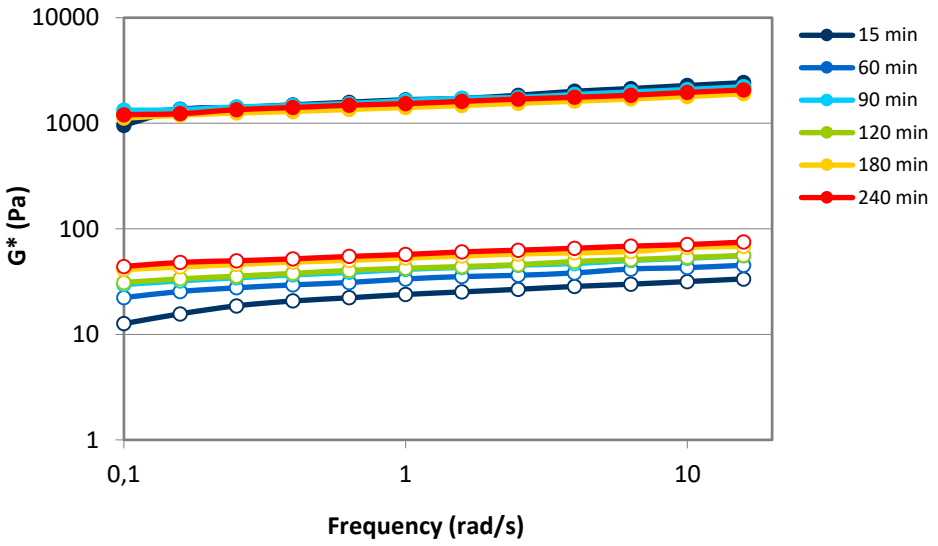

Figure 6.3 Complex modulus (*G**) of Finola (full circles) and Carmagnola (hollow symbols) M-HSM water dispersion (25% w/v) as a function of frequency, measured at different time ranging between 15 and 240 min.

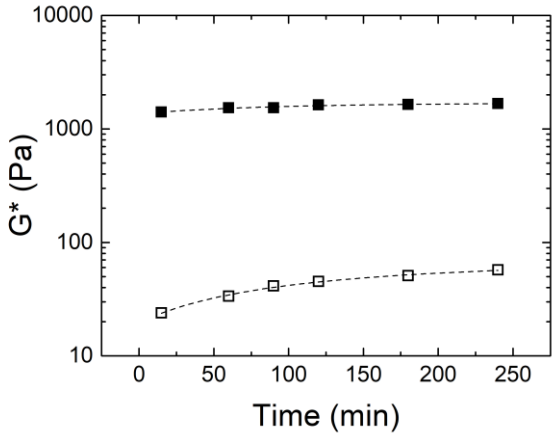

Figure 6.4 Kinetic profile of the complex modulus (*G**) of Finola (full circles) and Carmagnola (hollow symbols) M-HSM water dispersion (30% w/v).

If we consider Finola HSM, *G** curves are overlapped, with no show significant differences, already after one hour; on the other hand, the same parameters underwent an increase in time for

several hours for Carmagnola HSM. In **figure 6.4**, the G* values measured at a frequency of 1 rad/s are plotted as a function of the time to evidence the kinetical evolution of the structuring properties. The kinetic profiles followed a first order kinetic and were described using the exponential model:

$$G^* = G^*_{max} + a\ exp\ (time/\tau) \qquad \text{(eq. 6.1)}$$

where τ represents the growth constant (min). The present elaboration allowed to quantify the rate of the structuring phenomenon (k; min^{-1}), which is the inverse of the growth constant $\tau = 1/k$, for the two samples. The rate was equal to 6.40 and $10.71 \cdot 10^{-3}$ Pa/min for Carmagnola and Finola HSM, respectively. The different values of k indicate that Finola components evolve their organization after hydration in a faster manner compared to Carmagnola ones, reaching faster an equilibrium state. This behavior may be ascribed to the different composition, mainly in terms of protein content and profile. However, it is not excluded that fibers and particles structural organization (e.g. the presence of pores) can contribute to accelerate the network formation kinetic.

Viscoelastic properties

The dynamic frequency sweep results for three concentrations of M-HSM aqueous suspensions are shown in **figure 6.5**. Considering Finola products, all the shapes of the *G'* and *G"* curves were parallel and *G'* were almost one order of magnitude greater than *G".* The values of *G'* and *G"* were almost independent on the frequency, with $G' \approx \omega^{0.1}$. The values of tanδ were in the range of 0.1-0.3. This implied that the hemp seed meal exhibited viscoelastic solid-like properties. These results are in agreement with other studies focused on vegetal protein dispersions, such as lupin and soy (Xu & Mohamed, 2003; Shimada & Matsushita, 1980; Tan *et al.*, 2014).

These observations were true also for Carmagnola products, with the exception of the sample at 10% (w/v). In this case, dynamic moduli were almost overlapped, with tan(δ) ranged between 0.3 and 0.6, and a significant dependence on frequency. It means that Carmagnola M-HSM behave as a really weak gel at this concentration, while all the other samples exert dynamic properties typical of strong gels (Chen *et al.*, 2010). These differences in viscoelastic behavior between the two cultivars can be due to the different protein content, that is noticeably lower (about one half) in Carmagnola HSM.

It is also evident from the **figure 6.6** that the response of HSM dispersions is strongly dependent on the concentration. Thus, the G^* values obtained at 1 rad/s were plotted as a function of the concentration, for both M-HSM and S-HSM. Since it appeared a quite linear distribution of the values in the log-log plot, for Finola samples we can hypothesize that G^* have a power law dependence on the concentration, according to the equation $G^* = G^*_0 + kc^{\beta}$, where the exponent parameter β reflects the structural properties of the whole suspension. Finola S-HSM and M-HSM presented a β value equal to 5.13 and 5.42 Pa·ml/g (R2 = 0.999). This is characteristic of colloidal aggregates (Daniel & Audebert, 1999). A power law dependence was found also for the two highest concentrations (20% and 30% w/v) of Carmagnola HSM dispersions, with a similar slope as highlighted in **figure 6.6b**, while the dispersion at 10% (w/v) deviated from this model. It can be explained by the fact that model applicable to strong polymeric gels (Guenet, 2000), that is not the case of HSM dispersions at 10%.

We can deduce that the HSM variety, which is reflected in a different composition, significantly affected the viscoelastic properties of the materials. At the lower concentrations (10 and 20 %) Carmagnola HSM is characterized by a weaker structure than Finola samples, and this finding

agrees with the smaller value of protein concentration. At 30%, the situation is reverse, and to explain the fact, it can be hypothesized that other compounds (e.g. fibers), exceeded a critical threshold of concentration, can contribute to the material structuring.

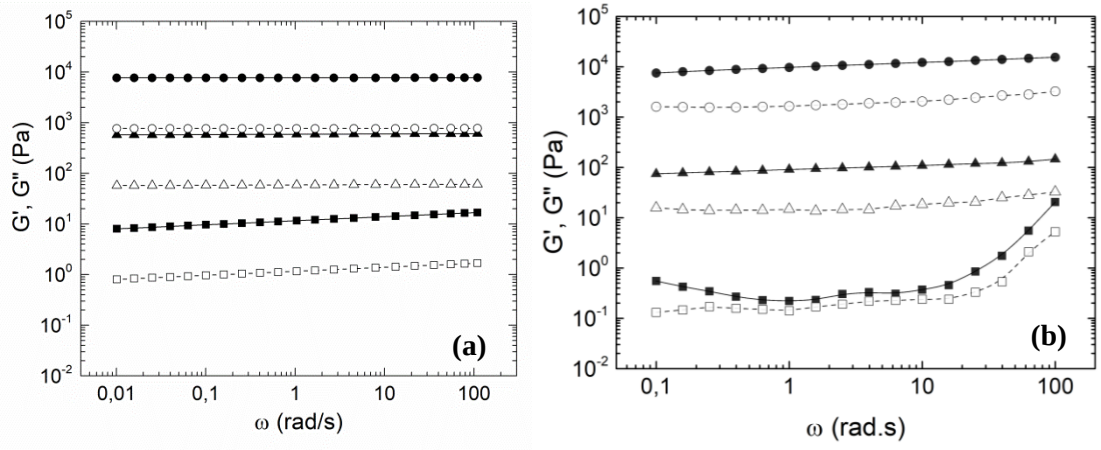

Figure 6.5 Dynamic moduli (*G'*, full symbol, and *G"*, hollow symbol) of Finola (a) and Carmagnola (b) M-HSM at different concentration (10%: square, 20%: triangle, 30%: circle) as a function of frequency.

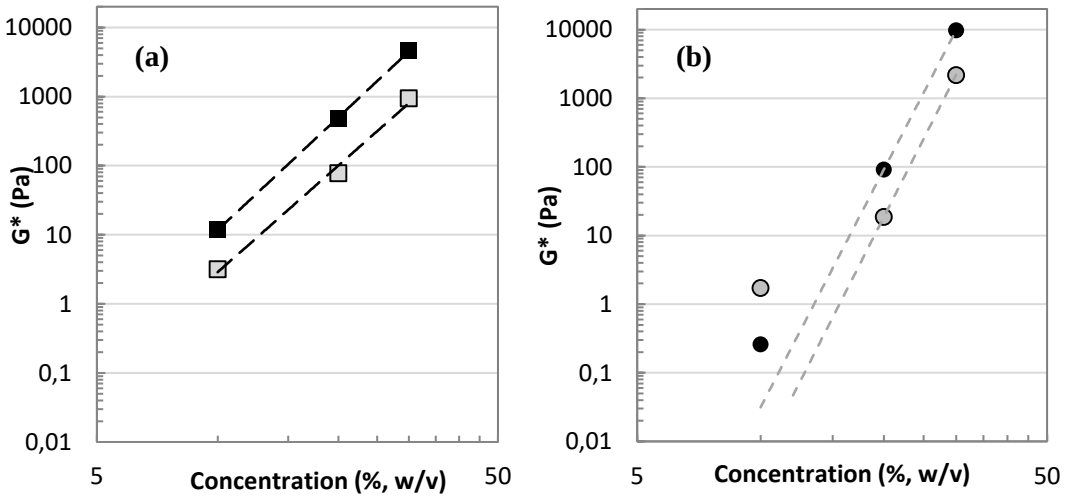

Figure 6.6 Complex modulus (*G**) dependence on the concentration for Finola (a) and Carmagnola (b) HSM with particle size < 125 μm (black symbols) and < 90 μm (grey symbols). The power law fitting for Finola HSM is reported as black dotted line ($R^2 > 0.99$).

6.2.5 Functional properties assessment

Beyond their roles in nutrition, bioactivity, and health, the value of food proteins extends to include functional properties such as solubility, water binding, fat absorption, emulsifying, foaming, and gelation. These properties make food proteins versatile and useful ingredients in a wide range of product development, formulation, and other applications (Arvee, Agyei & Udenigwe, 2017). Thus, these specific functional properties (water and oil binding capacity, WBC and OBC, foaming capacity and stability, FC and FS) were selected as indices of HSM technological performance, to investigate how it is influence by modifying productive factor and conditions (cultivar, granulometry, pH).

Cultivar and pre-treatment effect

The values of functional parameters (*WBC*, *FHC*, *FC*, *FS*) for HSM from both cultivars, before and after defatting, are reported in **figure 6.7**. Concerning the ability of retaining water and oil,

Finola samples showed higher values of *WBC* and *OBC* than Carmagnola material when tested as it is. The different behaviour can be explained both by the qualitative and quantitative differences in the protein fraction. On the other hand, physical entrapping (Cadden, 1987) would be favoured by the higher granulometry of Carmagnola meal but it seems to have a minor impact on the final results.

Defatting pre-treatment determined an increase in retention parameters for all samples, likely because the steric hindrance of hemp seed oil limited the binding of both water and oil (Galla & Dubasi, 2010). Despite the similar fat content, Finola-derived ingredient showed a more significant improvement in technological performance after defatting confirming the primary role of protein affinity in solvent retention. In particular, Finola HSM displayed more affinity to oil than water, differently from Carmagnola HSM that exerted similar values for *WBC* and *OBC*. Indeed, from SDS-PAGE (**figure 6.2**), Finola protein extracts seem to be relatively more rich in globulin (i.e. edestin) than Carmagnola extracts, with more intense profile in correspondence of albumin bands. It is known (Malomo et al., 2015) that globular protein in hemp seed have a higher content of hydrophobic groups and it may be reflected in a higher affinity to non-polar media.

These observations related to cultivar effect were confirmed also by foaming properties assessment. Carmagnola HSM containing particles with size > 125 μm was not able to produce enough foam for measurements, thus only defatted HSM with granulometry < 125 μm were compared. In this case *FC* is doubled for Finola compared to Carmagnola, and also the stability of the two foams was significantly different. It may be explained by the minor protein content in Carmagnola HSM, since proteins are able to form viscoelastic interfacial membranes through protein-protein interactions and enhance resistance of air bubbles to destabilization. These results agree with previous works (Aluko *et al.*, 2009; Malomo *et al.*, 2015), which showed that samples with higher protein concentration formed more stable foams than samples with lower protein content.

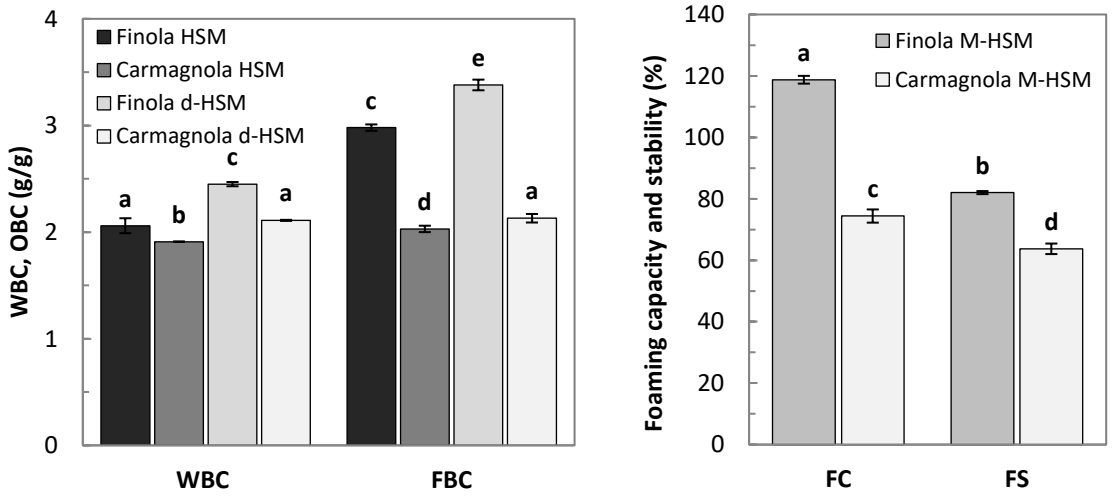

Figure 6.7 (Left) Water and oil binding capacity (*WBC* and *OBC*) and (right) foaming capacity and stability (*FC* and *FS*) of hemp seed meal products obtained from different cultivars, before and after defatting pre-treatment.

Granulometry effect

The *WBC* and *OBC* values recorded for HSM products with three different particle size distributions are shown in **figure 6.8**. The ability to retain water was maximized by increasing the sample granulometry, on the contrary oil retention reached its minimum value for samples with the smallest particle size. It can also be highlighted that the finest sample (S-HSM) displayed a

more pronounced affinity for oil than water (*OBC>WBC*), but the situation was completely reversed for the material with greater particle size (which display a higher affinity for water than oil: *WBC > OBC*). Water retention may be favored by the higher fibers content, which are mainly constituted by hull fibres containing largely water-insoluble polysaccharides (i.e. cellulose, hemicelluloses, lignin) (Tosh & Yada, 2010, Gorecka *et al.*, 2000). Since these polysaccharide chains are rich in –OH groups, they bind high amount of water to get complete hydration. This hypothesis is supported by the fact that *WBC* values for L-HSM are in agreement with results obtained for hull from other seeds, typically ranging between 2-4 ml/g (Gorecka *et al*., 2010). Concerning oil absorption, this phenomenon seems to be favored by size reduction, likely due to the higher protein concentration (Kaur & Singh, 2005). Indeed, hemp seed proteins are rich in hydrophobic residues that can act as oil binding sites (Malomo & Aluko, 2015), and *OBC* values are comparable with results obtained for hemp protein isolates (Yin *et al.*, 2008).

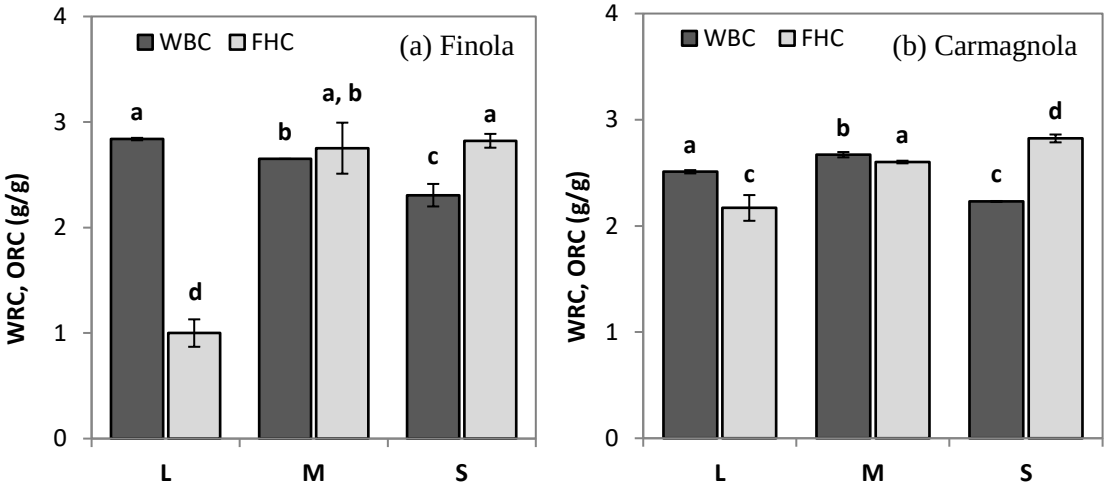

Figure 6.8 Water and oil binding capacity (*WBC* and *OBC*) of hemp seed meal products characterized by different particle size (L-HSM: > 125 μm; M-HSM: < 125 μm; S-HSM: < 90 μm) obtained from Finola (a) and Carmagnola (b) cultivars.

As evident in **figure 6.9**, both foaming capacity and stability reached a maximum value in correspondence of HSM with particle size < 125 μm (respectively: 118.75 and 74.39 % for Finola, 82.02 and 63.72 % for Carmagnola). Products with the greatest particle dimension (> 125 μm) displayed the lowest foaming capacity. It is likely that the presence of large particles in the cell wall of a foam promotes rupture of the wall (Frye & Berg, 1989) and hinders, in some cases inhibits, foam formation. Moreover, L-HSM contains less proteins than the other two samples, confirming the primary role of the protein fraction in foaming ability by reducing surface tension between oil and aqueous phases. Comparing M-HSM and S-HSM, the foaming parameters for the coarser meal are almost doubled than the same parameters for the finer meal. If we recall that the two materials have almost the same protein content, the difference in the functional response cannot be attributed to surface activity but foaming could be favored by the higher viscosity of the material (as shown in **figure 6.10**) or the presence of solid particles that increase the rigidity of the interfaces. Indeed, it is known that foam can be stabilized through a combination of proteins and polysaccharides, reducing surface tension between oil and aqueous phases and augmenting viscosity (Georgieva *et al.*, 2008).

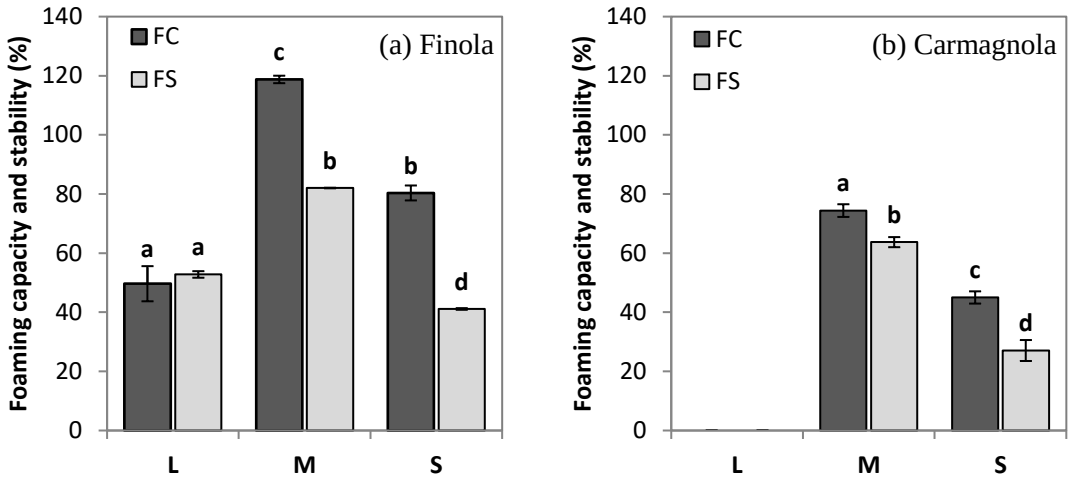

Figure 6.9 Foaming capacity and stability (*FC* and *FS*) of hemp seed meal products characterized by different particle size (L-HSM: > 125 μm; M-HSM: < 125 μm; S-HSM: < 90 μm) obtained from Finola (a) and Carmagnola (b) cultivars.

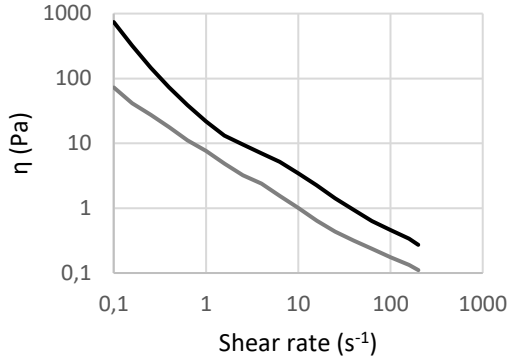

Figure 6.10 Viscosity of M-HSM (black) and S-HSM (grey) water suspensions at 20% (w/v) of Finola HSM.

We can conclude that the different granulometry seems to affect the fiber and protein distribution in the products, with important consequences on the interaction with solvents and foaming abilities. In support of this thesis, a similar behavior was observed by comparing functional properties of hemp seed meal and protein isolate in a previous study (Malomo *et al*., 2014).

Effect of pH

Figure 6.11 and **6.12** display *WBC*, *FC* and *FS* values for M-HSM obtained from both cultivars and dispersed in water media at different pH in order to investigate the effect of pH conditions on the functionality of these materials. According to statistical analysis, only the samples dispersed in water media at pH 4 showed a significantly lower value. This behavior could be correlated to hemp seed proteins solubility, especially globulin, which reaches its minimum at pH conditions lower than 5 (Tang *et al.*, 2006; Malomo *et al.*, 2015).

The poor functional properties of HSM at pH 4 is confirmed observing foaming properties as well. The results showed that the *FC* of HSM was consistent with the solubility properties across the pH range studied. According to the literature, the formation of covalent disulfide bonds between individual proteins and subsequent aggregation at acidic pH limit their solubility (Malomo *et al.*, 2015) and also the availability of protein chains at the interface (Tang *et al.*, 2006). No significant differences were detected at pH 7 e 10.

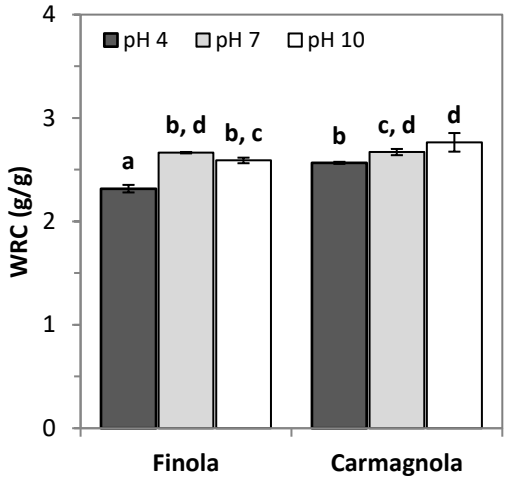

Figure 6.11 Water binding capacity (*WBC*) of hemp seed meal obtained from Finola and Carmagnola cultivars dispersed in water media at controlled pH (4, 7, 10).

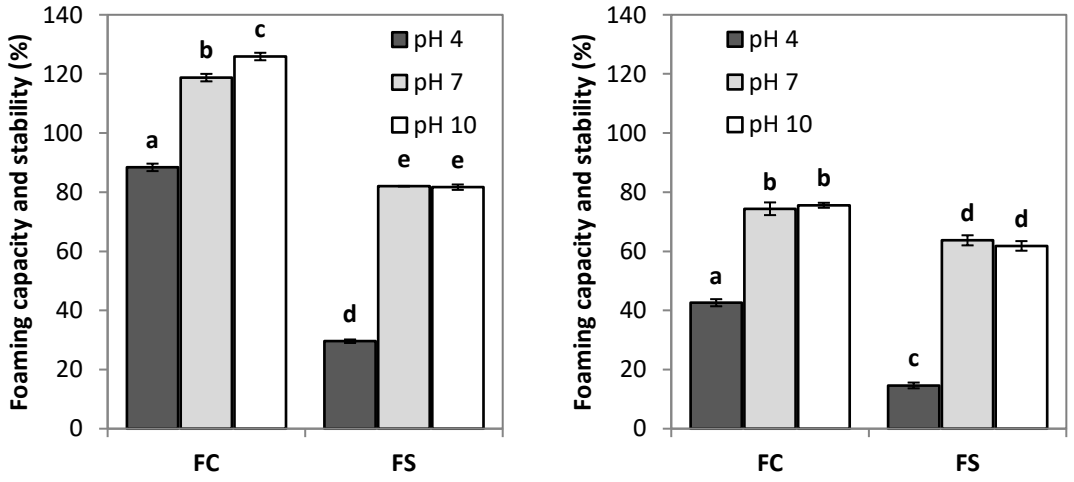

Figure 6.12 Foaming capacity and stability (*FC* and *FS*) of hemp seed meal products dispersed in water media at controlled pH (4, 7, 10) and obtained from Finola (a) and Carmagnola (b) cultivars.

3.6 Multiple light scattering

Interfacial activity of HSM was also evaluated at oil-water interface, which is characterized by higher hydrophobicity than air-water interface of foam. Emulsion stability was quantified by monitoring through multiple light scattering measurements. The differential backscattering and transmission profiles as a function of the sample height are reported in **figure 6.13**. In this way, the physical evolution of this process is followed without disturbing the original system and with good accuracy and reproducibility (Mengual *et al.*, 1999). Modifications of the curves during time can be ascribed to three different phenomena. Sedimentation of the largest particles to the bottom (0-1.5 mm), creaming in the center (1.5-29 mm) and raising of free oil onto the top of the sample.

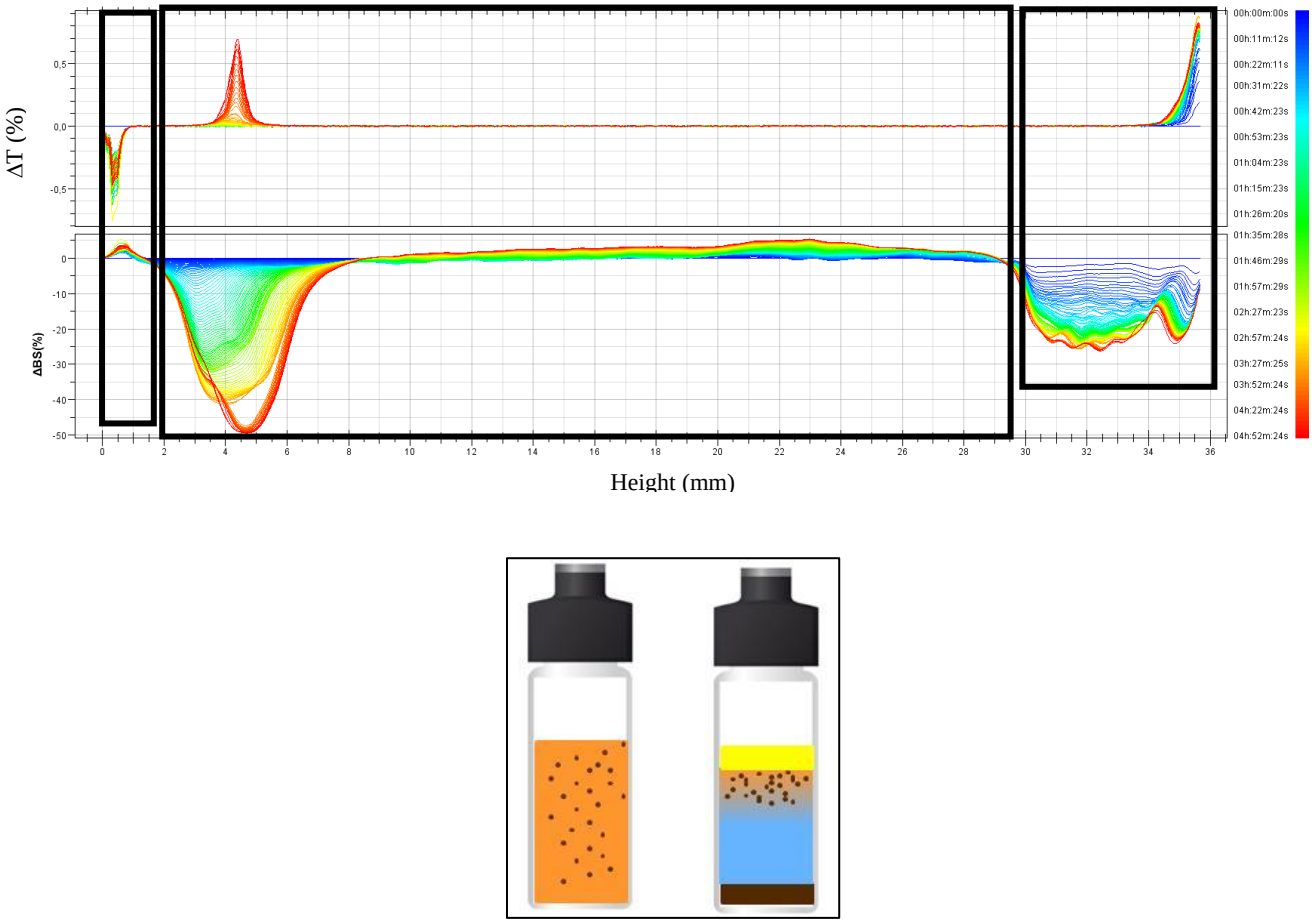

Figure 6.13 Evolution of transmission and backscattering profiles of Finola M-HSM emulsions at pH 10, as examples. Data are reported as a function of sample height in the tube, the backscattering profile at *t*=0 was regarded as the base line (Δ). Schematic representation of the instability phenomena taking place in the samples: (a) large particles sedimentation, (b) creaming, (c) free oil separation.

The creaming, that is a migration phenomenon by which emulsion droplets tend to rise to the top of a container, can be recognized by analyzing the emulsions backscattering parameter. For all the emulsions the backscattering of light was fairly constant along their entire height at the beginning of the experiment because there was an even distribution of droplets throughout the system. Over time the droplets moved upwards due to gravity which caused a decrease in the backscattering at the bottom of the emulsions (because the droplet concentration decreased) and an increase at the top (because the droplet concentration increased). The migration of oil droplets in HSM-stabilized emulsions led to the appearance of a negative peak in ΔBS% plot at about 4 mm, due to the clarification at the bottom of creaming phenomenon, that became larger as migration extended in samples. In the case of samples at pH 4, this tendency/dilution effect was so important that allowed the measurement of the transmittance signal, as reported in **figure 6.14a**. In the upper region (about 8-28 mm in **figure 6.13**), the BS values increased as a consequence of the concentration and the average of ΔBS% values measured in this region are reported as a function of time in **figure 6.14b** in order to quantify the kinetic rate of creaming. The kinetic could be described using a first order equation:

$$\Delta BS = \Delta BS_{max} + a \exp(-k^{*}\text{time}) \qquad \text{(eq. 6.2)}$$

where k is the rate of the instability phenomenon (min^{-1}). The results are shown in **table 6.3**. Samples at pH 4 were the most unstable, since they have the highest k and no statistical difference is observed between the two cultivars. If we consider emulsions produced at pH 10, Finola HSM induced a faster destabilization, with k equal to 1.01 min^{-1} that is almost double rate than Canola HSM.

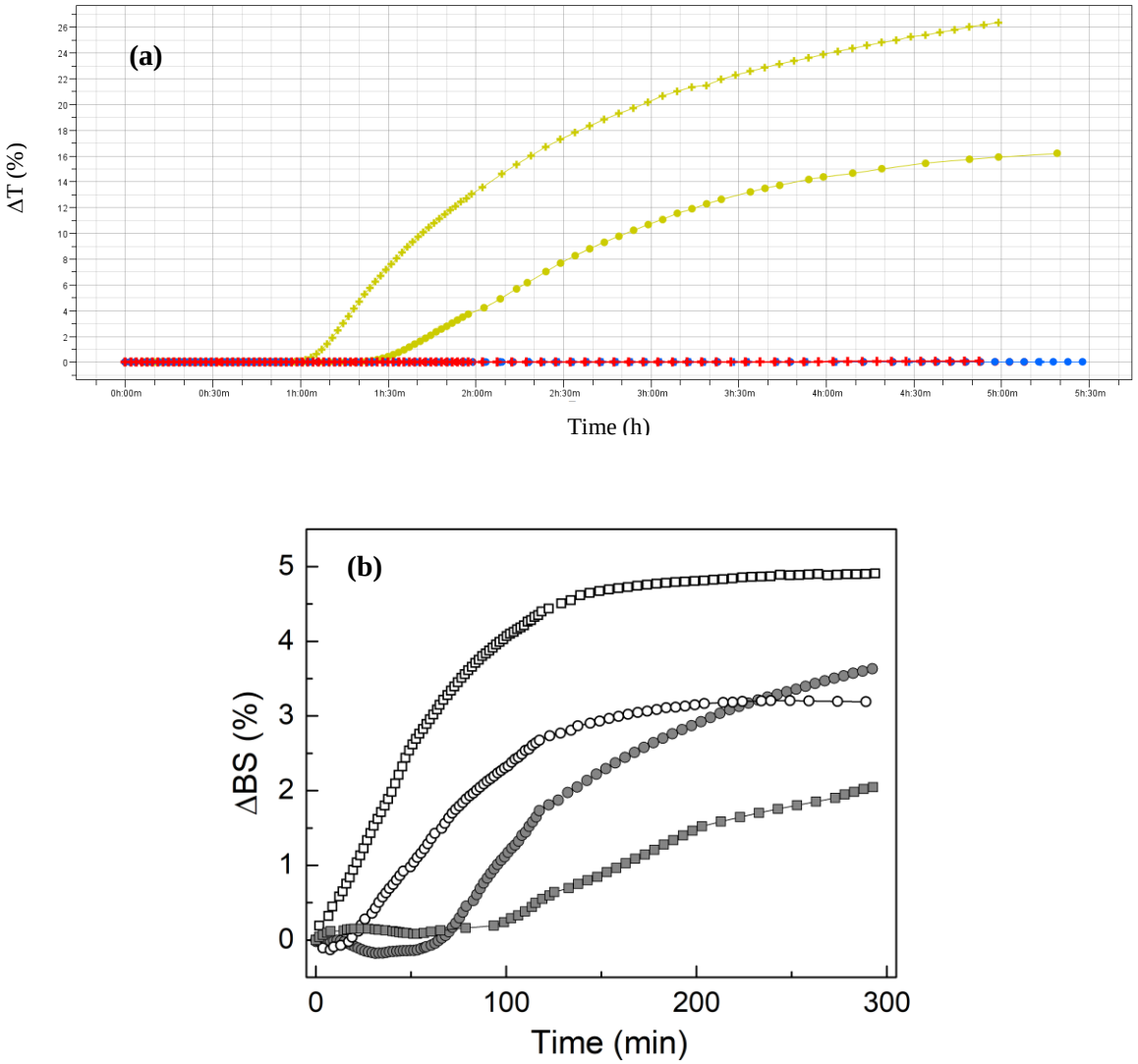

Figure 6.14 (a) Clarification in the bottom region of emulsions (4-5 mm) measured as transmittance signal, ΔT (%), during time with pH 4 (yellow) and 10 (red), and (b) evolution in time of backscattering, expressed as ΔBS (%), of emulsions in the central region (8–28 mm), where concentration of particles took place. Emulsions were stabilized with 8.33% (w/v) of M-HSM from Finola (circles) and Carmagnola (squares) at different pH conditions (pH 4: white symbols; pH 10: grey symbols).

Table 6.3 Rate of creaming (*k*, min $^{-1}$) calculated from the first-order kinetic model (**eq. 6.2**) for the emulsions were stabilized with 8.33% (w/v) of M-HSM from Finola and Carmagnola at different pH conditions.

	***k* (min^{-1})**	
	pH 4	*pH 10*
Finola HSM	1,74	1,01
Carmagnola HSM	1,77	0,52

Conclusions

The defatting treatment had a positive effect improving elastic response, WBC, OBC and foaming production ability. Particle size proved to affect functional properties as well; both WBC and OBC indicates that polarity is inversely proportional to granulometry, excepting for powders with particles size < 90 μm which shown a noticeably increased hydrophobicity. The fraction with particle size < 125 μm displayed the higher foaming ability value (almost 10-fold higher than

commercial sample), further maximized correcting pH at 7. In conclusion physical processing can be successfully applied to HSM powder with the aim of optimizing its technological performance, likely as effect of tuning material composition and structure

Aknoledgements

I thank Professor Gabriella Roda, and Dr. Gilda Aiello (Dept. of Pharmaceutical Science, UNIMI) for performing the quantification of cannabinoids and the characterization of the protein fraction.

References

Aiello, G., Fasoli, E., Boschin, G., Lammi, C., Zanoni, C., Citterio, A., & Arnoldi, A. (2016). Proteomic characterization of hemp seed (*Cannabis sativa* L.). *Journal of proteomics*, 147, 187-196.

Aluko, R. E., Mofolasayo, O. A., & Watts, B. M. (2009). Emulsifying and foaming properties of commercial yellow pea (Pisum sativum L.) seed flours. *Journal of agricultural and food chemistry*, 57(20), 9793-9800.

ANKOM. (2008). *Crude Fiber Analysis in Feeds by Filter Bag Technique. AOCS Approved Procedure Ba 6a-05*.

AOAC 2001.11:2005. *Protein (crude) in animal feed, Forage (plant tissue), Grain and oilseeds. Block digestion method using copper catalyst and steam distillation into boric acid.*

Ashton, C. H. (1999). Biomedical benefits of cannabinoids?. *Addiction biology*, 4(2), 111-126.

Decreto Ministeriale 1999. Approvazione dei metodi di analisi per il controllo ufficiale degli alimenti per animali e soppressione di altri metodi inerenti al controllo del medesimo settore merceologico. *Gazzetta Ufficiale della Repubblica Italiana* 31, 41

Frye, G. C., & Berg, J. C. (1989). Antifoam action by solid particles. *Journal of colloid and interface science*, 127(1), 222-238.

Georgieva, D., Cagna, A., & Langevin, D. (2009). Link between surface elasticity and foam stability. *Soft Matter*, 5(10), 2063-2071.

Grotenhermen, F., Karus, M., & Lohmeyer, D. (1998). THC-limits for food: a scientific study. *Journal of the International Hemp Association*, 5(2), 101-105.

Guenet, J. M. (2000). Structure versus rheological properties in fibrillar thermoreversible gels from polymers and biopolymers. *Journal of Rheology*, 44(4), 947-960.

House, J. D., Neufeld, J., & Leson, G. (2010). Evaluating the quality of protein from hemp seed (Cannabis sativa L.) products through the use of the protein digestibility-corrected amino acid score method. *Journal of agricultural and food chemistry*, 58(22), 11801-11807.

Latif, S., & Anwar, F. (2009). Physicochemical studies of hemp (Cannabis sativa) seed oil using enzyme-assisted cold-pressing. *European Journal of Lipid Science and Technology*, 111(10), 1042-1048.

Leizer, C., Ribnicky, D., Poulev, A., Dushenkov, S., & Raskin, I. (2000). The composition of hemp seed oil and its potential as an important source of nutrition. *Journal of Nutraceuticals, functional & medical foods*, 2(4), 35-53.

Lemarchand, C., Couvreur, P., Vauthier, C., Costantini, D., & Gref, R. (2003). Study of emulsion stabilization by graft copolymers using the optical analyzer Turbiscan. *International journal of pharmaceutics*, 254(1), 77-82.

Malomo, S. A., He, R., & Aluko, R. E. (2014). Structural and functional properties of hemp seed protein products. *Journal of food science*, 79(8), C1512-C1521.

Malomo, S. A., & Aluko, R. E. (2015). Conversion of a low protein hemp seed meal into a functional protein concentrate through enzymatic digestion of fibre coupled with membrane ultrafiltration. *Innovative Food Science & Emerging Technologies*, 31, 151-159.

Mengual, O., Meunier, G., Cayré, I., Puech, K., & Snabre, P. (1999). TURBISCAN MA 2000: multiple light scattering measurement for concentrated emulsion and suspension instability analysis. *Talanta*, 50(2), 445-456.

Pojić, M., Mišan, A., Sakač, M., Dapčević Hadnađev, T., Šarić, B., Milovanović, I., & Hadnađev, M. (2014). Characterization of byproducts originating from hemp oil processing. *Journal of agricultural and food chemistry*, 62(51), 12436-12442.

Russo, R., & Reggiani, R. (2015). Evaluation of protein concentration, amino acid profile and antinutritional compounds in hemp seed meal from dioecious and monoecious varieties. *American Journal of Plant Sciences*, 6(01), 14.

Thiex, N., Novotny, L., & Crawford, A. (2012). Determination of ash in animal feed: AOAC official method 942.05 revisited. *Journal of AOAC International*, 95(5), 1392-1397.

Vonapartis, E., Aubin, M. P., Seguin, P., Mustafa, A. F., & Charron, J. B. (2015). Seed composition of ten industrial hemp cultivars approved for production in Canada. *Journal of Food Composition and Analysis*, 39, 8-12.

Wang, X. S., Tang, C. H., Yang, X. Q., & Gao, W. R. (2008). Characterization, amino acid composition and in vitro digestibility of hemp (*Cannabis sativa* L.) proteins. *Food Chemistry*, 107(1), 11-18.

Williams, P. A., & Phillips, G. O. (2009). Gum arabic. In *Handbook of Hydrocolloids* (Second Edition) (pp. 252-273).

Experiment 7:

Functionality-driven fractionation of Hemp Seed Meal into finished unrefined ingredients and thermal stability

HMS may be subjected to critical temperatures (> 60 °C) both during cold-pressing for oil extraction and during transformation manufacturing when used as food ingredient (i.e. bakery goods, pasta production). An extensive literature is available for thermal treatment of HSM in hydrated conditions, reporting the denaturation temperature at 90-95 °C and the onset of the phenomenon at about 80 °C (Tang *et al.*, 2006). But, to our knowledge there is very few information about effect of thermal treatments on macromolecules stability and functionality in a multicomposite system.

Thus, this project aims at evaluating the possibility of obtaining protein-enriched products by simple dry-fractionation of hemp seed meal (HSM) to improve their technological performance and investigating the thermal stability of HSM protein fraction after a pasteurization treatment in view of the application of this material in a real food system.

7.1 Materials and Methods

7.1.1 Materials

Terre Basse Hemp Seed Meal (HSM) commercial product was kindly provided by KDM S.r.l. (Mantua, Italy), and it is constituted by a mixture of OSI 31 and Futura 75 varieties. After cold-pressing (at a maximum temperature of 40 °C), the seed are subjected to milling and drying, at 35 °C for 30 hours, before commercialization. All the chemicals were at analytical grade and were supplied by Sigma-Aldrich S.r.l. (Germany).

7.1.2 Thermal treatments

HSM were heated according to two different procedures, toasting and wet-heating. For both treatments, the material was maintained at the selected temperature for 45 minutes, and the temperature values considered were 45, 65, 90 and 95 °C, beyond a control treatment without heating (NT).

In the case of toasting, HSM powder were poured into thermoresistant plates, and heated in a oven (Sanyo, OMT Oven). Regarding wet-heating, HSM was hydrated for two hours in water (5% w/v). Subsequently the samples were heated on a thermostated plate (MR 3001 K, Heidolph) under magnetic stirring. The cooled HSM dispersion was frozen at -25 °C in aluminium vessels and subjected to freeze-drying using vacuum modulus (Edwards, Ero Electronics).

7.1.3 HSM pre-treatments

During HSM characterization, some analyses (i.e. rheological characterization, proteins extraction) required a defatting step for the material. The oil was removed through solvent extraction using hexan 1:20 ratio w/v in agitated condition with a magnetic stirrer for 5 hours. Later, hexan/oil mixture was filtered with filter paper n. 113v (Whatman International LDT, UK) and the solid residue was dried overnight.

Since granulometry was considered as a critical factor for HSM expressing its technological performance, samples were sieved by means of the analytical sieve shaker Octagon Digital (Endecotts Ltd., England), by using certified sieves with pore size of 90, 125, 250, and 500 μm.

7.1.4 Protein Analysis

Hemp Seed Proteins Extraction

Before applying the extraction protocol, HSM were defatted as described in **paragraph 7.1.3**. For all the samples tested, the protein component was selectively solubilised using a buffer (Trizma-base) constituted by 100 mM Tris-HCL, 50 mM NaCl at pH 8. The defatted material was dispersed in the buffer (10% w/v) and maintained under magnetic at 4 °C stirring overnight. Then, the HSM dispersion was centrifuged at 4 °C at 10000 rpm for 30 min to remove the insoluble residues, and the surnatante was recovered obtaining the Hemp Protein Extract (HPE).

Sodium dodecyl sulfate polyacrylamide gel electrophoresis (SDS-PAGE)

The HPE was diluted in the loading buffer (15 μm in 10 μm) and loaded onto the SDS-PAGE gel. The gel was composed of a 4% polyacrylamide stacking gel over a 12% resolving polyacrylamide gel. The cathodic and anodic compartments were filled with Tris–glycine buffer, pH 8.3, containing 0.1%, m/v, SDS. The electrophoresis was conducted at 100 V until the dye front reached the gel bottom. Staining was performed with colloidal Coomassie Blue and destaining with 7% (v/v) acetic acid in water.

Bradford Assay

The protein concentration of HPE was determined using the Bradford assay reagent with bovine serum albumin as the standard. The absorbance of the standards and unknown sample was determined at 595 nm.

7.1.5 Cannabinoids Quantification

The quantitative determination of the cannabinoids was carried out after methanol extraction dispersing 50 mg of HSM sample in 1 ml of solvent. After 3 cycles at vortex for 1 minute, samples were centrifuged 85 min at 4000 rpm) and the supernatant was decanted. The methanol extract was analysed through Shimadzu HPLC-UV system.

7.1.6 Physico-Chemical Characterization

Colorimetric Quantification

The colour parameters of different granulometry classes of HSM powder were measured using a tri-stimulus reflectance colorimeter Chroma Meter II (Konica-Minolta, Japan), with standard illuminant C. Results are expressed in CIE *L*a*b** scale as the mean of eight determinations.

Water Binding Capacity

The water binding capacity (*WBC*) and fat binding capacity (*FBC*) were assessed according to the method described by Malomo *et al*. (2014) with slight modifications. Protein sample (2 g) was dispersed in 10 mL distilled water in a 15 mL preweighted centrifuge tube. The dispersions were allowed to stand for 30 min and then centrifuged at 7000 g for 25 min at room temperature. The supernatant was decanted, and the tube containing the precipitate was weighed again to determine amount of water retained per gram of sample.

Foaming Capacity

For foaming capacity (*FC*) determination, the sample was suspended in deionized water at 2% (w/v) in order to investigate the effect of the pH on this parameter. The suspension was homogenized at 20000 rpm for 1 min using an Ultra-Turrax (Ika, Germany) homogenizer (shaft S-25N-10G). The capacity of the continuous phase to include air (*FC*) was determined as follows:

$$FC = \frac{V_f - V_i}{V_i} \qquad \text{(eq. 7.1).}$$

Where V_f is the volume of the suspension after homogenization and V_i is the volume of the suspension before homogenization.

7.1.7 Rheological Analysis

Rheological measurements were carried out on HSM water dispersion 30 w/v by using the HSM fraction with a particle size < 125 μm. After adding water, the material was left at rest for 3 hours in order to guarantee the complete hydration. The test were performed with a CMT rheometer (DHR-2, TA Instruments, USA) equipped with a 40 mm diameter plate-plate geometry, with a gap of 1 mm. A solvent trap provided by the manufacturer for liquid samples was used to prevent loss of solvent.

Oscillatory rheometry was applied to samples heated at different temperatures and hydration conditions. Preliminary strain sweeps were performed at 10 rad/s with a deformation varying between 0.1 and 100, in order to determine the linear viscoelasticity (LVE) region. Subsequently, HSM water dispersions underwent a frequency sweep test at 23 °C with 0.2% of deformation (determined within the LVE region) in the frequency range of 0.1-100 rad/s. The rheological

properties of HSM samples were also studied at different temperatures (21-61 °C) applying the frequency sweep protocol described above.

The structuring kinetic of the material was assessed by monitoring the evolution of the complex modulus (G^*) during time, starting when HSM (with particle size < 125 μm) came in contact with water. Time sweep measurements (strain: 0.2%, frequency: 1 rad/s, duration: 10 s) were performed every 10 minutes at 23 °C.

7.2 Results and Discussion

7.2.1 Dry fractionation of hempseed meal aimed at protein-rich functional fraction production

Hemp Seeds Meals were physically fractionated in order to evaluate the size distribution of the material in view of the technological application. **Figure 7.1** shows the relative fraction of hempseed flour for each dimensional class. HSM had more than 85% of particles ranged between 125 and 500 μm, but no material with size < 90 μm was recovered. However, the main difference at a macroscopic level was detected for fractions with particle size greater and smaller than 250 μm, with a significant differentiation in colour.

Hunter scale was used to quantify chromatic variations, especially parameter b^* whose value is related to the yellowness of the sample, and the results are displayed in **tables 7.1**. Fractions with a particle size < 250 μm showed significantly higher values of b^*, and an increased brightness (L^*).

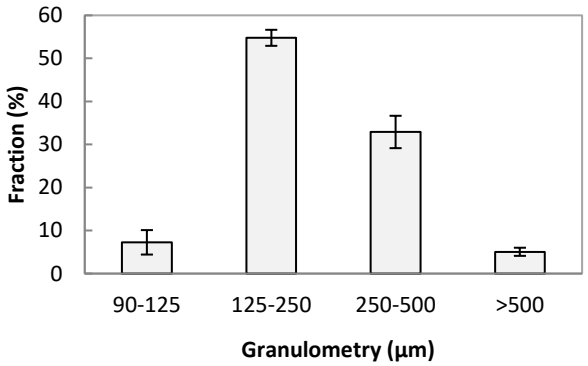

Figure 7.1 HSM distribution in classes on the basis of granulometry dimension

Table 7.1 Colour characteristics of HSM and its fractions.

	Whole HSM	HSM fractions			
		> 500 μm	250-500 μm	125-250 μm	90-125 μm
L^*	9.01±0.96 [a]	6.20±0.66 [b]	2.46±0.53 [c]	7.80±0.85 [b]	11.14±1.14 [a]
a^*	1.73±0.34 [a]	1.00±0.16 [a]	0.88±0.23 [b]	1.68±0.16 [a]	2.25±0.23 [d]
b^*	8.16±1.17 [a]	4.50±0.99 [b]	3.10±0.43 [b]	8.14±0.98 [a]	8.78±0.87 [a]

Note: data are expressed as mean ± S.D. Means within a row with different letters are significantly different (P < 0.05).

The differences observed at a macroscopic level were hypothesized to be related to a diversity in composition for HSM fractions. In order to gain insight into the effect of granulometry on protein distribution, protein extracts were qualitatively and quantitatively analyzed. **Figure 7.2** display the SDS-PAGE profiles for whole HSM and its different fractions (< 125, 125-250, > 250 μm). From the electrophoretic separation, it is clearly detected a band at about 55 kDa corresponding to the acidic-basic subunit of edestin (Raikos *et al.*, 2015). It is reported to be the main constituent of HSM protein fraction, rich in sulfur amminoacids, and it is synthesized by the plant as a storage polymer (Tang *et al.*, 2006; Odani & Odani, 1998). The four protein extracts showed a similar

distribution of the bands, indicative of the fact that dry fractionation did not modified qualitatively the protein profile of the material. But, the coarser fraction (> 250 μm) profile was less intense suggesting a significant reduction of proteins concentration, which was quantified through Bradford assay.

As clear from the results reported in **figure 7.3**, the protein content in HPE showed a progressive concentration from 2.86 g/ml to 7.06 g/ml by reducing the particle size. The protein content for the finest fraction (< 125 μm) was doubled compared to the coarsest one (> 250 μm). The increase in protein concentration is hypothesized to be due to partial removal of the fiber components, whose content generally settle around 20% of HSM, and is mainly constituted by insoluble compounds (Pate, 1999). It is the major constituent of the epicarp, which is preserved during cold-pressing as filtration adjutant but it might represent a hindrance to HSM application as food ingredient.

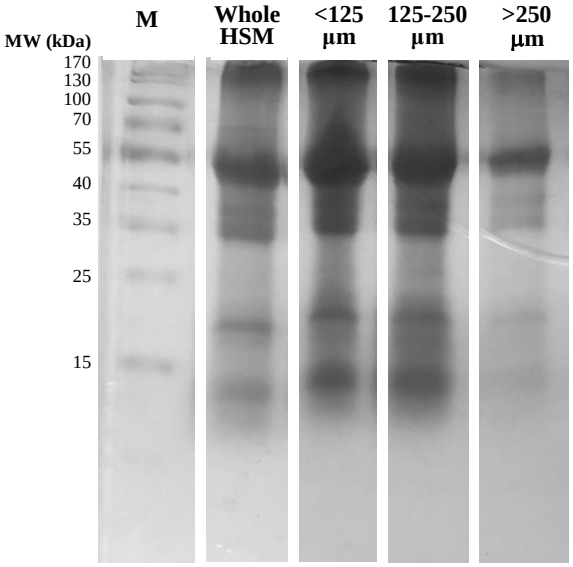

Figure 7.2 SDS- PAGE profile of hemp seed protein extract obtained from fractions with different granulometry. M: molecular mass ladder. Stained with micellar Coomassie blue.

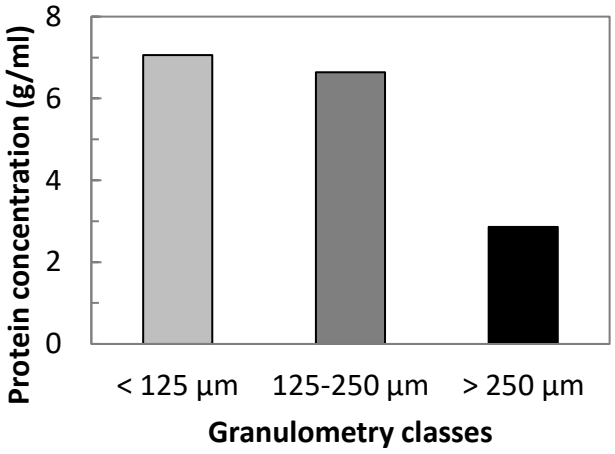

Figure 7.3 Protein concentration in PE obtained from different HSM fraction measured through Bradford analysis.

Cannabinoids (CBD and THC) content was also quantified for the different fractions but no significant changes were found except for the CBDA concentration that was not detectable (because under the instrument sensibility) for the coarser fraction (> 250 μm). The THC content

confirmed to be below the legal limit of 0.2% for hempseeds derivatives food-use as set by European Recommendation (EU) 2016/2115.

Table 7.2 Chemical quantification of cannabinoids content for HSM fractions.

	Whole HSM	**HSM fractions**	
		> 250 μm	<125 μm
CBD (mg/g)	0.01%	0.01%	0.01%
CBDA (mg/g)	0.01%	n.q.	0.01%

Higher technological performances are expected from the HSM fraction < 250 μm, that accounts for more than 55% of the whole HSM mass. A physical fractionation process is recommendable to be scaled on an industrial scale. It should be highlighted that physical dry fractionation by sieving requires far less energy for processing (<1%) compared to traditional wet fractionation (Schutyser & van der Goot, 2011).

7.2.2 Effect of heat treatments on technological properties of HSM

Water binding capacity (WBC) and foaming capacity (FC) were selected as macroscopic indices to monitor HSM technological performance. The first parameter is indicative of the material ability to interact with water and retain it, while FC was used to evaluate possible modification in interfacial properties. Results for HSM subjected to both heat treatments are reported in **figure 7.4**.

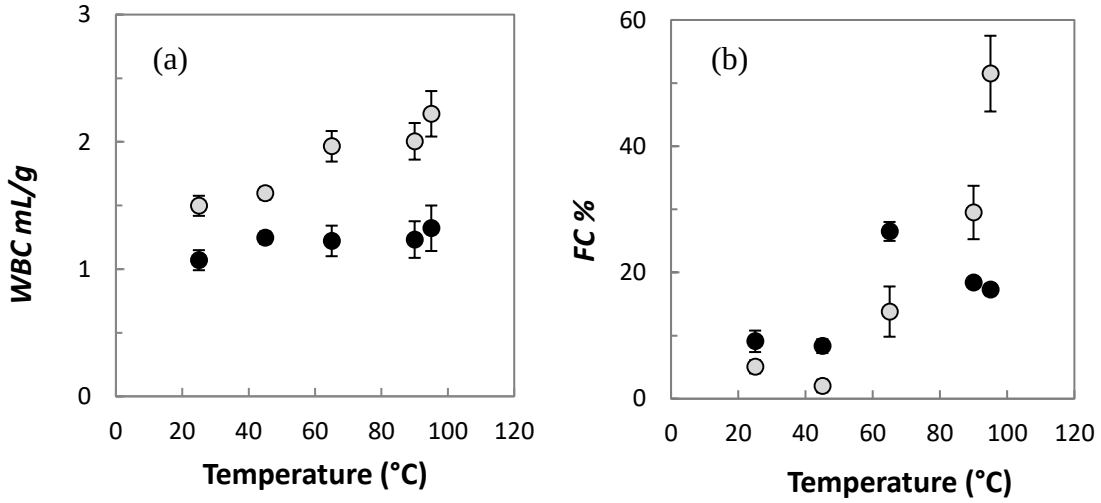

Figure 7.4 Effect of toasting (black circles) and wet-heating (grey circles) at different temperatures on HSM technological properties: WBC (a) and FC (b).

In the case of toasting, none significant effect of heating on HSM functionality was highlighted. Indeed, the two indices displayed a quite constant trend, suggesting a stable behaviour at different temperatures. We can suggest that the possible increase of temperature during pressing for oil recovery cannot affect significantly the proteins capability to hydrate and their foaming functionality.

The presence of water during the heat treatment (wet-heating) determined a significant increase in functional parameters values for HSM subjected to temperature ≥ 65 °C. Heating of hydrated HSM was already proved to account for proteins denaturation, which induces the formation of aggregates due to the formation of covalent disulphide bonds via sulfhydryl-disulphide interchange (Tang *et al.*, 2006; Raikos *et al.*,2015). The altered structural characteristics of the

aggregated protein systems can in some case provide additional protein-water interaction by means of imbibition of water within the newly formed structural network, such as the gelation of globular proteins upon heating and cooling (Chou & Morr, 1979), explaining the increase in WBC values. Moreover, previous studies reported that proteins unfolding and the consequent aggregation can be reflected into an improvement of surface functional properties due to the greater ability to reduce surface tension of the resultant soluble chains (Zhu & Damodaran, 1994; Sorgentini *et al.*, 1995; Damodaran, 2005).

7.2.3 Effect of heat treatments on structuring properties of HSM

The effect of thermal treatments on the viscoelastic behaviour of defatted HSM fractions, with a particle size < 125 μm, dispersed in water was studied by dynamic oscillatory measurements. **Figure 7.5** shows the behaviour of the dynamic moduli (*G'* and *G"*) as a function of the frequency applied.

For all the samples tested, the storage modulus was one order of magnitude higher than the loss modulus, and the *G'* displayed a power law dependence on frequency as follows:

$$G' \propto \omega^n \qquad \text{(eq.7.2)}$$

where ω is the frequency and *n* represents the slope of the curve and was found to be always lower than 0.1. It can be inferred that HSM exerted a solid-like behaviour, given the predominance of *G'* on *G"* and the independent behaviour of the storage modulus on the angular frequency. The toasting treatment did not affect significantly the rheology of HSM, as highlighted in **figure 7.5a** where we can observe unmodified dynamic moduli comparing the materials heated at different temperatures. Similar values of *G'* and *G"* were measured for HSM after wet-heating at temperature ≤ 65 °C in **figure 7.5b**. On the contrary, heating at 90 and 95 °C in hydrated conditions increased both the moduli, which could be related to the strength of interactions between units in the material (Phillips & Williams, 2009). The higher stiffness of the gel could be easily related to the increased number of interactions taking place after the thermal denaturation of the proteins, as already observed for a number of similar protein systems (Rankema & van Vliet, 2002; Rankema *et al.*, 2002; Foegeding *et al.*, 2002).

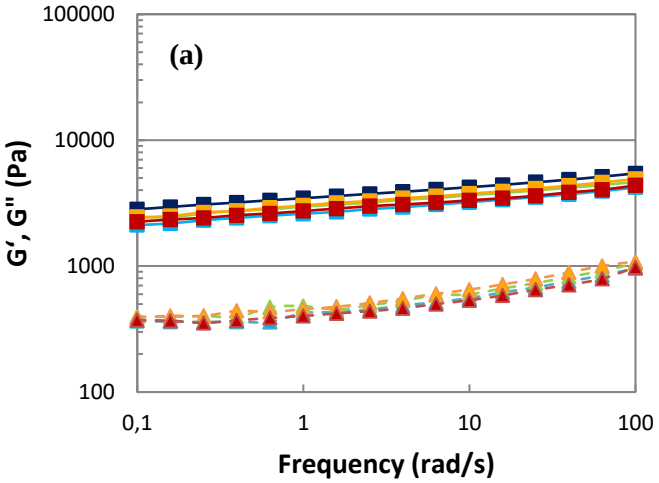

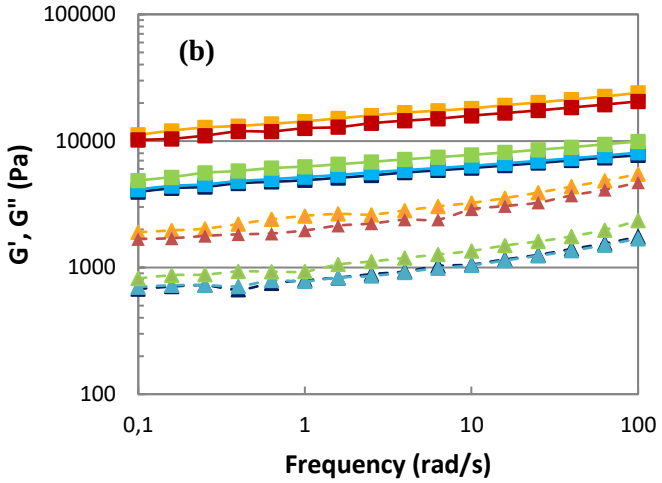

Figure 7.5 Dynamic moduli (*G'*: circles; *G"*: triangles) of HSM water dispersions (30% w/v). Effect of toasting (a) and wet-heating (b) at different temperatures: 25 (blue), 45 (light blue), 65 (green), 90 (orange) and 95 °C (red).

Subsequently, few samples (non-treated, toasted and wet-heated at 95 °C HSM) were selected for a deeper investigation.

The Boltzmann time-temperature superposition principle is based on the possibility to enhance the processes involved in molecular relaxation or rearrangements in viscoelastic materials with increasing temperature determines a direct equivalency between time (expressed as its inverse, ω) and temperature (Neviere, 2006). This approach allowed to explore the rheological behaviour of the material at very long timescales, corresponding to low frequencies not experimentally available by the instrument.

Oscillatory data obtained from HSM aqueous dispersions at 30% (w/v) and collected at different temperatures (**figure 7.6a**) were converged onto a master-curve (**figure 7.6b**), with a suitable scaling of mechanical spectra in the horizontal direction with a shift factor: $aT = \omega(T)/\omega(T_0)$. Thermally-induced phase changes, which would have produced deviations or irreversible changes in thermal responses, were not observed in the temperature range used (20-60 °C), in accordance with results from previous calorimetric analyses (Tang *et al.*, 2006).

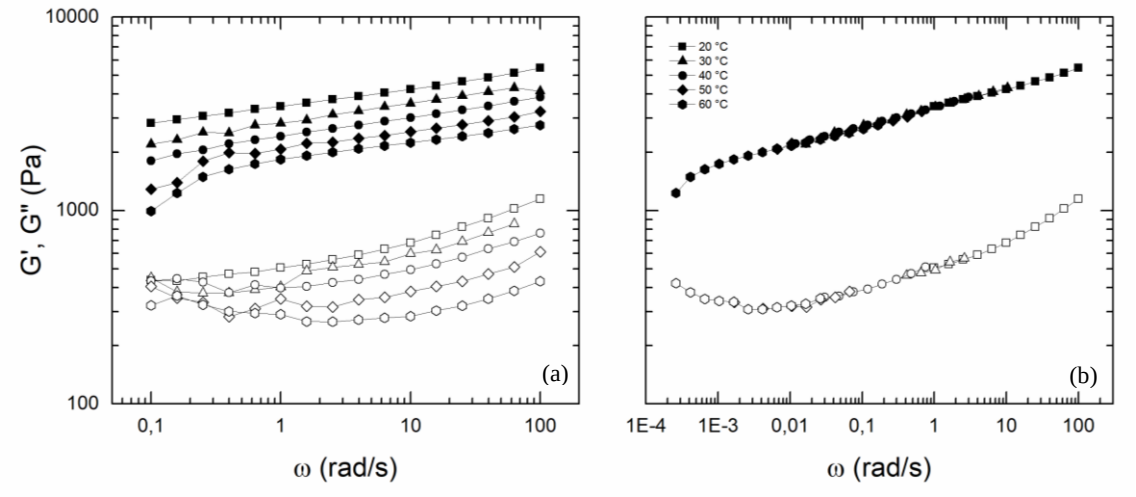

Figure 7.6 (a) Frequency sweep of 30% (w/v) aqueous dispersion of non-treated HSM with particle size < 125 μm at different temperatures ranged between 20 and 60 °C. (b) Master curves generated by the horizontal shifting of the frequency sweep curves. (G' full symbols, G" hollow symbols).

The theoretical interest in calculating a relaxation spectrum is based on the supposition that it reflects molecular movements of macromolecules, and thus can be used to deduce structural information of technological importance. In our study, relaxation spectrum was obtained by fitting $G'(\omega)$ and $G''(\omega)$ experimental data with Fredholm integral equations (Hansen, 2008). The spectrum (**figure 7.7**) resolved a quick peak of relaxing components with τ value approximately 6 10^{-2} s, with a noticeable width given by the heterogeneity of the system. The existence of a slower peak at a longer timescale, with $\tau > 10^5$, can be presumed. The identification of the nature of the fast, and slow relaxation modes is far from being fully described, but they can be related to the protein network.

After toasting, the spectrum maintained a similar trend compared to the non treated sample. While, it is evident that multiple relaxation modes appeared for wet-heated HSM, with τ values at about 0.8 and 10^3 s. These variations are indicative of modifications in the pattern of relaxing components, likely due to a different interaction between macromolecules (Mao *et al.*, 2000). In addition, we can notice a significant increment of the distribution function $H(\tau)$ for at higher relaxation time values ($\tau > 10^4$), that could be related to greater relaxing entities possibly product of aggregation phenomena.

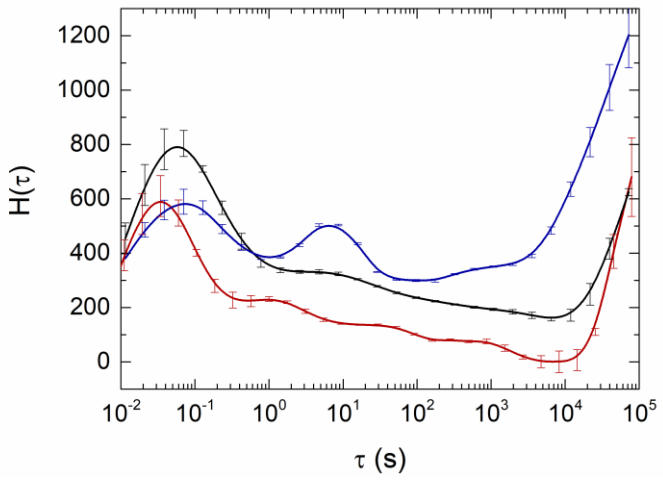

Figure 7.7 Continuous relaxation time distribution function H(τ) of 30% aqueous dispersion of HSM, with particle size < 125 μm. Not thermal treated (black), toasted (red), and wet-heated (blue) HSM.

7.2.4 Structuring kinetic of HSM: effect of thermal treatments and role of the macrocomponents

A time-cure test was performed in order to understand the structuring behaviour of HSM proteins under hydration and the complex modulus (G^*) evolution was monitored during time.

The kinetic profiles for the toasted HSM are reported in **figure 7.8**. For all the samples, the viscoelasticity growth clearly followed a first order kinetic until about 90-120 minutes, while a second minor phenomenon (about 10% compared to the first one) can be detected at longer time. According to the different toasting temperature, two main behaviours can be recognized. In **figure 7.8a**, concerning HSM toasted at 45 and 65 °C, the second structuring event can be distinguished after 120 minutes of test. While for HSM toasted at 90 and 95 °C (**figure 7.8b**), the appearance of the second structuring phenomenon is anticipated at 60-70 minutes. In **figure 7.9a**, it is reported the complex modulus of the first structuring phenomenon normalized for its plateau value. In the case of wet-heated HSM the structuring kinetic is characterized by a single phenomenon, and the

normalized curves, where the value 1 corresponds to the maximum degree of structuring, are reported in **figure 7.9b**.

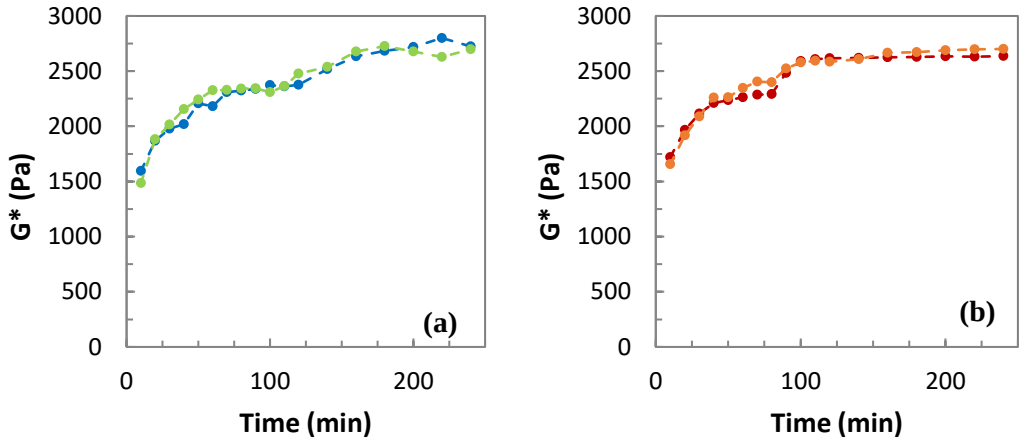

Figure 7.8 Complex modulus as a function of time for toasted HSM (30% w/v) treated at 45 (blue), 65 (green), 90 (orange) and 95 (red) °C.

All the samples initially displayed a typical exponential trend, and the structuring behaviour was described through a first order kinetic model:

$$G^* = 1 - e^{kt} \qquad \text{(eq. 7.3)}$$

where d k is the rate constant. The rate values calculated are shown as a function of the treatment temperature in **figure 7.10**.

Wet-heated HSM was characterized by a structuring rate about one order of magnitude higher than toasted HSM. The structuring ability of the materials is limited by the access of the water to the structuring components. Thus, the faster structuring kinetic for samples heated in hydrated conditions is hypothesized to be due to the re-organization of the soluble molecules. Indeed water acts as a solvent for water-soluble proteins, fibers, minerals (Maolomo *et al.*, 2014; Bao-yao & Jie, 2004), which are solubilized in the medium. After freeze-drying, the water-soluble proteins are ready accessible to the solvent. On the contrary, the organization of toasted HSM particles was not significantly altered by the thermal treatment and it was characterized by a compact cellular structure that slowed down the water absorption and migration toward buried compounds. In addition, the structuring kinetic for wet-heated HSM is significantly accelerated for samples treated at a temperature higher than 45 °C, since the formation of further interaction between protein chains is favoured by the heat-induced aggregation.

It should be reported that also toasted HSM structuring rate is affected by the thermal treatment conditions. From **figure 7.10**, we can appreciate that samples heated at 90 and 95 °C showed a faster kinetic, that could be related to a more rapid hydration of the particles. It is well-known that toasting determines microfractures into the cellular structure (Wolf & Baker, 1975; Hale *et al.*, 1999), easing the complete hydration of the particle.

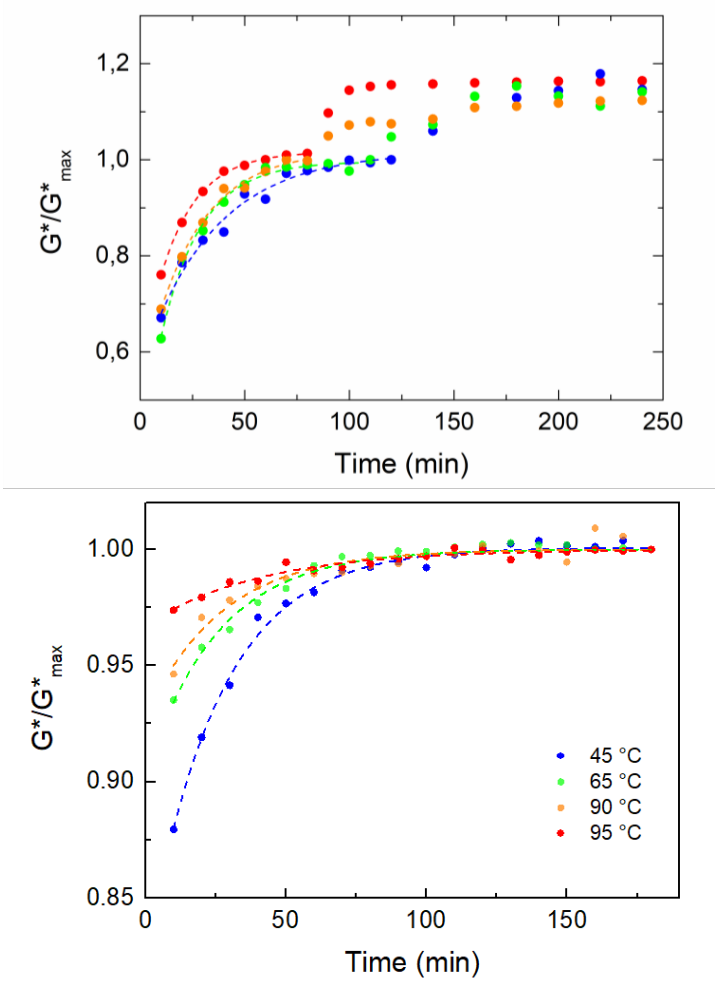

Figure 7.9 Normalized complex modulus as a function of time for toasted (a) and wet-heated (b) HSM (30% w/v) treated at 45 (blue), 65 (green), 90 (orange) and 95 (red) °C. Dotted line represents the exponential fitting of the curve.

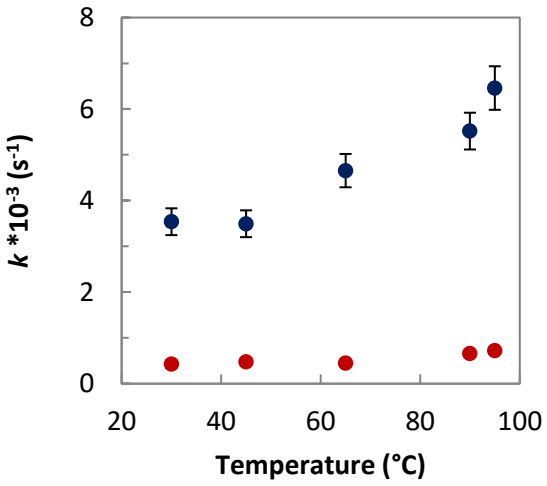

Figure 7.10 Rate of the structuring kinetic calculated for toasted (red) and wet-heated (blue) HSM water dispersions (30%w/v). Error bars are expressed as standard error.

In order to verify the contribution of the two main components (i.e. proteins and fiber) to the two structuring events, the role of the fibers in the structuring kinetic was investigated by substituting HSM with a particle size < 125 μm with two different levels (10 and 20%) of fiber-enriched HSM,

with the same particle size but obtained by grinding of the coarser fraction. The evolution of *G** in time for toasted HSM treated at 65 °C with different enrichment in fibers is reported in **figure 7.11**, and revealed a reduction in the rheological response of the material by increasing the fiber fraction. This behaviour can be explained by an effect of dilution in protein concentration, while most of the polysaccharide components are represented by insoluble chains (Pate, 1999) acting as inert material. Also in this case, the structuring kinetic was described using a first order model (**eq. 7.3**) and the results for the rate parameter are reported as a function of the substitution level in the **inset** of **figure 7.11**. The rate constant underwent a slight reduction for increased content of fibers, suggesting a slowing down effect of these compounds on the structuring kinetic. These results confirmed the prevalent role of the protein fraction in structuring properties of HSM.

In addition, altering the percentage of protein and fibers, both the importance and the delay time of the second structuring phenomenon did not change. It means that its occurrence is not caused by the different distribution of water between the different macrocomponents but likely to the organization of HSM particles. Indeed, the structuring kinetic of wet-heated HSM, where cellular compartmentation is hypothesized to underwent significant modifications, is characterized by a single phenomenon

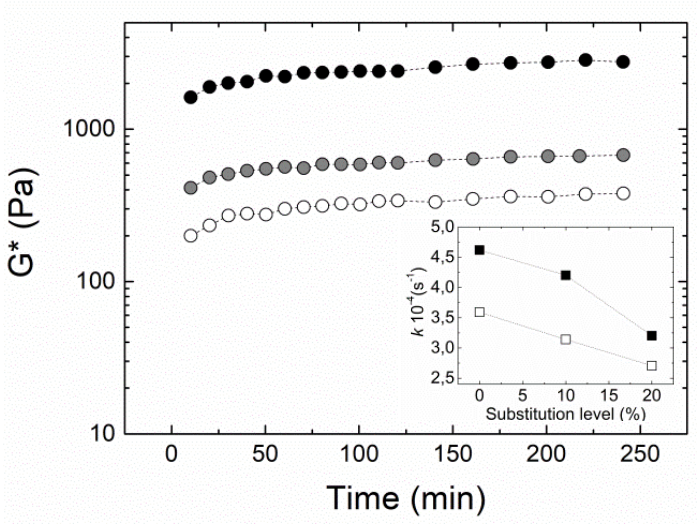

Figure 7.11 Complex modulus as a function of time for toasted HSM at 65 °C (30% w/v) without (black) and with a partial substitution (10% in grey and 20% in white) of the fraction < 125 μm with the fiber-enriched. Inset: Rate constant as a function of the degree of substitution for the first (black) and the second (white) structuring phenomena.

7.2.5 Analysis of HSM Protein: Thermal Stability

Figure 7.12 provides the SDS-PAGE profiles of protein extracted from HSM subjected to the heat treatments. The position of the bands is quite constant for the samples and, as expected, edestin was the main component, recognized through the acidic-basic subunits corresponding to the band with molecular weight (MW) of about 52 kDa (Wang *et al.*, 2008).

Toasted HSM did not show significant differences also in terms of profile intensity all over the investigated temperature range while the intensity of the bands is progressively and significantly reduced for the samples wet-heated at 90 °C and above. This behaviour suggested that no aggregation occurred during toasting. Differently, SDS-PAGE profile revealed that wet-heating produced a reduction in protein concentration likely due to the formation of insoluble aggregates consequent to proteins denaturation. Indeed, the formation of intermolecular disulphuric bonds was previously reported to take place for HSM protein isolates when heating in hydrated conditions, favoured by the presence of water molecules (Tang *et al.*, 2006).

The protein concentration of the extracts was quantified by means of Bradford analysis and the results are presented in figure **7.13**. The increase of toasting temperature did not affect the protein concentration (**figure 7.13a**), confirming the stability of these biopolymers in dry conditions. Conversely, a slight reduction in protein concentration was detected at 65°C and the parameter was almost halved at 90 and 95 °C (**figure 7.13a**), in agreement with SDS-PAGE results.

Protein analysis also confirmed that a re-organization of the soluble compounds likely took place during wet-heating treatment, as hypothesized in **paragraph 7.2.4**. Indeed, contrarily to the results obtained for non-treated HSM (**figure 7.3**), samples treated at room temperature (25 °C) and hydrated conditions showed quite similar protein concentration values, regardless of the granulometry class considered (**figure 7.14**). The homogenous distribution of proteins for different HSM particle sizes suggested that wet-heating induced a modification of the particle structure at a tissue and cellular level.

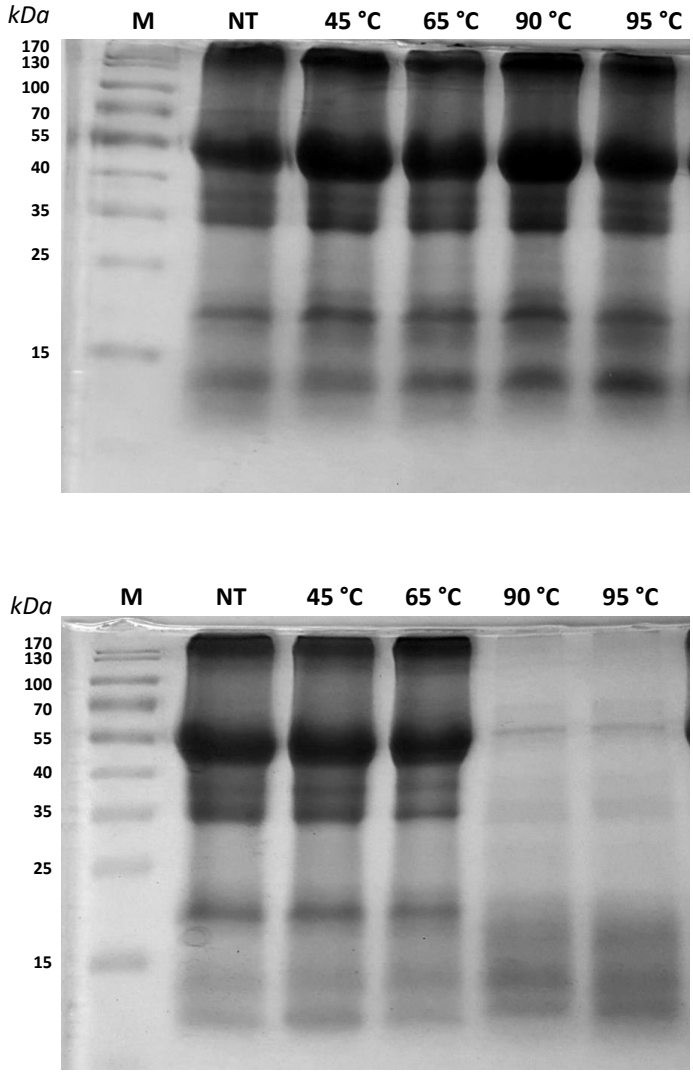

Figure 7.12 SDS-PAGE profile of hempseed protein extract after (a) toasting and (b) wet-heating: M (marker BSA), 10−170 kDa.

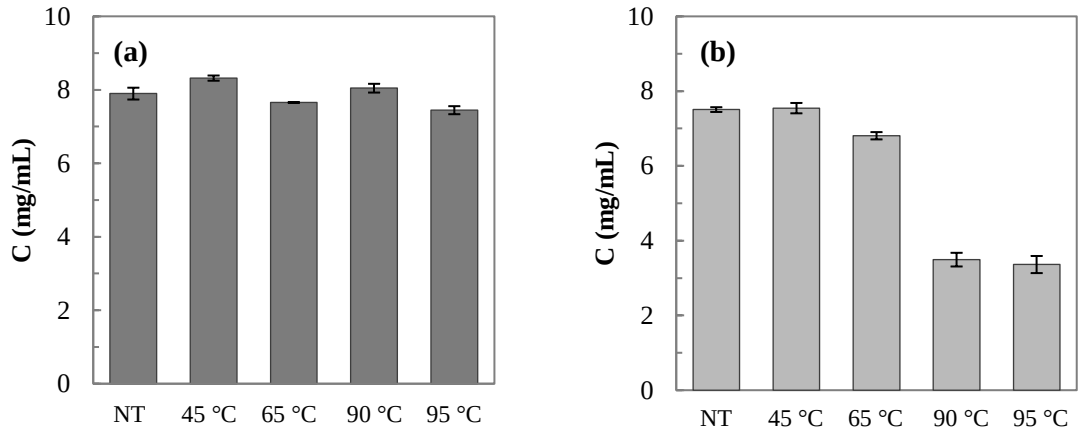

Figura 7.13 Protein concentration of hempseed protein extracts after (a) toasting and (b) wet-heating, quantified through Bradford assay.

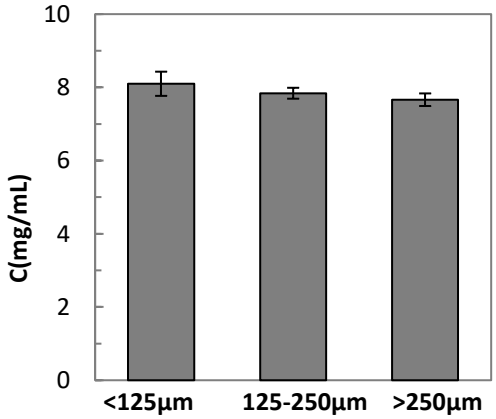

Figure 7.14 Protein concentration of hempseed protein extracts from HSM with different particle size, quantified through Bradford assay.

Conclusions

In conclusion, dry fractionation was selected as a suitable method to produce fraction of HSM rich in proteins. Toasting had no significant effect on protein stability and functionality. Heating of HSM in dry conditions (toasting) did not significantly affect proteins organization and functionality; even though it was found to modify the cellular structure with the consequent modification of HSM behaviour during hydration and structuring processes. Heating of HSM in wet conditions resulted in the denaturation and the subsequent aggregation of the proteins, with improved technological properties.

The present study provides not only useful information for the final utilization, but also indications about the management of pre-treatment conditions in order to tailor the material performances.

Aknoledgements

I thank Professor Gabriella Roda, and Dr. Gilda Aiello (Dept. of Pharmaceutical Science, UNIMI) for performing the quantification of cannabinoids and the characterization of the protein fraction.

References

Bao-yao, B. Y. G. W., & Jie, T. J. W. L. (2004). Extraction isolation and purification of water-soluble polysaccharides from hemp seed [J]. *Food Science and Technology*, 6, 031.

Chou, D. H., & Morr, C. V. (1979). Protein-water interactions and functional properties. *Journal of the American Oil Chemists' Society*, 56(1), A53-A62.

Damodaran, S. (2005). Protein stabilization of emulsions and foams. Journal of Food Science, 70(3), R54-R66.

Foegeding, E. A., Davis, J. P., Doucet, D., & McGuffey, M. K. (2002). Advances in modifying and understanding whey protein functionality. *Trends in Food Science & Technology*, 13(5), 151-159.

Hale, M. D., Mccafferty, K., Larmie, E., Newton, J., & Swan, J. S. (1999). The influence of oak seasoning and toasting parameters on the composition and quality of wine. *American Journal of Enology and Viticulture*, 50(4), 495-502.

Hansen, S. (2008). Estimation of the relaxation spectrum from dynamic experiments using Bayesian analysis and a new regularization constraint. *Rheologica Acta*, 47(2): 169-178.

Malomo, S. A., He, R., & Aluko, R. E. (2014). Structural and functional properties of hemp seed protein products. *Journal of food science*, 79(8), C1512-C1521.

Mao, R., Tang, J., & Swanson, B. G. (2000). Relaxation time spectrum of hydrogels by CONTIN analysis. *Journal of food science*, 65(3): 374-381.

Neviere, R. (2006). An extension of the time–temperature superposition principle to non-linear viscoelastic solids. *International journal of solids and structures*, 43(17), 5295-5306.

Odani, S., & Odani, S. (1998). Isolation and primary structure of a methionine-and cystine-rich seed protein of *Cannabis sativa*. *Bioscience, biotechnology, and biochemistry*, 62(4), 650-654.

Pate, D. W. (1999). Hemp seed: a valuable food source. *Advances in hemp research*, 243-255.

Phillips, G. O., & Williams, P. A. (2009). *Gums and stabilisers for the food industry 12*. Royal Society of Chemistry.

Raikos, V., Duthie, G., & Ranawana, V. (2015). Denaturation and oxidative stability of hemp seed (*Cannabis sativa* L.) Protein isolate as affected by heat treatment. *Plant foods for human nutrition*, 70(3), 304-309.

Renkema, J. M., Gruppen, H., & Van Vliet, T. (2002). Influence of pH and ionic strength on heat-induced formation and rheological properties of soy protein gels in relation to denaturation and their protein compositions. *Journal of Agricultural and Food Chemistry*, 50(21), 6064-6071.

Renkema, J. M., & van Vliet, T. (2002). Heat-induced gel formation by soy proteins at neutral pH. *Journal of agricultural and food chemistry*, 50(6), 1569-1573.

Schutyser, M. A. I., & Van der Goot, A. J. (2011). The potential of dry fractionation processes for sustainable plant protein production. *Trends in food science & technology*, **22**(4): 154-164.

Sorgentini, D. A., Wagner, J. R., & Anon, M. C. (1995). Effects of thermal treatment of soy protein isolate on the characteristics and structure-function relationship of soluble and insoluble fractions. *Journal of Agricultural and Food Chemistry*, 43(9), 2471-2479.

Tang, C. H., Ten, Z., Wang, X. S., & Yang, X. Q. (2006). Physicochemical and functional properties of hemp (*Cannabis sativa* L.) protein isolate. *Journal of agricultural and food chemistry*, 54(23), 8945-8950.

Wang, X. S., Tang, C. H., Yang, X. Q., & Gao, W. R. (2008). Characterization, amino acid composition and in vitro digestibility of hemp (*Cannabis sativa* L.) proteins. *Food Chemistry*, 107(1): 11-18.

Wolf, W. J., & Baker, F. L. (1975). Scanning electron microscopy of soybeans, soy flours, protein concentrates, and protein isolates. *Cereal Chem*, 52(387).

Zhu, H., & Damodaran, S. (1994). Heat-induced conformational changes in whey protein isolate and its relation to foaming properties. *Journal of Agricultural and Food Chemistry*, 42(4), 846-855.

Topic 4:

BIOTECHNOLOGICAL TRANSFORMATION

Waste produced by food processing and consumption still contains ~60% of organic matter (Lin *et al*., 2013), and thus it can be considered an interesting source of nutrients to be used as substrate for microbiological fermentation substrate to produce value-added products of microbial origin (Rodriguez Couto, 2008). In light of the possibility offered by biotechnological transformation, the production of cellulose through microbial conversion arises a renewed interest in food technological applications since it can be obtained from renewable resources and sustainable processes, and it is biodegradable (Siracusa et al., 2008).

Apart being the major polysaccharide in plant cell walls, cellulose is also synthesized by several bacterial species, mainly *Gluconobacter xylinium* and *Komogateibacter sucrofermentas*, and marine organisms. Bacterial cellulose (BNC) display the same molecular formula as plant-derived cellulose but it is fundamentally different because of its nanofiber architecture. Glucose units are the monomeric molecules forming a linear chain polymer, and the hydroxyl groups are in the thermodynamically preferred $^4C_1$ conformation. Microbial-derived fibres are characterized by nanosized diameter (4-30 nm) and they can form highly regular intra- and inter molecular hydrogen bonds, which induce nanofibers to merge into randomly assembled ribbon-shaped fibrils with highly levels of crystallinity (Klemm *et al.*, 2005; Pääkko *et al.*, 2007). Hence, nanofibrils of BNC are immobilized in a stable three-dimensional network. This peculiar organization accounts for distinctive advantages over traditional sources of cellulose such as plants. In particular, BNC has lower density, higher crystallinity, higher water retention, gelling ability, higher mechanical strength, and higher purity (Iguchi *et al.*, 2000). Indeed, the well-separated nano- and microfibrils of BNC create an extensive surface area, which means much more surface hydroxyl and ether groups than other cellulose to interact with the solvent, other molecules, or other cellulose chains (Li *et al.*, 2009). Such properties are really attractive for industrial exploitation and already found application in papermaking, acoustics, optics (Shi *et al.*, 2014), tissue engineering, cosmetics, and pharmaceutics to incorporate drugs and control their release (Mori *et al.*, 2011). In the recent years, food industry has also addressed its attention toward BNC because of its nature of multifunctional food additive, able to combine different functionalities: controlling food system rheology, retaining bioactive molecules, reinforcing agent in packaging materials. At the moment, the development of nanocomposites containing BNC for packaging represents one of the main fields of interest in food research, but the use of this matrix as ingredient seems to offer wider perspectives in product innovation. However, the overall functionality of this material has not been completely explored, thus the definition and the study of functional properties with potential interest for food formulations is still a critical step.

Hong, F., Guo, X., Zhang, S., Han, S. F., Yang, G., & Jönsson, L. J. (2012). Bacterial cellulose production from cotton-based waste textiles: enzymatic saccharification enhanced by ionic liquid pretreatment. *Bioresource Technology*, 104, 503-508.

Iguchi, M., Yamanaka, S., & Budhiono, A. (2000). Bacterial cellulose—a masterpiece of nature's arts. *Journal of Materials Science*, *35*(2), 261-270.

Klemm, D., Heublein, B., Fink, H. P., & Bohn, A. (2005). Cellulose: fascinating biopolymer and sustainable raw material. *Angewandte Chemie International Edition*, *44*(22), 3358-3393.

Kurosumi, A., Sasaki, C., Yamashita, Y., & Nakamura, Y. (2009). Utilization of various fruit juices as carbon source for production of bacterial cellulose by Acetobacter xylinum NBRC 13693. Carbohydrate Polymers, 76(2), 333-335.

Li, X., Chen, S., Hu, W., Shi, S., Shen, W., Zhang, X., & Wang, H. (2009). In situ synthesis of CdS nanoparticles on bacterial cellulose nanofibers. *Carbohydrate Polymers*, *76*(4), 509-512.

Lin, C. S. K., Pfaltzgraff, L. A., Herrero-Davila, L., Mubofu, E. B., Abderrahim, S., Clark, J. H., ... & Thankappan, S. (2013). Food waste as a valuable resource for the production of chemicals, materials and fuels. Current situation and global perspective. *Energy & Environmental Science*, 6(2), 426-464.

Mori, R., Nakai, T., Enomoto, K., Uchio, Y., & Yoshino, K. (2011). Increased antibiotic release from a bone cement containing bacterial cellulose. *Clinical Orthopaedics and Related Research*, *469*(2), 600-606.

Pääkkö, M., Ankerfors, M., Kosonen, H., Nykänen, A., Ahola, S., Österberg, M., ... & Lindström, T. (2007). Enzymatic hydrolysis combined with mechanical shearing and high-pressure homogenization for nanoscale cellulose fibrils and strong gels. *Biomacromolecules*, *8*(6), 1934-1941.

Rodríguez Couto, S. (2008). Exploitation of biological wastes for the production of value-added products under solid-state fermentation conditions. *Biotechnology Journal: Healthcare Nutrition Technology*, 3(7), 859-870.

Shi, Z., Zhang, Y., Phillips, G. O., & Yang, G. (2014). Utilization of bacterial cellulose in food. *Food Hydrocolloids*, *35*, 539-545.

Siracusa, V., Rocculi, P., Romani, S., & Dalla Rosa, M. (2008). Biodegradable polymers for food packaging: a review. Trends in Food Science & Technology, 19(12), 634-643.

Experiment 8:

Technological functionality of bacterial nanocellulose intended as supporting matrix for volatile molecules

The technology implying the use of flavours (and fragrances) supported or encapsulated on different materials is constantly evolving since years, with the aim of increasing the retention efficiency of these volatile molecules on the supporting materials. The loss of the flavour of supported or encapsulated compounds during storage time is a crucial issue for their industrial application, and thus a lot of attention is payed to lengthen shelf-life values. The bacterial cellulose has been identified as a promising candidate to improve efficiency of adsorption and retention of volatile compounds, due to its peculiar structure. The present study aims to study the ability of the bacterial cellulose to retain volatile compounds, in a model system, in order to lay the basis for a primary justification of its industrial exploitation.

The aim of the experiment was to verify if the two cellulosic materials have a different ability to retain two volatile compounds, so that only the stereochemical structure influences the absorption capacity.

8.1 Materials and methods

8.1.1 Materials

A commercial blend of celluloses (CB), constituted by carboxymethylcellulose and microcrystalline cellulose (namely Avicel 611 F) was purchased from Sigma-Aldrich, Germany, and used as reference material. Bacterial nanocrystalline cellulose (BNC) was produced on a lab scale as shown in the following **paragraph** (**8.1.2**).

8.1.2 Bacterial cellulose production

Komogateibacter sucrofermentas (DSMZ 15973) was used for the bio-synthesis of the bacterial cellulose hydrogel. The bacterium was cultured in a Hestrin and Schramm (HS) medium, which was composed of 2 wt.% glucose, 0.5 wt.% yeast extract, 0.5 wt.% peptone, 0.27 wt.% disodium phosphate, and 0.15 wt.% citric acid. After incubating for 7-10 days at 30 °C in static conditions, the hydrogel was dipped into deionized water, and then steamed by boiling in a 1 M NaOH solution for 30 mins to remove cells eventually present into the pellicles. Afterwards, the samples of bacterial cellulose hydrogels were purified by washing in deionized water until their pH value approached 7. The pellicles obtained were homogenized, and then freeze-dried.

8.1.3 Preparation of cellulose suspensions

Dispersions of microcrystalline and commercial cellulose were prepared blending powders in deionized water by magnetic stirring until a complete hydration. As regards bacterial cellulose, the lyophilized sample was ground in water by means of a heavy-duty blender (Waring Laboratory, Torrington, CT), performing 3 cycles of 3 minutes at 18500 rpm. Thereafter, BNC suspensions were sonicated with a sonicator (VS-F100b, As One Corp.) for 30 minutes to separate cellulose fibrils (Wong, Kasapis & Huang, 2012). All samples were stored at 4 °C.

8.1.4 Films preparation

To prepare the BNC films, 0.25 g of bacterial cellulose in the form of a diluted suspension (1% w/v) were poured in a Petri dish and dried at room temperature. The dried samples were placed in a desiccator containing saturated NaBr, providing a constant RH of 60% at 25 °C. In order to improve the mechanical properties of the films, glycerol was eventually added to the cellulose suspension with a final concentration of 30% and 60% (w/w on dry matter).

8.1.5 Rheological Analysis

The rheological behavior of BNC and CB at different concentrations dispersions was characterized using a CMT (combined motor and transducer) rheometer (DHR-2, TA Instruments). All measurements were performed using stainless steel parallel plate geometry (40 mm diameter) at 23°C. A solvent trap provided by the manufacturer for liquid samples was used to prevent loss of solvent. Initially, oscillatory stress sweeps were performed to determine the linear viscoelastic region for each sample, at frequency condition of 1 rad/s. Subsequently, a dynamic frequency sweep was conducted by applying a constant strain of 0.2% selected within the linear viscoelastic region for all the samples, with a frequency range between 0.2 and 30 rad/s. From that, dynamic moduli (*G'* and *G"*) and complex viscosity as a function of frequency were obtained.

8.1.6 Retention of volatile compounds

Isoamyl acetate (IsoA) and n-amyl acetate (n-A) were selected as model molecules. The same amount of solution containing the volatile compounds was used for the experiments, and it was supported on the minimum amount of cellulose able to retain the solution. Two parallel experiences were performed, adopting the same operative parameters, so that the release phenomena were influenced only by the type of material.

Once the compounds were adsorbed on cellulosic materials, the samples were maintained into sealed Pyrex 250 mL round media bottle sealed with a screwcap equipped with a septum to perform the analysis. This system enables an SPME (solid phase microextraction) needle to enter the airtight container at regular intervals, and to be exposed to the Pyrex headspace for a define period. The test was performed at room temperature and 50 °C for both the cellulosic materials, in order to investigate the effect of temperature.

HS-SPME and GC/MS conditions

The headspace of each 250 ml bottle Pyrex was sampled during a total experimental period of 66 or 77 hours (according to the temperature conditions). The quantification of the release during time was carried out combining a SPME (solid phase micro-extraction) technique and gas chromatography/mass spectrometry (GC/MS). SPME was performed using the 50/30 DVB/CAR/PDMS fibre (2 cm) to adsorb volatile molecules present in the Pyrex headspace. GC/MS analyses were performed in a Shimadzu 2010 gas chromatograph coupled to a Shimadzu QP-2010 MSD quadrupole mass spectrometer (Shimadzu, Milan, Italy). The gas chromatograph was equipped with a Equity-1701, 30 m x 0.25 mm, 0.25 µm film thickness (Supelco – Italia). The injector was operated in split mode (1:5) at T = 220 °C. Before sampling, the fibre was reconditioned for 10 min in the GC injection port at 220 °C. The operating conditions for the GC/MS were: helium flow 1.0 ml/min, and oven temperature 40 °C for 1 min, increased to 240 °C at a rate of 5 °C/min. The temperature of the ion source was 200 °C, the electron energy was 70 eV, and the interface temperature was 240 °C. Mass spectra were acquired over the mass range 40–300 a.m.u..

Release Parameters Calculation

Once the amount of volatile compound adsorbed on the SPME fiber was measured, the results were expressed as relative release index (RR) described as the percentage ratio between the amount of volatile measured in the headspace at a specific sampling time and the amount of volatile initially loaded in the system (75 and 157 µg for IsoA and n-A respectively). The cumulative release was calculated as the sum of the amount of volatile compound detected until a given time (*t)*, while the overall relative release represents the sum of the total volatile compounds amount measured at all sampling times. In the end, the partition coefficient (*P*) was obtained by dividing the amount of volatile compound adsorbed on the fiber at a specific sampling time to the amount of the same compound residual in the system at the same moment. The parameter definitions are resumed as follows:

$RR = m_t/m_0$ *(eq. 8.1)*

$\text{Cumulative release} = \sum_{t=1}^{n} m_t/m_0$ *(eq. 8.2)*

$P = m_t/m_r$ *(eq. 8.3)*

where m_t is the amount of volatile adsorbed by the fiber at time *t*, m_0 is the amount of volatile initially loaded in the system (75 and 157 µg for IsoA and n-A respectively), and m_r is expressed as:

$m_r = m_0 - \sum_{t=1}^{n} m_t$ *(eq. 8.4)*

8.1.7 Dynamic-mechanical thermal analysis

Dynamic mechanical properties of the BNC films were measured using a Rheometric Scientific DMTA V, USA, working in tensile mode and equipped with a film tension clamp. A preload force of 0.01 N was applied. Strain-stress curves were recorded, at 30 °C, ramping the tensile force at 2 N/min until the rupture of the sample. Temperature ramp measurements were carried out at a constant frequency of 1 Hz, a strain amplitude of 0.05%, in a temperature range of 30–350 °C, with a heating rate of 5 °C/min and gap distance of 20 mm. The samples were prepared

by cutting 5 mm wide strips from the films. The device was previously calibrated, and a total of 5 measurements for each sample were performed in order to ensure the reproducibility of the results. The softening point (*Ts*) is defined as the extrapolated onset of the drop of storage modulus. The glass transition temperature (*Tg*) is indicated by the peak of tan δ curve (Puoplin *et al*, 1999).

2.1.9 Mathematical analysis

For all the curves, the fitting was performed with OriginLab Version 9.1 software.

8.2 Results and discussion

8.2.1 Viscoelastic properties

Rheological investigation of viscoelastic properties with small amplitude oscillatory shear (SAOS) technique was carried out to assess the structural and functional properties of bacterial cellulose suspensions.

The rheological behaviour of the bacterial cellulose and the commercial blend was compared through rheological parameters obtained under dynamic conditions of non-destructive oscillatory tests in the frequency range of 0.2-30 rad/s. This approach allowed to investigate the properties of the polymeric dispersions under conditions close to the at-rest state, without the disruption of the internal structure of the material unlike steady state regime. Indeed BNC gel is constituted by microfibrils, and its orientation is irreversibly changed by flow leading to a shear history dependent rheology (Iguchi et al., 2000). The storage and the viscous moduli of BNC suspensions at different concentration values (ranging from 0.1% to 1% w/v) as a function of frequency (ω) are provided in **figure 8.1a**. *G'* is about one order of magnitude greater than *G"* for all the BNC concentrations investigated, suggesting that the system manifests a solid-like behavior. In addition, it is generally recognized that the dynamic moduli (*G'* and *G"*) of biopolymer networks scales as $G'(\omega) \approx \omega^n$, $G''(\omega) \approx \omega^n$ following a power law trend characteristic of each system (Torres *et al.*, 2009). Our samples of bacterial cellulose showed a power law exponent (*n*) value of about 0.08, and thus *G'* and *G"* can be considered almost independent of the angular frequency. On the basis of this information and the parallelism between moduli in mechanical spectra, a gel-like behaviour was observed for all the concentrations, even for the lowest value (0.1% w/v). That is, the fibers formed network structure over the whole system even at the lowest concentrations considered. On the contrary, mechanical spectra of the commercial blend (**figure 8.1b**), showed a significantly higher dependence on the frequency, with *n* equal to 0.72 and 0.83 at 1% and 0.5% of concentration. This behaviour is representative of the absence of a strong gel network.

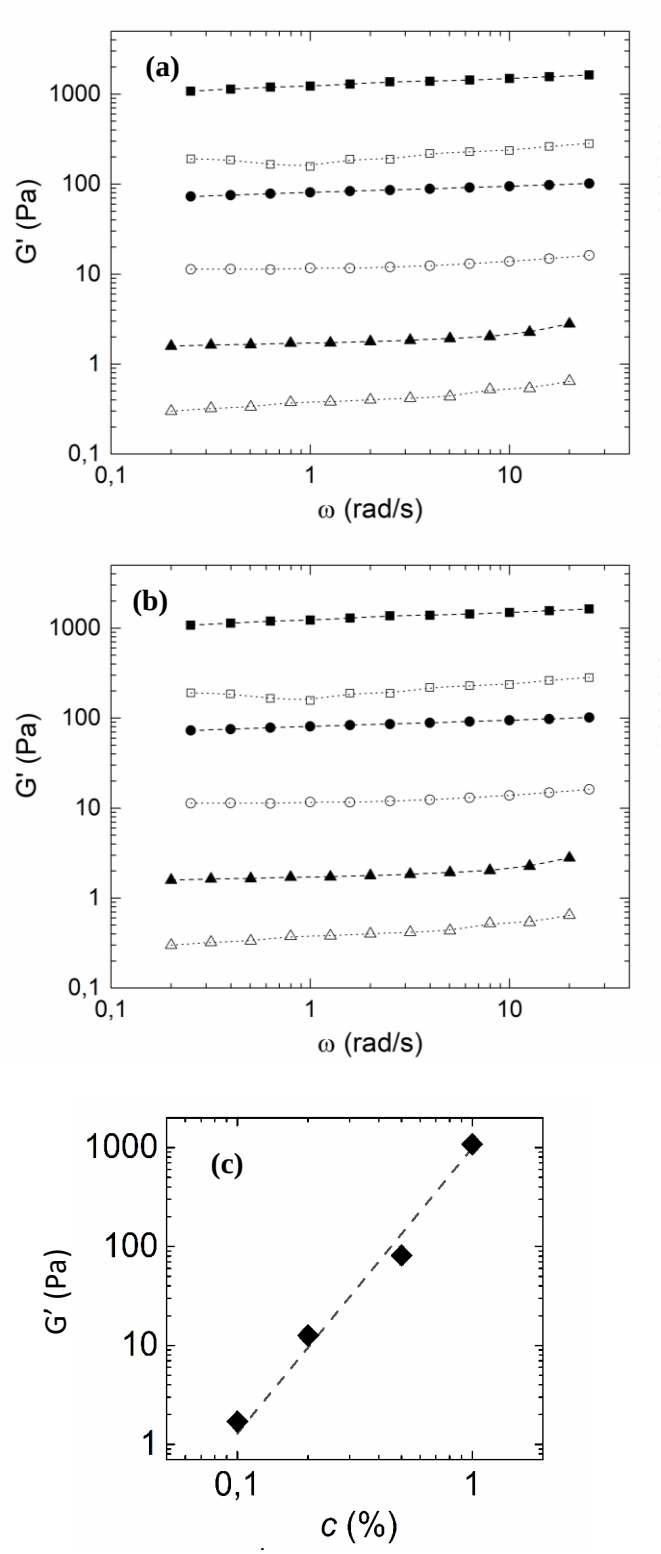

Figure 8.1 Dynamic modul (*G'*: full symbols; *G"*: hollow symbols) as a function of the frequency (ω) of the cellulose dispersions of BNC (a) and commercial blend (b) at 1% (■), 0.5% (●) and 0.1% (▶). (c) *G'* value obtained from amplitude sweep in the LVE as a function of the concentration (w/v).

Figure 8.1 also highlights the strong dependence of the elastic modulus on the concentration. In **figure 8.1c**, *G'* value obtained from amplitude sweep in the LVE region (at rest-state) was plotted as a function of the concentration (w/v). A power law relation was fitted to the dynamic data of BNC: $G' = kc^{\beta}$(eq. 8.5), where k and β are two characteristic constants (Tatsumi & Matsumoto, 2007). The exponent value (β) was found to be equal to 2.23. The power obtained agrees with

previous works (Tatsumi *et al.*, 1999) where the elastic modulus for cellulosic fibers increased in proportion to $c^{9/4}$ regardless of the types of the fibers. Indeed, the parameter, β, reflects the structural properties of the whole system that can be defined a fibrillar gel (Guenet, 2000). In addition, such exponent values agreed with the value determined for polymers gels in a good solvent by the use of the scaling theory (Daoud *et al.*, 2007) confirming the formation of a gel-like network independently on concentration. Conversely, the front factor *k* was associated to the individual characteristics of the fibers such as the axial ratio and the elastic modulus of the fiber (Tatsumi & Matsumoto, 2007). In our case, the *k* value is 700. Previous works (Tatsumi *et al.*, 2002) reported 1080 and 120 for bacterial cellulose and hydrolysed bacterial cellulose respectively. The intermediate value obtained in our work are hypothesized to be related to the freeze-drying process. Removing water induces a collapse of the network and the formation of interfibrillar aggregates limiting the solvent accessibility, causing a decrease in viscoelastic properties as already reported for similar systems (Liu et al., 2017; Pääkkö *et al.*, 2007; Tatsumi & Matsumoto, 2007).

8.2.2 Cox-Merz plot

Figure 8.2 depicts the Cox-Merz plots, where the complex viscosity (η^*) is reported as a function of the angular frequency (ω). Indeed, according to the Cox-Merz empirical rule (Cox & Merz, 1958), the steady-flow viscosity can be correlated with the dynamic viscosity and for gel structures the value of the complex dynamic viscosity is a monotonically decreasing function of applied frequency. Both the materials have non-Newtonian flows, as observed for similar fiber suspensions. It was found that the viscosity curves present a constant decrease with increasing frequency, indicating a shear-thinning behaviour (Lin *et al*, 2015; Yu *et al*., 2014).

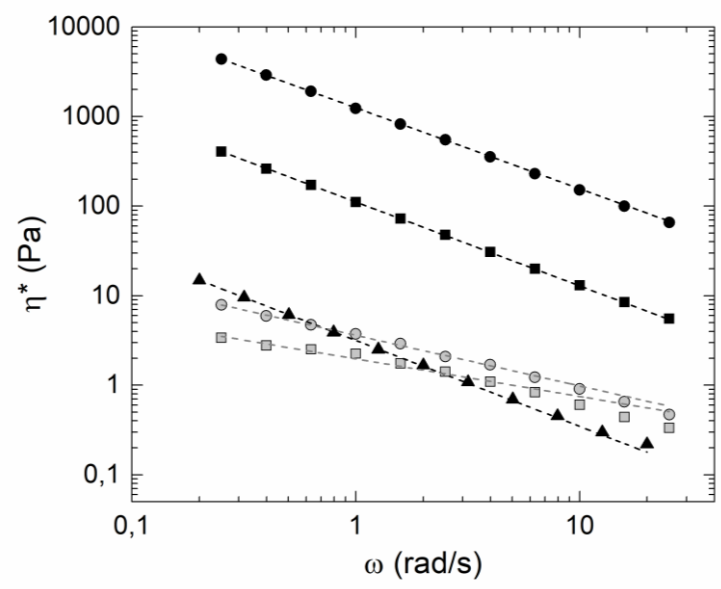

Figure 8.2 Complex viscosity (η^*) as a function of the frequency (ω), according to Cox-Merz representation, of cellulose dispersions of BNC (full symbols) and commercial blend (hollow symbols) at 1% (o), 0.5% (■) and 0.1% (►).

The behaviour can be described as a power law, using Ostwald model as follows:

$$\eta^* = K^* \omega^{n-1} \qquad \text{(eq. 8.6)}$$

The exponent *n*, which expresses the degree of non-Newtonian behaviour, displayed similar values for each material (BNC and CB) at different concentrations. However, a significant difference in the curve slope between the two products is evident, with a *n* value of 0.07 and 0.44 for BNC and CB respectively, and reflects a more pronounced shear-thinning behaviour of the microbial cellulose. The front parameter *K** represents the consistency index of the system and is named complex apparent viscosity. As highlighted in **table 8.1** by comparing the complex viscosity obtained at 0.1% and 1% of concentration, BNC exerts *K** values similar to CB samples 10-fold more concentrated.

Table 8.1 Value of the apparent complex viscosity (*K**) obtained from Ostwald model describing the complex viscosity as a function of the frequency.

	c (%)	**BNC**	**CB**
	0.1%	1.63	-
K* (Pa s)	0.5%	113.33	0.38
	1%	1253.72	3.60

8.2.3 Volatile compounds retention

Bacterial cellulose possesses potentiality to be applied as support to transport and protect volatile molecules. In this experimental set up, the adsorption of the two molecules used for the study, isoamyl and n-amyl acetate, on the SPME can only be influenced by the retention ability of the two types of cellulose, and thus by their physical state. Indeed, the headspace and its composition exclusively result by the retention ability of the cellulose placed at the bottom of the confined space.

After SPME absorption from headspace, a GC/MS quantification of the released amount of aromatic compounds was carried out in order to determine the ability of cellulosic materials to retain the two amyl acetate (iso- and n-). **Figure 8.3** compares the overall relative release values of both volatile molecules from the two cellulosic supports. The commercial blend shows an overall RR index (**eq. 8.1**) corresponding to 21.86% and 29.29%, for isoamyl and n-amyl acetate respectively. Regarding bacterial cellulose, RR values are 1.58% and 1.86% for isoamyl and n-amyl acetate, almost 15-fold lower than the reference ones. It can be deduced that microbial cellulose retains more than 98% of the initial amount of volatile molecules after 73 hours of monitoring at room temperature. On the contrary the commercial blend is able to retain between 70% and 80% of the adsorbed compounds for the same period of time.

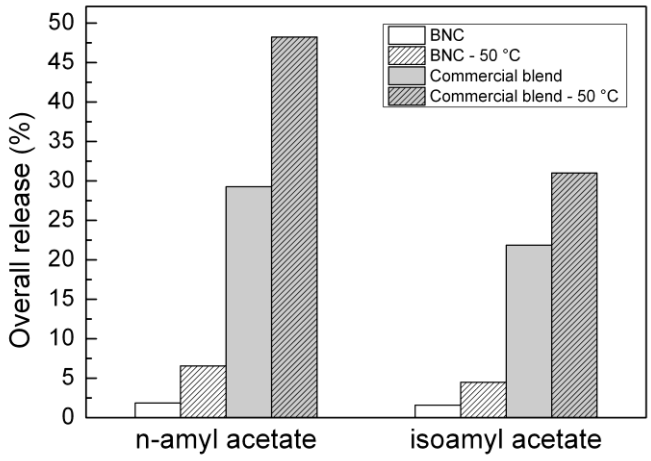

Figure 8. 3 Overall amount of released isoamyl and n-amyl acetate from commercial blend (Avicel CL611-F) and bacterial cellulose at room temperature and 50 °C at the end of the experimental time.

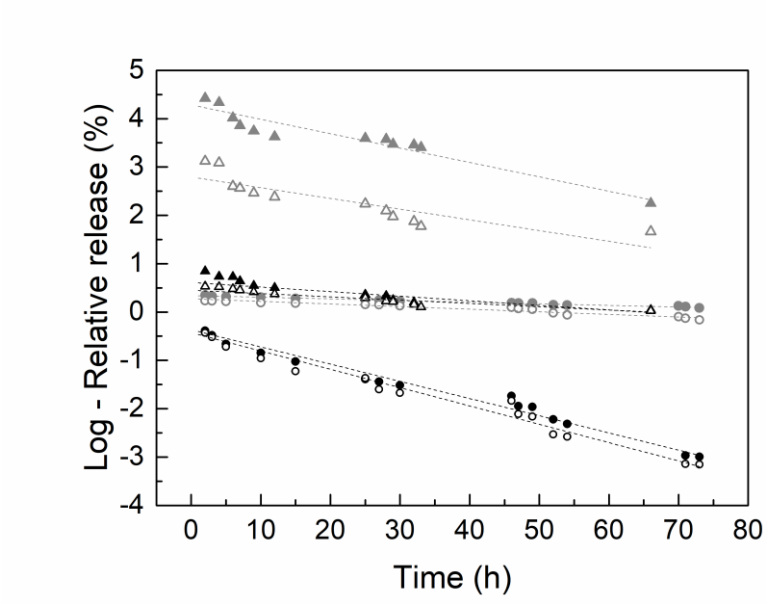

Figure 8.4 Relative release curves of isoamyl acetate (hollow symbols) and n-amyl acetate (full symbols) at room temperature (black) and 50 °C (grey) from commercial blend (triangles) and bacterial cellulose (circles) during the experimental time.

The performance of the two materials was also monitored during time, as shown in **figure 8.4** where the relative amounts of released aromatic molecules are plotted on a logarithmic scale as a function of the experimental time. The initial part of the release curves (until 10 hours) displays a fast release phenomenon. Once this event ceased, BNC curves get a plateau value, characterized by negligible amounts of released compounds (lower than 0.1%). On the contrary, regarding CB curves, the initial exponential fast release is followed by a slower kinetic of desorption. The linear trend of the relative release in the logarithmic scale highlights its exponential dependence on the experimental time. As evident from the **table 8.2**, the slopes obtained from the bacterial cellulose are about one order of magnitude higher than the same parameter calculated from the commercial blend curves. It means that the volatile molecules reach a state of null release faster when adsorbed on bacterial cellulose than on the commercial blend.

Table 8.2 Parameters related to the retention ability of the two cellulosic materials.

		-k **(g/s)**	**Maximum cumulative release (%)**
Room temperature	BNC + n-amyl acetate	35.58±1.36	1.86 (R^2=0.993)
	BNC + iso-amyl acetate	37.92±1.58	1.58 (R^2=0.996)
	CB + n-amyl acetate	3.38±0.36	50.45 (R^2=0.991)
	CB + iso-amyl acetate	5.39±0.44	23.69 (R^2=0.980)
50 °C	BNC + n-amyl acetate	9.45±0.18	6.73 (R^2=0.984)
	BNC + iso-amyl acetate	6.79±0.84	4.63 (R^2=0.984)
	CB + n-amyl acetate	29.74±2.54	---
	CB + iso-amyl acetate	22.16±3.78	---

Note: The value of the calculated parameter *–k* are expressed as mean ± standard error.

The slower desorption event (t > 20 h) was found to be significant only for commercial blend samples while bacterial cellulose displayed a negligible release after 15 hours. The results suggest a higher affinity between volatile molecules and bacterial cellulose during time. This feature may be related to the higher surface area of BNC (Gelin *et al.*, 2007), because of its peculiar three-dimensional network structure compared to hierarchical organization of plant-derived cellulose used in the commercial blend. It means that BNC possess a considerably higher number of hydroxyl groups available for binding volatile molecules (Liu *et al.*, 2017). Therefore, it is important to discriminate between the volatile free to be released, the potion entrapped into the cellulosic matrix and the total fraction of the compounds.

Phase partitioning is one of the key factors affecting the flavor release, and it is strongly influenced by the fraction of free molecules, which are the only ones able to exert a vapor pressure (de Roos, 2000). The partitioning phenomenon was quantified through a specific parameter, the partitioning coefficient, *P*, corresponding to the ratio of the amount of volatile compound adsorbed on the SPME fiber and the total amount of residual volatile compound still present in the system (**eq. 8.3**). In **figure 8.5**, the value of *P* shows a decreasing trend when plotted as a function of the relative release, indicating that proceeding with the release test always less volatile molecules are available to be released. The BNC curves, where the release at the longer time is negligible, tend to intercept the abscissa at RR values lower than 2%. The dependence of the partition coefficient as a function of the cumulative release was modeled by means of a descriptive mathematical equation:

P = ((log(-a *cumulative release* + c)+b)/d (eq. 8.6)

where *a*, *b*, *c* and *d* are descriptive constants.

The present model was able to properly describe the BNC curves, since the R^2 after fitting data was higher than 0.99 for all the samples, as also evident from the **inset** in **figure 8.5**. In addition, the descriptive mathematical model can be used to identify the cumulative release value corresponding to a null partitioning coefficient. When *P* is equal to zero, it means that all the volatile molecules present in the system are bond to the cellulosic support and cannot be released. The corresponding cumulative amount of volatile released (cumulative release) at that time is inversely proportional to the ability of the celluloses to retain it. The values of cumulative release extrapolated (at *P*=0) are reported in **table 8.2**. A similar behavior was hypothesized also for the CB samples, and the curves were described with the same mathematical model with the R^2 values corresponding to 0.98 and 0.97 for n-amyl and isoamyl release respectively. Despite the values reported in **table 8.2** are subjected to the error related to the extrapolation, the great difference

between the values obtained with the different volatile molecules and the cellulosic materials enables to discriminate a very diverse behavior. When the partitioning coefficient approaches the zero, it means that the system is moving toward a kinetic equilibrium between the amounts of released and adsorbed volatile compound. As expected, the bacterial releases a relative amount of the supported compound one order of magnitude lower than the commercial blend.

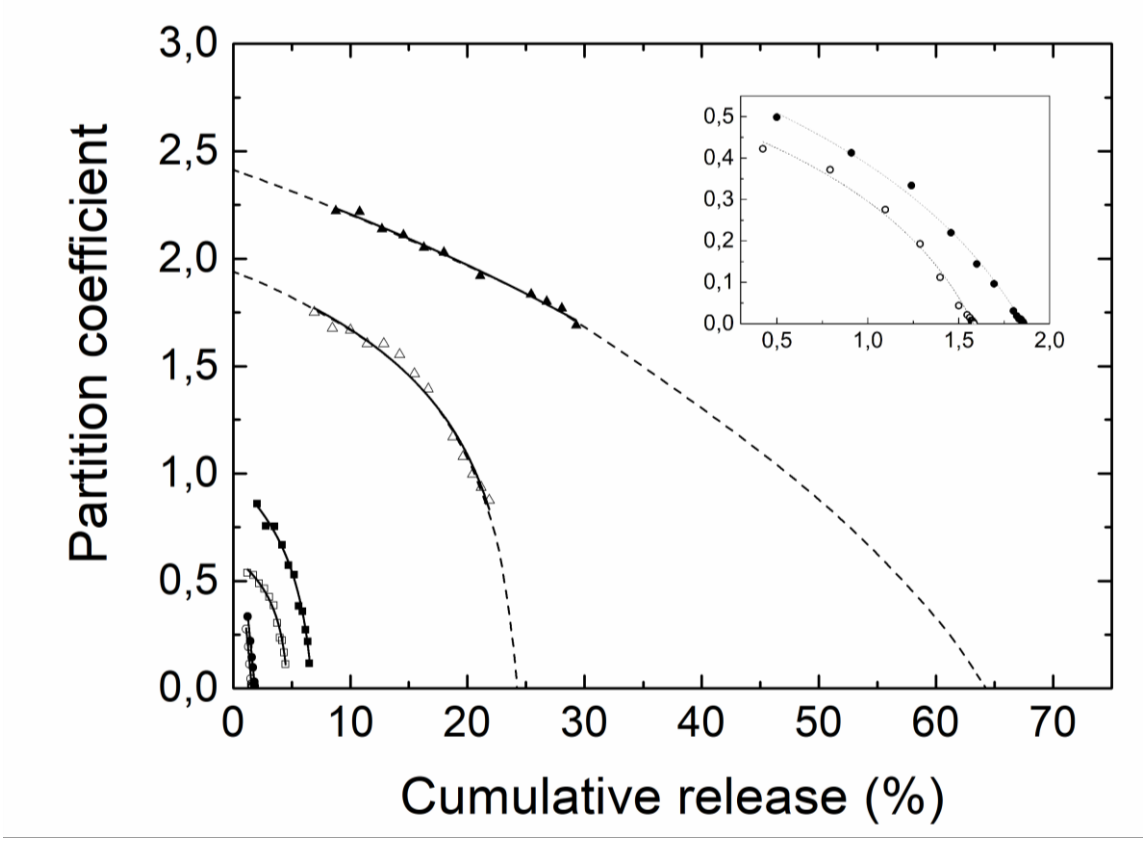

Figure 8.5 Partitioning coefficient of isoamyl (hollow circles) and n-amyl acetate (full circles) in BNC (o) and commercial blend (■) at room temperature and BNC at 50 °C (▶) as a function of the cumulative release.

Effect of the temperature on volatile retention on cellulose supports

The retention ability was also evaluated at a higher temperature, 50 °C, in order to evaluate the performance of bacterial cellulose under critical conditions. The retention in bacterial cellulose seems to be strongly influenced by the increased temperature, which is reflected into a three times higher overall release compared to the value at room temperature (**figure 8.3**). On the contrary the values obtained for the commercial blend are not even doubled. Anyway, it should be considered that the released amount of the two volatile components from BNC is limited, and also at 50 °C the microbial cellulose is able to retain more than 90% of the initial value.

In this case none of the supporting materials reaches a negligible release at the end of the experimental time. The different behavior of the bacterial cellulose at enhanced thermal conditions is highlighted also by the slope values obtained from the first-order kinetic model (*k*), which was reduced by one-third. In addition, at this condition, the relative amount released from the bacterial cellulose is significantly different according to the volatile compound considered, contrary to the overlapping of the two corresponding curves at room temperature. The phase partitioning of the volatile compound was studied also at this temperature condition (50 °C), and its plot as a function of the cumulative relative release is shown in **figure 8.5**. In this case the maximum portion of the initial volatile amount released is 3-4 fold higher.

The effect of the temperature is strictly related to the concept of dynamic equilibrium which take place in the system. The volatile molecules can interact with the hydroxyl groups of the cellulose through their oxygen. These binding are continuously formed and disrupted reversibly, but the system at the equilibrium maintains a constant ratio between the compound desorbed and the adsorbed one. Increasing the temperature, a higher level of energy is furnished to the volatile molecules to migrate into the matrix and thus the equilibrium state is shifted toward greater amount of released compound. In addition, the higher number of available –OH groups in the bacterial cellulose structure compared to the commercial blend makes volatile molecules statistically more prone to be bond or rebond to them increasing the affinity to the cellulosic material. At a macroscopic scale, these events are translated into a higher retention of the volatile compounds. When the partition coefficient is null, it is hypothesized that volatile molecules dissociate from the cellulosic matrix and move toward headspace, but they promptly interact with a close free hydroxyl groups of the polymeric chain.

The results, reported in **table 8.2**, confirm that the retention ability of volatile compounds is significantly affected by the physical state of the cellulose, and that the bacterial cellulose presents an extensively much higher retention ability of volatile molecules.

Effect of the volatile molecules structure on their retention on cellulosic supports
Beyond the effect of the architecture of the two cellulose samples, the molecular structure of the two volatile molecules showed a significant influence on the retention ability. It was previously reported that iso-amyl acetate presents the higher amounts of compound retained into the cellulose supports at the end of the experimental time compared to the results obtained for the n-amyl acetate. The different behavior can be ascribed to the different molecular structure, given the two compounds have the same molecular weight; indeed n-amyl acetate is more linear than iso-amyl acetate, which presents a side methyl group. We can conclude that molecular branching may hinder the migration of the molecule through the cellulose network.

8.2.4 Dynamical-mechanical analysis

DMTA analysis enabled the assessment of the mechanical performances of cellulosic films, and the evaluation of the possibility to improve their functional properties through the addition of a plasticizer (glycerol). Indeed, the interaction between the polysaccharide and the polyol can induce modifications of the structural arrangement, which are translated into different macroscopic performances. **Figure 8.6** displays stress-strain curves for BNC films in presence and absence of glycerol, as plasticizer. The curve for microbial cellulose films, without plasticizer, show an initial steep constant slope corresponding to the linear elastic interval. The linear region is followed by a deformation stage with a continuous decrease in the stress-strain slope until a break point at relatively low strain (3.31%). Thus, BNC films show a tension curve with a shape typical for hard and brittle materials. Mechanical properties of films were characterized by measuring elongation at break (*EB*) and the Young's modulus (E_1), as reported in **table 8.3**, which are key indicators of a film's flexibility and elasticity. As expected, the presence of glycerol had a significant plasticizing effect decreasing the initial slope from 32.25 to 16.35 and 14.18 MPa (for 0, 30 and 60 % w/w of glycerol respectively), and almost doubling the degree of elongation at breaking point. Moreover, in presence of the glycerol, a second constant slope is reached over the plastic deformation stage, corresponding to the plastic index (E_2). Its value is quite similar for the two degree of addition (3.16 MPa for 30% and 2.97 MPa for and 60 % w/w of glycerol), as for the Young's modulus. It can be hypothesized a saturation effect after a critical value of glycerol addition (lower than 30%). We can conclude that the inclusion of glycerol determines an

effective plasticization of the system, related to the effect of competition between hydroxyl groups of the polymer and of the additive which causes a reduction of internal hydrogen bonding in cellulose film (McHugh *et al.*,1994).

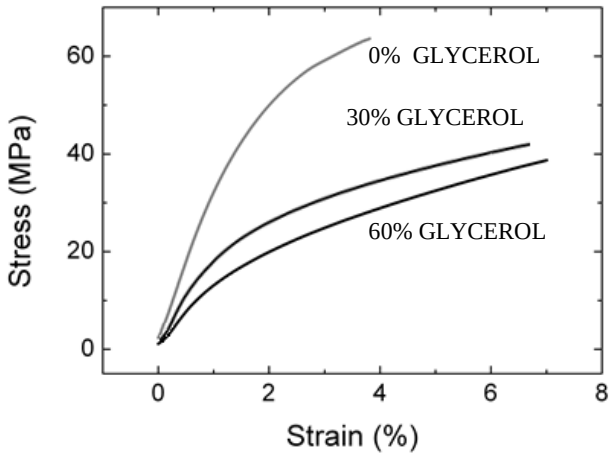

Figure 8.6 Stress-strain curves for the BNC film curve with (grey) and without (black) glycerol.

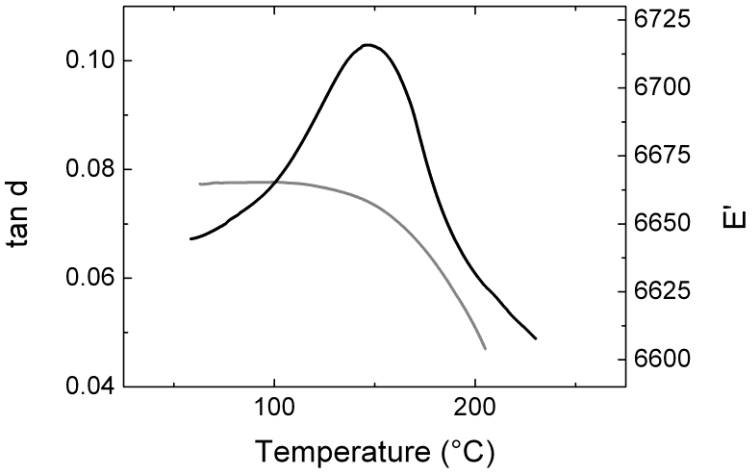

Figure 8.7 Typical DMTA plot of a BNC filmed (without plasticizer) cured in a temperature ramp: tan(δ) is reported as a black line, E' as a grey line.

Moreover, dynamic mechanical thermal analysis (DMTA) was carried out to obtain information about the microstructure of a cured film. The storage modulus, *E'*, and *tan*(*δ*) curves as a function of temperature (**figure 8.7**) were used to assess the compatibility between glycerol and cellulosic fibers. The Ts/Tg ratio expresses the width of tan δ peak. It is a rule that a higher Ts/Tg ratio leads to a narrow tan(*δ*) peak, indicating the formation of more homogeneous film (Patel *et al.*, 2012). All the type of film displayed a single tan(*δ*) peak, and it is representative of an effective compatibility between cellulose and glycerol (Pouplin *et al.*, 1999). Though *Ts/Tg* ratio underwent a slight reduction, indicative of a less homogeneous system.

Table 8.3 DMTA characterization of bacterial cellulose film in presence and absence of glycerol. Elongation at break (*EB*), the Young's modulus (E_1), and plastic index (E_2) obtained through tensile analysis. Glass transition temperature (T_g) and homogeneity index (T_s/T_g) from ramp temperature testing.

	E_1 (MPa)	E_2 (MPa)	EB (%)	T_g (°C)	T_s/T_g
BNC	32.25	-	3.31	229 ± 9	0.73
BNC + 30% gly	16.35	2.97	6.80	146 ± 5	0.61
BNC + 60% gly	14.18	3.16	7.01	152 ± 7	0.58

Conclusions

The present study offers an overview of the most significant technological properties for the exploitation of bacterial cellulose as novel food ingredient. Films of BNC proved to be an optimal support for aromatic molecules, and indeed more than 98% of the initial amount of volatile molecule adsorbed was recovered into the film after 73 hours of analysis. Hydration, structuring and retention properties exerted by bacterial cellulose are mainly related to its striking greater surface area, compared to traditional sources of cellulose, and the consequent number of hydroxyl groups available for interacting both with water and volatile molecules. Concerning the setup of films production, the addition of a plasticizer (glycerol) was found to improve technological performances and likely induce modifications in structural organization.

Aknoledgements

I thank Professor Diego Romano (Dept. of Food, Environmental and Nutritional Sciences, UNIMI) for the kind gift of bacterial cellulose, and Dr. Monica Bononi (Dept. of Environmental Science and Policy, UNIMI) for performing the volatile quantification in release kinetic studies.

References

Cox, W. P., & Merz, E. H. (1958). Correlation of dynamic and steady flow viscosities. *Journal of Polymer Scienc*e, 28(118), 619-622.

Daoud, M., Stanley, H. E., & Stauffer, D. (2007). Scaling, Exponents, and Fractal Dimensions. In *Physical Properties of Polymers Handbook* (pp. 83-89). Springer, New York, NY.

de Roos, K. B. (2000). Physiochemical models of flavor release from foods. In D. D. Roberts & A. J. Taylor (Eds.), *Flavour release* (p. 126-141). American Chemical Society.

Gelin, K., Bodin, A., Gatenholm, P., Mihranyan, A., Edwards, K., & Strømme, M. (2007). Characterization of water in bacterial cellulose using dielectric spectroscopy and electron microscopy. *Polymer*, *48*(26), 7623-7631.

Guenet, J. M. (2000). Structure versus rheological properties in fibrillar thermoreversible gels from polymers and biopolymers. *Journal of Rheology*, 44(4), 947-960.

Iguchi, M., Yamanaka, S., & Budhiono, A. (2000). Bacterial cellulose—a masterpiece of nature's arts. *Journal of Materials Science*, *35*(2), 261-270.

Lin, D., Li, R., Lopez-Sanchez, P., & Li, Z. (2015). Physical properties of bacterial cellulose aqueous suspensions treated by high pressure homogenizer. *Food Hydrocolloids*, *44*, 435-442.

Liu, D., Martinez-Sanz, M., Lopez-Sanchez, P., Gilbert, E. P., & Gidley, M. J. (2017). Adsorption behaviour of polyphenols on cellulose is affected by processing history. *Food Hydrocolloids*, *63*, 496-507.

McHugh, T. H., Aujard, J. F. & Krochta, J. M. (1994). Plasticized whey protein edible films: water vapor permeability properties. *Journal of Food Science*, *59*(2), 416-419.

Pääkkö, M., Ankerfors, M., Kosonen, H., Nykänen, A., Ahola, S., Österberg, M., ... & Lindström, T. (2007). Enzymatic hydrolysis combined with mechanical shearing and high-pressure homogenization for nanoscale cellulose fibrils and strong gels. *Biomacromolecules*, *8*(6), 1934-1941.

Patel, M. M., Patel, C. J., & Patel, N. K. (2012) Study of Thermal Properties on UV-Curable Coatings Derived from Oleochemical Polyols. *Chemical Science Transactions*, *1*(2), 289-296

Pouplin, M., Redl, A., & Gontard, N. (1999). Glass transition of wheat gluten plasticized with water, glycerol, or sorbitol. *Journal of agricultural and food chemistry*, *47*(2), 538-543.

Tatsumi, D., Ishioka, S., & Matsumoto, T. (1999). Effect of particle and salt concentrations on the rheological properties of cellulose fibrous suspensions.*Nihon Reoroji Gakkaishi*, *27*(4), 243-248.

Tatsumi, D., Ishioka, S., & Matsumoto, T. (2002). Effect of fiber concentration and axial ratio on the rheological properties of cellulose fiber suspensions. *Nihon Reoroji Gakkaishi*, *30*(1), 27-32.

Tatsumi, D., & Matsumoto, T. (2007). Rheological properties of cellulose fiber wet webs. *Journal of Central South University of Technology*, *14*, 250-253.

Torres, F. G., Troncoso, O. P., Lopez, D., Grande, C., & Gomez, C. M. (2009). Reversible stress softening and stress recovery of cellulose networks. *Soft Matter*, *5*(21), 4185-4190.

Wong, S. S., Kasapis, S., & Huang, D. (2012). Molecular weight and crystallinity alteration of cellulose via prolonged ultrasound fragmentation. *Food Hydrocolloids*, *26*(2), 365-369.

Yu, D., Zeng, J. S., Chen, K. F., Feng, Y. C., & Yang, X. (2014). Rheological measurement of concentrated pulp fiber suspensions in oscillatory shear using a novel device. *BioResources*, *10*(1), 182-195.

Overall Conclusion

The research presented in this PhD thesis gives an overview of the technological performance of novel food ingredients derived from food processing residues. The conversion of sidestreams by-products into functional materials for the food formulation was operated with different approaches, spanning from functional-driven extractions with different degree of selectivity to microbial biotransformation.

The characterization of cellulose nanocrystals rheo-optical behaviour provided an insight into the relationship between nematic ordering and kinetic arrest. At the moment, the results are far from a complete understanding of its rheological behaviour and how it is influenced by the anisotropic transition, but useful information were obtained in order to perform a correct characterization and avoid artefacts due to the complexity of the system.
Cell wall materials were studied as carrier of bioactive compounds. Despite their permeable, it was investigated the possibility of tuning wall matrix composition and architecture through the control of the extraction process in order to obtained a more sustained release.
The texturing and structuring abilities of hemp seed meal were found to be strictly correlated to both compositional and structural features. In particular, HSM particles are characterized by a really complex organization, and a full knowledge of the phenomena involved in their functionality absolutely requires a multiscale point of view.
Bacterial cellulose demonstrated to be an excellent support for flavour molecules retain. Compared to commercial cellulosic materials, its three-dimensional network provided a unique support for volatile molecules binding.

The exploitation of agro-food residues for the production of food ingredients was not only advantageous in terms of sustainability and resources saving. The complexity and variability in composition, and the peculiar structures obtained from these ingredients is reflected in an improved functionality compared to purified ingredients.

SCIENTIFIC PRODUCTS

Non peer-reviewed publications

Zanchetta, G., Rocchi, E., & Piazza, L. (2017). Seeing Is Believing: Coupling Between Liquid Crystalline Ordering and Rheological Behaviour in Cellulose Nanocrystals Suspensions. *Chemical Engineering Transactions*, 57, 1933-1938.

Piazza, L., & Rocchi, E. (2017). Preliminary Study on the Reduced Pressure Cold Plasma Processing of Fresh Cut Salads: Rheological Assessment of Modifications in the Plant Tissue Structure. *Chemical Engineering Transactions*, 57, 1867-1872.

Proceedings of National and International Conferences

Rocchi, E., Zanchetta G.& Piazza, L. (2016) Rheo-optical characterization of cellulose nanocrystals suspensions extracted from waste plant biomass. **Oral presentation** at *Italian Soft Days – Second Edition, 23-24 June 2016.* Milan, Italy.

Rocchi, E. (2016) Preliminary data on Cell Wall Material intended as micro-reactor for in situ-preparation and targeted delivery of active components. **Poster presentation** at *21st Workshop on the Developments in the Italian PhD Research on Food Science Technology and Biotechnology, 14-16 September 2016*. Portici, Italy.

Piazza L., Rocchi E., Malegori C., Mazzitelli D., Picozzi C., Ortenzi M.A., Gazzotti S., Altomare A., Orioli M. & Carini M. (2016) BOMBYX project: Valorisation of high value proteins and lipids extracted from silkworm pupae. **Oral presentation** at *30th EFFoST Conference, 26-28 November 2016*. Vienna, Austria.

Rocchi, E., Romano D., Malgori C. & Piazza L. (2016) Assessment of physico-chemical properties of bacterial nanocellulose intended for food formulations improvement. **Poster presentation** at *30th EFFoST Conference, 26-28 November 2016.* Vienna, Austria.

Piazza L., Rocchi E., Malegori C., Mazzitelli D., Picozzi C., Ortenzi M.A., Gazzotti S., Altomare A., Orioli M. & Carini M. (2017)

Piazza L., Brambilla A.E., Rocchi E., Spinelli L., Torricelli A. & Rizzolo A. (2017) Rheology and microstructure of blueberry purees: influence of the processing design. **Oral presentation** at *Food Innova 2017, 31 Jenuary-03 February 2017*. Cesena, Italy.

Rocchi, E. (2017) Kinetic study of the release mechanism from plant-derived supramolecular aggregates, intended as carrier of bioactive compounds. **Poster presentation** at *22nd Workshop on the Developments in the Italian PhD Research on Food Science Technology and Biotechnology, 20-22 September 2017*. Bolzano, Italy.

Rocchi, E. (2018) Functionality-driven fractionation of materials collected during the mainstream plant processing into finished unrefined ingredients. **Oral presentation** at *23rd Workshop on the Developments in the Italian PhD Research on Food Science Technology and Biotechnology, 20-22 September 2017*. Oristano, Italy.

Acknowledgments

Firstly, I would like to express my gratitude to my advisor Prof. Laura Piazza for the opportunity of performing this exciting research activity and strengthening my analytical expertise, facing always new challenges.

My sincere thanks also go to Dr. Giuliano Zanchetta, who provided me an opportunity to join the point of view of Physics. His patient support and guidance were essential for travelling through the complex behaviour of Nanocrystalline cellulose.

I also wish to express my gratitude to Dr. Monica Bononi for sharing her expertise in volatiles release and for the precious time she dedicated to our work. As well, thanks to Prof. Gabriella Roda and Dr. Gilda Aiello for the fruitful collaboration and the interesting debates, which were translated in a multidisciplinary and stimulating perspective for the characterization of hempseed meals.

I thank Dr. Marco Signorelli and Francesca Saitta for sharing daily ideas, friendship and coffee. They are cheering up fellows against turbulences and wise counsellors for academic (but not only) doubts.

I am grateful to Maria Eletta Moriano for the long trip and the great memories together. In particular, in her office I always found a chair where to seat, words to find comfort, and understanding to not feel alone.

I extend sincere thanks to all the people I met at the 'fifth floor', who supported and inspired me since my bachelor degree. Thanks also to the dept. of Food and Environmental Science that gave access to the laboratory and research facilities. A special thanks goes to Simona Ratti for sharing with me her laboratory experience, hard work moments and her sincere speaking.

I want to acknowledge my parents for their support and nearness; without them I would have never got the privilege of reaching this goal today. To Giorgio, thanks for his unconditional confidence in my abilities, the motivational speeches and the attentions in critical moments. He gave priority to my realization even when it meant to sacrifice time, and I am really grateful for this.

In the end, I thank all my friends because 'walking with a friend in the darkness is better than walking alone in the light'.